University of Birmingham

Doctoral Thesis

FLOW AND TEMPERATURE DYNAMICS IN THE HYPORHEIC ZONES

Author:
Tanu Singh

Supervisor(s):
Prof. Stefan Krause
Dr Jesus D. Gomez-Velez
Prof. David M. Hannah

A thesis submitted to the *University of Birmingham* for the degree of
DOCTOR OF PHILOSOPHY

School of Geography, Earth and Environmental Sciences
College of Life and Environmental Sciences
University of Birmingham
September 2019

ABSTRACT

Hyporheic zones (HZs) are key compartments in river-aquifer systems, characterized by continuous exchange of water, solutes, nutrients and bacteria between stream water and aquifers. Flow in the HZs is driven and controlled by interplay between bedform topography, stream stage fluctuations, temperature oscillations in stream water temperature, hydraulic conductivity, channel gradients and other sediment properties. Resultant hyporheic exchange fluxes affect biogeochemical turnover and is a determinant of biogeochemical hot-spots and hot-moments. While previous studies have improved our understanding of hyporheic exchange processes for steady state flow and temperature conditions, little attention has been paid to the *transient* behaviour of HZs. To evaluate the dynamic development of HZ characteristics in response to transience in surface-water flow and temperature, a two-dimensional flow and transport model with a time-varying boundary condition at the sediment-water interface is used. The impacts of single peak-flow events, repeated and superimposed events and diurnal variations in surface-water temperature are systematically explored. Moreover, we quantify the adequacy of reduced-order models to represent the hyporheic characteristics under transient flow conditions by comparing our numerical results with field-observations.

Peak-flow events cause the expansion and contraction of the HZ, which is controlled by events yet is modulated by ambient groundwater flow. Discharge of older hyporheic water is observed for higher bedform aspect ratio (*i.e.* ratio between the bedform amplitude and wavelength) and lower channel slopes. Variations in residence times during peak-flow events lead to the development of larger areas of potential nitrification and denitrification in the HZ for longer duration. However, when superimposed and repeated peak-flow events were taken into account, we observed that separation between the occurrence of two events largely determines the discharge of older or younger hyporheic waters. Increased time-lag between two events show higher variability in residence time distribution. Moreover, flatter numerical breakthrough curves for events with increased separation and longer duration of the events are observed. Also, when temperature-dependent flow is considered in ripple-like bedforms, significant variations in hyporheic exchange fluxes are highlighted. Temperature signals leaving the HZs are cooled and lagged which are dependent on the parameters determining the heat transport time scales (*i.e.* hydraulic conductivity and channel slopes). Furthermore, it is shown that the reduced-order models can adequately predict the dynamics of HZs for a step-pool bedform, however there are minor deviations for a low-gradient run when compared to field-observed data. The presented findings illustrate the importance of consideration of transience in hyporheic exchange processes and potential implications for river management and restoration. These findings also suggested that mechanistic knowledge derived from the reduced-order models should be considered with caution as there are limitations in our ability to upscale hyporheic exchange processes.

To maa, papa, bhai, nana and nani thank you for everything.

ACKNOWLEDGEMENTS

I owe my deepest thanks to my supervisors Prof Stefan Krause, Dr Jesus D. Gomez-Velez and Prof David Hannah for their continuous guidance and unwavering support over the course of my PhD studies. Without their advice and feedback this thesis would have not been possible.

I would also like to thank Nicolai Brekenfled, Liwen Wu, Dr Sophie Comer-Warner, Dr Sam Johansson, Prof Anders Wörman, friends at University of Birmingham and KTH, and my HypoTRAIN family who have provided invaluable help, support and advice throughout the period of my PhD study.

Thanks to my friends, Danny and Alex who started PhD studies with me in the same office in Birmingham and were always there to talk and listen to me in last four years. I really appreciate it!

I would also like to thank my parents and my brother for motivating and believing in me and making me capable of studying in the UK. My best friend Akanksha, I greatly appreciate her availability 24x7 to listen and moreover, sorting out all my problems from New Delhi. I will always cherish this friendship.

A very special thanks to my husband and my best friend, Dr Bradley Sean Cox, without whose love, constant support, encouragement, and understanding this journey would have been significantly difficult. I am grateful to him for always being there whenever I needed him. I really can't imagine finishing my thesis without his presence in my life. I am glad we were together in our PhD journeys, this made the journey even more special.

Finally, my sincere thanks goes to Marie Curie ITN HypoTRAIN which received funding from European Union's Horizon 2020 research and innovation programme under Marie Skłodowska-Curie [grant agreement No. 641939] and HiFreq RISE project [grant agreement No. 734317] for funding this research. I am thankful to HypoTRAIN for providing the training, exposure and network opportunities which would otherwise have not been possible.

Birmingham, September 2019 T. S.

CONTENTS

LIST OF FIGURES

LIST OF TABLES

ABBREVIATIONS

ADE	**A**dvection-**D**ispersion **E**quation
DOC	**D**issolved **O**rganic **C**arbon
HEF	**H**yporheic **E**xchange **F**lux
HTE	**H**eat **T**ransport **E**quation
HZ	**H**yporheic **Z**one
ROM	**R**educed-**O**rder **M**odel
RT	**R**esidence **T**ime
SWI	**S**ediment-**W**ater **I**nterface
VHG	**V**ertical **H**ydraulic **G**radient

NOMENCLATURE

Roman symbols

a_n	n^{th} moment of the residence time distribution
AR	Aspect Ratio of Streambed
BTC	Modelled breakthrough curve
C	Concentration
d_{b}	Depth of domain
$\mathbf{D}$	Dispersion-diffusion tensor
DN	Damköhler number
D_{m}	Effective molecular self-diffusion coefficient
$\boldsymbol{D}_{\text{T}}$	Hydrodynamic thermal dispersion tensor
d_{bkf}	Bankful depth
D_{c}	Grain-size diameter
E_{a}	Activation energy
g	Acceleration due to gravity
h	Hydraulic head
h_{d}	Intensity of dynamic head fluctuations
h_{d}	Intensity of dynamic head fluctuations
h_{SWI}	Head distribution at SWI
H_{generic}	Generic stage hydrograpg
H_0	Stage at baseflow
H_{p}	Stage increase at peak
H_{s}	Total stage
H_{sup}	Superimposed hydrograph
HZ_{eff}	Hyporheic zone efficiency
k_{f}	Thermal conductivity of fluid
k_{s}	Thermal conductivity of solids
k_{T}	Bulk thermal conductivity
K	Hydraulic conductivity
L	Total streamwise length
m_{out}	Total mass leaving the hyporheic zone
M_{in}	Total mass entering the streambed
p	Pressure head
Pe_{T}	Thermal Peclet number
$\boldsymbol{q}$	Darcy velocity
Q_{anoxic}	Anoxic hyporheic waters discharged to the stream
$Q_{\text{hz,out}}$	Hyporheic waters discharged to the stream
Q_{oxic}	Oxic hyporheic waters discharged to the stream
r_{T}	Reaction rate
R_{u}	Universal gas constant
S	Channel slope

Sk	Skewnwss of the event
t_{c}	Time-scale for heat transport
t_{d}	Duration of the event
t_{lag}	Time-lag between two paek-flow events
t_{p}	Time at peak of the event
T	Temperature
T_{amp}	Peak-amplitude of water column temperature
T_{s}	Temperature of water column
T_{sm}	Mean diurnal temperature
v_{s}	Mean velocity
$\boldsymbol{v}_{\mathrm{T}}$	Thermal front velocity
z	Reference elevation
Z_{SWI}	Streambed topography of stream-water interface

Greek symbols

α	Thermal expansion coefficient
α_{L}	Longitudinal dispersivity
α_{T}	Transverse dispersivity
β_{l}	Longitudunal thermal dispersivity coefficient
β_{t}	Transversal thermal dispersivity coefficient
δ	Constant determining the degree of assymetry
δ_{ij}	Kronecker delta function
Δ	Characteristic amplitude of streambed
η	Fraction defining lag between two events
θ	Porosity
κ	Permeability
λ	Wavelength of bedform
μ_d	Dynamic viscosity
μ	Mean residence time
μ_{max}	Maxima of first central moment of residence time
ρ	Fluid density
$\tau_{\mathrm{O_2}}$	Biogeochemical timescale for oxygen consumption
ϕ	Phase shift
ξ_{m}	Fluid tortuosity
ω	Frequency of the event
Ω	Modelling domain
$\partial\Omega_{\mathrm{b}}$	Base boundary
$\partial\Omega_{\mathrm{d}}$	Downstream lateral boundary
$\partial\Omega_{\mathrm{in}}$	Inflow sub-boundary
$\partial\Omega_{\mathrm{out}}$	Outflow sub-boundary
$\partial\Omega_{\mathrm{SWI}}$	Sediment water interface boundary
$\partial\Omega_{\mathrm{u}}$	Upstream lateral boundary

PUBLICATIONS

Some of the results presented in the thesis have been published in peer-reviewed journal. Chapter 2 is associated to publication [**J2**].

Journal articles

[**J1**] L. Wu, **T. Singh**, J. D. Gomez-Velez, G. Nützmann, A. Wörman, S. Krause, J. Lewandowski, 'Impact of Dynamically Changing Discharge on Hyporheic Exchange Processes Under Gaining and Losing Groundwater Conditions', *Water Resources Research*, **54**, 1–18, (2018).

[**J2**] **T. Singh**, L. Wu, J. D. Gomez-Velez, J. Lewandowski, D. H. Hannah, S. Krause, 'Dynamic Hyporheic Zones: Exploring the Role of Peak-Flow Events on Bedform-induced Hyporheic Exchange', *Water Resources Research*, **55**, 1–18, (2019).

[**J3**] B. Mojarrad, A. Betterle, **T. Singh**, C. Olid, A. Wörman, 'The effect of stream discharge on hyporheic exchange', *Water*, **11** (7), 1436, (2019).

[**J4**] A. Jaeger, C. Coll, M. Posselt, J. Mechelke, C. Rutere, A. Betterle, M. Raza, A. Mehrtens, K. Meinikmann, A. Portmann, **T. Singh**, P. J. Blaen, S. Krause, M. Horn, J. Hollender, J. P. Benskin, A. Sobek, J. Lewandowski, 'Using recirculating flumes and a response surface model to investigate the role of hyporheic exchange and bacterial diversity on micropollutant half-lives', *Environmental Science: Processes & Impacts*, (SUBMITTED) (2019).

[**J5**] L. Wu, J. D. Gomez-Velez, S. Krause, **T. Singh**, A. Wörman, J. Lewandowski, 'Impact of Dynamically Changing Discharge on Hyporheic Exchange Processes Under Gaining and Losing Groundwater Conditions', *Water Resources Research*, (SUBMITTED) (2019).

Conference contributions

[**C1**] **T. Singh***, L. Wu, J. D. Gomez-Velez, S. Krause, D. M. Hannah, J. Lewandowski, G. Nüetzmann, 'Effects of freshets on dynamics of hyporheic zones', *European Hyporheic Forum*, (June 2016).

[**C2**] **T. Singh***, L. Wu, J. Lewandowski, G. Nützmann, A. Wörman, D. M. Hannah, S. Krause, J. Gomez-Velez, 'Impacts of Freshets on Hyporheic Exchange Flow under Neutral Conditions', *AGU*, (December 2016).

[**C3**] L. Wu*, **T. Singh**, J. Lewandowski, G. Nützmann, A. Wörman, D. M. Hannah, S. Krause, J. Gomez-Velez, 'Impacts of Freshets on Hyporheic Exchange Flow under Gaining and Losing Conditions', *AGU*, (December 2016).

[**C4**] **T. Singh***, L. Wu, J. D. Gomez-Velez, S. Krause, D. M. Hannah, J. Lewandowski, G. Nüetzmann, 'Dynamic Hyporheic Zones: Impacts of Dynamic Forcing on Hyporheic Exchange Flows', *European Hyporheic Forum*, (April 2017).

[**C5**] L. Wu*, **T. Singh**, J. Lewandowski, G. Nützmann, A. Wörman, D. M. Hannah, S. Krause, J. Gomez-Velez, 'Dynamic Hyporheic Zones: Exploring the Role of Transient Flood Pulses on Bedform-induced Exchange under Gaining and Losing Conditions', *EGU*, **19**, 14565, (April 2017).

[**C6**] **T. Singh***, L. Wu, J. D. Gomez-Velez, S. Krause, D. M. Hannah, J. Lewandowski, G. Nüetzmann, 'Effects of transient hydrologic forcing on Hyporheic Exchange Flow', *HydroEco*, (June 2017).

[**C7**] L. Wu*, **T. Singh**, J. Lewandowski, G. Nützmann, A. Wörman, D. M. Hannah, S. Krause, J. Gomez-Velez, 'Impacts of Flood Pulses on Hyporheic Zones', *HydroEco*, (June 2017).

[**C8**] **T. Singh***, L. Wu, J. D. Gomez-Velez, S. Krause, D. M. Hannah, J. Lewandowski, G. Nüetzmann. 'Response of hyporheic zones to transient forcing', *AGU*, (December 2017).

[**C9**] **T. Singh***, L. Wu, J. D. Gomez-Velez, D. Hannah, S. Krause. 'Differential Heat Propagation in Ripples, Dunes and Riffle-Pool Bedforms and its Impact on Hyporheic Exchange Flows', *EGU*, **20**, 17203, (April 2018).

[**C10**] **T. Singh***, L. Wu, J. D. Gomez-Velez, D. Hannah, S. Krause, 'Exploring the dynamics of hyporheic zones', *EGU*, **20**, 17271, (April 2018).

[**C11**] L. Wu*, **T. Singh**, J. Gomez-Velez, J. Lewandowski, G. Nützmann, A. Wörman, S. Krause, 'Impacts of Flood on Bedform-driven Hyporheic Flux under Gaining and Losing Groundwater Conditions', *EGU*, **20**, 15411, (April 2018).

[**C12**] N. Brekenfeld*, S. Comer-Warner, **T. Singh**, P. J. Blaen, A. Lupon, L. Gómez-Gener, T. Blume, M. Morgner, H. Laudon, D. M. Hannah, K. Bishop, R. A. Sponseller, N. Kettridge, S. Krause, 'Stream channel characteristics and discharge mutually affect metabolic activity in a first-order boreal stream', *EGU*, **20**, 16195, (April 2018).

[**C13**] N. Brekenfeld*, S. Comer-Warner, **T. Singh**, P. J. Blaen, A. Lupon, L. Gómez-Gener, T. Blume, M. Morgner, H. Laudon, D. M. Hannah, K. Bishop, R. A. Sponseller, N. Kettridge, S. Krause, 'The effect of contrasting discharges on the metabolic activity of a small boreal stream' *EGU*, **20**, 15570, (April 2018).

[**C14**] L. Wu*, **T. Singh**, J. Gomez-Velez, G. Nützmann, A. Wörman, D. M. Hannah, S. Krause, J. Lewandowski, J. Riml, R. Earon, 'Exploring the Role of Transient Flood Pulses on Bedform-induced Hyporheic Exchange under Gaining and Losing Groundwater Conditions', *European Hyporheic Forum*, (April 2018).

[**C15**] S. Krause*, N. Brekenfeld, **T. Singh**, D. M. Hannah, S. Comer-Warner, P. Romeijn, J. D. Gomez-Velez, L. Wu, T. Blume, H. Laudon, K. H. Bishop, A. Robertson, J. Reiss, P. Blaen, 'Storm-driven variability of biogeochemical cycling at ecohydrological interfaces', *AGU*, (December 2018).

[**C16**] L. Wu*, **T. Singh**, J. D. Gomez-Velez, J. Lewandowski, A. L. E. Worman, G. Nuetzmann, S. Krause, 'Heat transport in dynamically-changing hyporheic zones', *AGU*, (December 2018).

[**C17**] N. Brekenfeld*, S. Comer-Warner, **T. Singh**, P. Blaen, A. Lupon, L. Gómez-Gener, T. Blume, M. Morgner, H. Laudon, D. M. Hannah, K. H. Bishop, R. Sponseller, N. Kettridge, S. Krause, 'The Hyporheic Zone as a Hotspot of C-Cycling in a Small Boreal Stream: Lessons Learnt from Experimental Flow Manipulations' *AGU*, (December 2018).

[**C18**] L. Wu, J. D. Gomez-Velez*, **T. Singh**, J. Lewandowski, A. Wörman, G. Nuetzmann, S. Krause, 'Exploring the role of river discharge and temperature regulation in hyporheic exchange processes', *EGU*, (April 2019).

[**C19**] M. Posselt*, C. Coll, J. Mechelke, A. Jäger, C. Rutere, R. Muhammad, A. Betterle, **T. Singh**, S. Krause, J. Hollender, A. Sobek, J. Lewandowski, M. Horn, K. Meinikmann, J. P. Benskin, 'Impacts of Bacterial Diversity and Hyporheic Exchange Flows on the Fate of Wastewater-derived Polar Organic Micropollutants: A Central Composite Face Designed Flume Study', *SETAC*, (May 2019).

*Presenting author

Chapter 1
INTRODUCTION

1.1 Motivation and problem description

River-aquifer systems are highly dynamic in nature, both spatially and temporally. They are associated with numerous physical, chemical and biological processes. Within this system, hyporheic zones (HZs) are key compartments that act as the liver of the river (Fischer et al. 2005). It is not only a habitat of many organisms but it also provides favourable reactive environments for attenuation of nutrients and contaminants (Krause, Hannah, Fleckenstein, Heppell, Kaeser, Pickup, Pinay, Robertson & Wood 2011, Boano et al. 2014, Zarnetske et al. 2011). Transformation and attenuation of nutrients and contaminants are the crucial ecological services that occurs within the HZs that require specific hydraulic, thermal and biological conditions. Moreover, the self-cleaning mechanism within these zones, often also associated with *reactive hotspots* involves complex behaviour as a result of dynamic and heterogeneous nature of these regions. This is because they are often exposed to external forces such as high-discharge events and extreme diurnal fluctuations in surface water temperature. Such changes have a high potential to effect the physical, chemical and biological processes in the HZs and therefore impact the water quality and the aquatic environments (Bruno et al. 2009, Wondzell & Swanson 1999).

Hyporheic zones cannot always be an effective natural biogeochemical reactor. This is because the biogeochemical reactions within the HZs are dependent on spatial and temporal hydraulic conditions. Hyporheic exchange is driven by bedform-induced hydrostatic and hydrodynamic conditions in streams that results in pressure

distribution along the sediment-water interface. The continuous exchange is a function of sediment heterogeneity, transient hydraulic conditions, hydraulic conductivity, channel gradient and geomorphological settings (Boano et al. 2006, Stonedahl et al. 2010, Gomez-Velez & Harvey 2014*a*, Krause, Hannah, Fleckenstein, Heppell, Kaeser, Pickup, Pinay, Robertson & Wood 2011, Azizian et al. 2017). Interplay between the aforementioned drivers and controls of hyporheic exchange can play a primary role in transport of water, heat, solutes and nutrients as well as contaminants deeper within the streambed for further enhancing biogeochemical transformations and redox reactions in the hyporheic zones. In addition to hydraulic conditions, appropriate thermal conditions helps temperature-sensitive bacterially mediated reactions to occur (Kaplan & Bott 1989, Comer-Warner et al. 2018, Webb et al. 2008). Hence, effects crucial biogeochemical reactions occurring in the hyporheic zones such as aerobic and anaerobic respiration, and nitrification and denitrification.

Spatio-temporal variance in flow regime can be a result of precipitation inputs, evapotranspiration, snow melt as well as anthropogenic activities such as from hydropower or waste-water treatment plants. The latter induces sharp discharges which can lead to effects such as hydro-peaking. When the ecology of the river system is also considered, it is clear that hydro-peaking can have negative effects on habitat of fish and benthic invertebrates (Bruno et al. 2009). This can be related to the impact of sharp discharges causing scouring of the streambed as well as clogging interstitial spaces of the sediment bed by the deposition of fine sediments and organic material (Ryan & Boufadel 2006, Brunke & Gonser 1997, Blaschke et al. 2003). Hydrologically, high-flow events have the potential to enhance surface water penetration into the streambed, which is usually rich in dissolved oxygen, dissolved organic matter, and nutrients. This can potentially increase the rate and types of biogeochemical

reactions (Casas-Mulet et al. 2015, Harvey et al. 2013). In addition, contaminants flushed to the surface water may be transported into the streambed (Fritz & Arntzen 2007) affecting the hyporheic environments and groundwater chemistry.

On the other hand, surface-water temperature fluctuations can occur due to anthropogenic perturbations such as thermal pollution, variations in flow dynamics or climate change (Caissie 2006). This dynamic temperature propagates in the streambed and results in complex flow and thermal distribution. This distribution of temperature in the streambed can have a critical impact on biogeochemical cycling rates (Boulton et al. 2010). This is because biogeochemical reactions are highly-dependent on thermal conditions in the streambed. Primarily, reactions which are facilitated by temperature-sensitive microbial activity are strongly affected by such perturbations (Krause, Hannah, Fleckenstein, Heppell, Kaeser, Pickup, Pinay, Robertson & Wood 2011, Comer-Warner et al. 2018, Fenchel et al. 2012). Hence, any abrupt rise in stream water temperature can deteriorate water quality and stream ecological functioning (Malcolm et al. 2004).

Hyporheic exchange flows do not necessarily occur at steady state discharge or thermal conditions as assumed by several studies in the past (Buffington & Tonina 2009, Tonina & Buffington 2009, Cardenas et al. 2004, Zheng et al. 2016). Discharge and temperature can considerably vary with space and time. This results in complex and dynamic patterns of flow velocities, exchange fluxes, residence times and temperature in the HZs. To date, a handful of research studies have considered the dynamic behaviour and characteristics of HZs (Malzone, Lowry & Ward 2016, Schmadel et al. 2016, Boano et al. 2007, Gomez-Velez et al. 2017, Trauth & Fleckenstein 2017, Zheng & Cardenas 2018) and helped to understand the importance of dynamics in HZs.

Process-based numerical models can be important tools that can help to achieve a mechanistic understanding of the dynamic behaviour of the HZs. Moreover, they can possibly provide explanations for the implications of dynamic flow conditions and diel temperature variations on biogeochemical cycling and hyporheic invertebrates. These numerical models can act as a tool to predict the regional-scale water quality outcomes by the accurate quantification of hyporheic exchange flows beginning from the small scale, and then translating to the regional scale.

The hyporheic exchange flows is driven by spatio-temporal variations in the pressure distribution along the sediment-water interface. The factors that control and drive the hyporheic exchange flow include bedform topography (bedform wavelength, bedform height), sediment hydraulic properties and heterogeneity, hydraulic conductivity, turbulent flows in the water column, channel slope, temperature fluctuations and groundwater influx and outflux (Krause, Hannah, Fleckenstein, Heppell, Kaeser, Pickup, Pinay, Robertson & Wood 2011, Boano et al. 2014, 2013, Wondzell & Swanson 1999, Tonina & Buffington 2009, Cardenas et al. 2004, Gomez-Velez et al. 2014). Depending on the focus of the study, model uses certain simplifications to enable us to study interactions between different drivers and controls of hyporheic exchange. The assumptions involved of stationery bedforms and homogeneous sediment bed in transient studies challenges the validity of the reduced-complexity models because high surface-water flow rates involves sediment transport that causes the migration of the bedform (Buffington & Tonina 2009) and alters the sediment hydraulic properties. Moreover, under high discharge conditions, turbulent flow patterns (e.g. hydraulic jumps) can be observed over local streambed variations which requires computationally expensive simulations of Navier-stokes equations. Thus, its should be noted that the reduced-complexity approach presented in this thesis overlooks

the local streamed pressure variations caused by such turbulent flows. In particular, the varied parameters in the presented thesis are chosen to capture the impact and importance of transient boundary conditions. Emphasis is given to the parameters such as channel slope that controls the groundwater underflow, hydraulic conductivity that controls the exchange flux, bedform height which depicts the spatial variations in the river systems and temperature that can change the flow velocities during various times of the day. Moreover, parameters involving peak-flow characteristics are also explored.

With an increased use of process-based reduced-complexity models, it is also important to quantify how accurate they are in prediction of hyporheic exchange processes. As hyporheic flows is a result of multiple scale interactions, it is important to evaluate the importance of different scales on biogeochmeical gradients developed in the HZs. Even though reduced-complexity models have vastly increased our mechanistic understanding of hyporheic exchange fluxes, retention time of water and solutes, and biogeochemical cycling in the river-aquifer systems under steady flow conditions and more recently under temporally-variable flow condition, the simulation results are seldom validated by field observations.

1.2 Research questions

To address the aforementioned knowledge gaps, this thesis aims to answer the following scientific questions

1. Effects of peak-flow events

- How does a transient single peak-flow event affect flow and transport in the HZs?
- How does repeated and superimposed peak-flow events affect flow and residence times in the HZs?
- How accurately can reduced-order models predict hyporheic exchange processes under transient conditions?

2. Effects of diurnal oscillations of surface water temperature

   - How does dynamic temperature oscillations propagate in the HZs and impact hyporheic characteristics?

1.3 Thesis structure

Structure of the thesis is to address above-mentioned research questions in each chapter. Chapter comprises of its own *abstract*, *introduction*, *methods*, *results*, *discussion* and *conclusions* designed for journal publication. All references are collated towards the end, in the Bibliography. Description of each chapter is as follows:

Chapter 2: Exploring the role of peak-flow events on bedform-induced hyporheic exchange: The research herein examines the effects of single peak-flow events on the characteristics of bedform-induced hyporheic exchange. We used a reduced-order model that couples flow and transport processes in an idealized, uniform and single type of bedform. We provide a systematic approach, explore a comprehensive parameter space and perform sensitivity analyses in order to identify the range of possible impacts by considering alterations of stream bedform geometries, channel gradient, peak-flow characteristics and biogeochemically relevant residence

time-scales in different bedforms like ripples, dunes and alternating bars. In addition to hyporheic exchange fluxes, we analyse hyporheic residence time distributions to quantify potential biogeochemical implications of time-varying streamflow. We therefore introduce a novel metric, the HZ efficiency for different time scales for oxygen consumption (using a definition of the Damköhler number. This chapter is published in Water Resources Research.

Chapter 3: Effects of the superimposed and repeated flow events on flow and residence times of dynamic hyporheic zones: This chapter is an extension to the previous chapter that includes the effect of single discharge events. However, river-aquifer systems, especially the urban rivers are fed with treated waste water from treatments plants twice in a day. Moreover, increases in the magnitude of discharge due to one precipitation event can be followed by one or more peak-flow events. This chapter explores the impacts of repeated and superimposed peak-flow events with different characteristics using flow and transport numerical models. We evaluate the effects by changing three different parameters, namely; (i) lag between two peak-flow events (t_{lag}); (ii) skewness of the events (t_p/t_d, Sk_1 and Sk_2); and (iii) duration of both the events (t_{d_1} and t_{d_2}). In addition to this, we also numerically model breakthrough curves to further decipher the potential contributions from the two events.

Chapter 4: Propagation of diurnal surface water temperature oscillations in ripples and impacts on hyporheic exchange fluxes: This chapter focuses on the propagation of diurnal surface water temperature oscillations within and below bedforms (ripples) through sequentially coupled reduced-order models of Darcy flow and heat-transport in the sediments using a temperature-dependent relationship of viscosity and density of water. The thermal forcing on the sediments caused

by diurnal fluctuations in water-column temperature is imposed at the sediment-water interface. For the systematic analyses we vary the peak amplitude of water column temperature (T_{amp}) to decipher its impacts on overall hyporheic and heat exchange within the system. Moreover, we quantify the relative contributions of convective and conductive heat transfer in the sediment bed using *Peclet number*. Furthermore, in order to to analyse the impact of diurnal temperature fluctuation on the spatial distribution of reaction rates in streambed sediments we evaluate dimensionless temperature-dependent reaction rate constants using the Arrhenius equation.

Chapter 5: Reduced-order models for simulating bedform-induced hyporheic exchange under transient flow conditions: This chapter focuses on testing the applicability of reduced-order models to represent hyporheic exchange processes. A step-pool and a low-gradient run are simulated using simplifications such as absence of sediment heterogeneity, constant hydraulic conductivity and neutral groundwater conditions. Model simulations are compared with field-observations of hydraulic heads and tracer breakthrough curves at different depths and under different flow conditions namely base, low and high-flow conditions in a first-order boreal stream in Northern Sweden.

Chapter 6: Conclusions and Future Work: This chapter concludes the research presented herein and discusses the potential scope for further advancements as well as the limitations to the current methods and findings.

Chapter 2
EXPLORING THE ROLE OF SINGLE PEAK-FLOW EVENTS ON BEDFORM INDUCED HYPORHEIC EXCHANGE*

Discharge varies in space and time, driving hyporheic exchange processes in river corridors that affect biogeochemical cycling and ultimately control the dynamics of biogeochemical hot-spots and hot-moments. Herein, we use a reduced-order model to conduct the systematic analysis of the interplay between discharge variability (peak-flow intensities, duration and skewness) and streambed topography (bedform aspect ratios, channel slopes) and their role in the flow and transport characteristics of hyporheic zones (HZ). We use a simple and robust conceptualization of single peak-flow events for a series of periodic sinusoidal bedforms. Using the model, we estimate the spatial extent of the HZ, the total amount of exchange, and the residence time of water and solutes within the reactive environment and its duration relative to typical timescales for oxygen consumption (i.e. a measure of the denitrification potential). Our results demonstrate that HZ expansion and contraction is controlled by events yet modulated by ambient groundwater flow. Even though the change in hyporheic exchange flux (%), relative to baseflow conditions is invariant for different values of channel slopes, absolute magnitudes varied substantially. Primarily, peak-flow events cause more discharge of older water for the higher aspect ratios (i.e for dunes and ripples) and lower channel slopes. Variations in residence times during peak-flow events lead to the development of larger areas of potential nitrification and denitrification in the HZ for longer durations. These findings have potential implications for river management and restoration, particularly the need for (re)consideration of the importance of hyporheic exchange under dynamic flow conditions.

*The bulk of material presented in this chapter is published in Water Resources Research. T.S. undertook analysis and processed the data. T.S. , L.W., J.G.V. and S.K. interpreted the data. T.S. wrote the manuscript with contributions from all other authors. All authors contributed to the final edits of the manuscript

2.1 Introduction

2.1.1 Functional significance of groundwater-surface water interactions in the hyporheic zone

Hyporheic exchange flows occurring at the sediment-water interface (SWI) are characterized by continuous, bidirectional exchange of water, solutes and energy between the river's main channel and its surrounding sediments (Tonina & Buffington 2011, Gomez-Velez et al. 2014). This exchange process has been found to control biogeochemical cycling (Krause et al. 2013, Boano et al. 2014, Pinay et al. 2015, Cardenas 2015), regulate stream temperature (Packman et al. 2004, Hannah et al. 2009, Krause, Hannah & Blume 2011) and impact ecological functioning (Brunke & Gonser 1997, Boulton et al. 1998, Harvey & Gooseff 2015) along river corridors. Mechanistic understanding of dynamic hyporheic processes requires detailed knowledge of the interplay between drivers and controls for exchange such as dynamics in discharge, streambed morphology, sediment hydraulic conductivity and porosity, ambient groundwater flow, channel sinuosity, planform morphology and channel geometry and slope (Boano et al. 2006, O'Connor & Harvey 2008, Stonedahl et al. 2010, Krause, Hannah, Fleckenstein, Heppell, Kaeser, Pickup, Pinay, Robertson & Wood 2011, Gomez-Velez et al. 2014). These complex interactions and exchange mechanisms play a key role in influencing the magnitude of hyporheic exchange flux (HEF), residence time of water and solutes in the streambed, and the location of stagnation zones. As a consequence, the area and depth in the streambed (see Figure 2.1) exposed to variations in physical, chemical and biological processes is also affected (Krause, Hannah, Fleckenstein, Heppell, Kaeser, Pickup, Pinay, Robertson &

Wood 2011, Zarnetske et al. 2011, Gomez-Velez et al. 2012, Gomez-Velez & Wilson 2013, Kaufman et al. 2017, Gomez-Velez et al. 2017).

2.1.2 Drivers and controls of hyporheic exchange

Hyporheic exchange occurs over a wide range of spatial and temporal scales (Krause, Hannah, Fleckenstein, Heppell, Kaeser, Pickup, Pinay, Robertson & Wood 2011, Boano et al. 2014, Cardenas 2015), ranging from millimeter-scale eddies that transfer momentum and solutes into the streambed over a few seconds to kilometer-scale flow paths along meander bends that exchange mass and solutes over time scales of decades and longer. The exchange process is driven by the spatial and temporal variations in the pressure distribution along the sediment-water interface (SWI), which is a function of discharge, channel geometry and slope and streambed topography (Wondzell & Swanson 1999, Buffington & Tonina 2009, Tonina & Buffington 2009, Boano et al. 2014). At the same time, the exchange process is controlled by the sediment hydraulic properties and their heterogeneity (Ryan & Boufadel 2006, Gomez-Velez & Harvey 2014*a*) and the ambient groundwater flow (Cardenas et al. 2004, Buffington & Tonina 2009).

2.1.3 Influence of transient stream flow on hyporheic exchange

While the aforementioned drivers and controls for hyporheic exchange have been intensively studied over the last three decades, particularly for steady-state flow conditions (Cardenas et al. 2004, Buffington & Tonina 2009, Tonina & Buffington

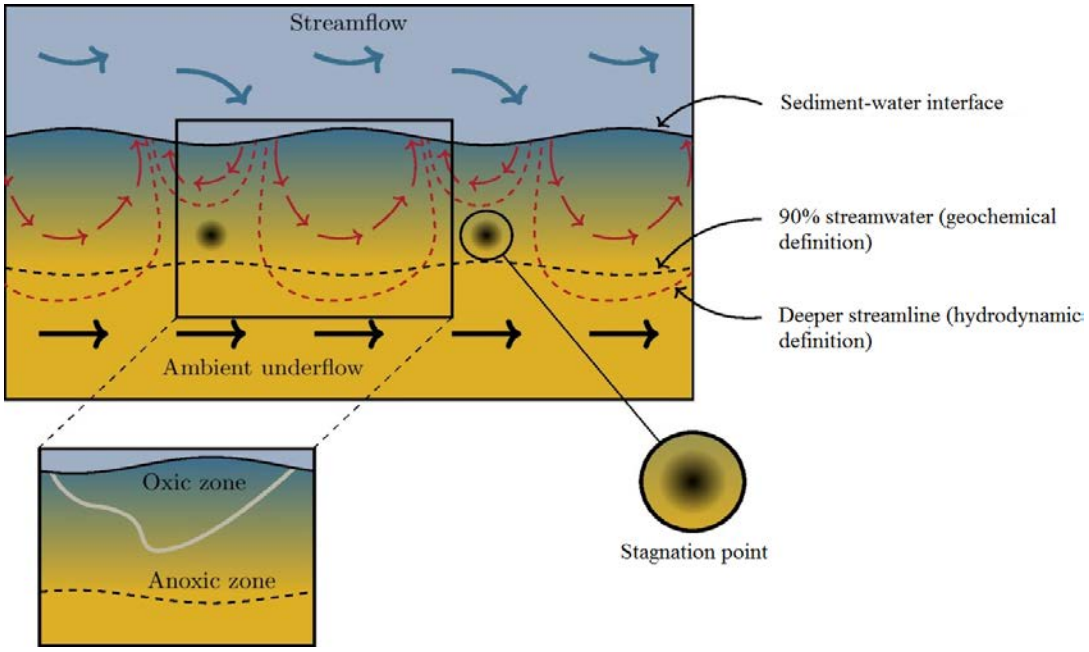

FIGURE 2.1: Conceptual sketch for the exchange processes. This image depicts the hydrodynamic (red dashed line depicting deeper streamline) and biogeochemical (black dashed line depicting biogeochemically active region with 90% of streamwater) definitions of the HZ, the location of stagnation points, and the transition boundary (grey line) from oxic to anoxic zones during peak flows. These characteristics vary in space and time due to discharge dynamics.

2009), we are only starting to understand the importance of transience in stream-flow (Boano et al. 2007, Tonina & Buffington 2011, Trauth & Fleckenstein 2017, Schmadel et al. 2016, Malzone, Lowry & Ward 2016, Gomez-Velez et al. 2017). Time-variance in stream flow can result from natural variation of precipitation inputs, evapotranspiration or snow melt as well as from anthropogenic activity in wastewater treatment plants or dam operations, which can lead to effects such as hydro-peaking and thermal-peaking. During peak flow events, the potential for enhanced surface water downwelling which is usually richer in oxygen, dissolved organic matter, and nutrients can impact the type and rates of streambed biogeochemical processes including aerobic and anaerobic carbon respiration, nitrification and denitrification (Gu et al. 2008, Harvey et al. 2013, Trauth & Fleckenstein 2017). Moreover, surface water-borne contaminants along with the water and other solutes may be transported into the streambed (Fritz & Arntzen 2007), potentially reaching greater depths and larger streambed areas (Figure 2.1) (Bruno et al. 2009, 2013, Jones 2014, Casas-Mulet et al. 2015). Consequently, fluctuations in stream stage and flow can effect benthic invertebrates, nutrient cycling and thermal conditions in hyporheic and benthic environments (Sawyer et al. 2009, Bruno et al. 2013, Jones 2014, Casas-Mulet et al. 2015).

Recent studies have shown the importance of understanding the dynamic nature of river corridors (Boano et al. 2013, Ward et al. 2013, Dudley-Southern & Binley 2015, Malzone, Anseeuw, Lowry & Allen-King 2016, Malzone, Lowry & Ward 2016, Schmadel et al. 2016, McCallum & Shanafield 2016, Trauth & Fleckenstein 2017, Gomez-Velez et al. 2017, Ward et al. 2018) and identified dominant drivers and controls of hypoheic exchange flows during transient stream flow conditions. For example, Malzone, Lowry & Ward (2016) showed that the annual and storm-induced

groundwater fluctuations is the key control on the volume of HZ and Schmadel et al. (2016) highlighted the importance of controls such as hillslope lag, amplitude of the hillslope and cross-valley and down-valley slopes on hyporheic flow path and residence times. McCallum & Shanafield (2016) found alterations in the residence time distributions of bank inflows and outflows for different discharge events. Trauth & Fleckenstein (2017) highlighted the importance of peak discharge and duration of the events on the mean age of the water and solutes which lead to higher rates of aerobic and anaerobic respiration. In the most recent work by Gomez-Velez et al. (2017), the authors explored the combined role of flow characteristics with varying channel planimetry, channel gradient and morphology on the spatial and temporal evolution of river bank storage and sinuosity-driven hyporheic exchange using a dimensionless framework. However, none of the previous dynamic studies integrated the hydrological and geomorphorhic controls of hypoheic exchange flows with biogeochemical potential systematically.

2.1.4 Aims and objectives

In this chapter, we provide a systematic approach to decipher the potential impacts of transient forcing on hypoheic exchange flows, using reduced-order models of idealized, uniform and single type of bedform-induced hyporheic exchange. Here, we use the term "reduced-order" to emphasize that the model formulation only attempts to capture first-order drivers and controls of the exchange process, ignoring some of the complexities such as heterogeneity and coupling of turbulent flow in the water column with groundwater flow in the sediment. These assumptions allow us to gain comprehensive understanding from many simulations. Using reduced-order models, we explore a comprehensive parameter space and perform sensitivity analyses in

order to identify the range of possible impacts by considering alterations of stream bedform geometries, channel gradient, peak-flow characteristics and biogeochemically relevant residence time-scales in different bedforms like ripples, dunes and alternating bars. In addition to HEF, we analyze hyporheic residence time distributions to quantify potential biogeochemical implications of time-varying streamflow. We therefore introduce a novel metric, the HZ efficiency for different time scales for oxygen consumption (using a definition of the Damköhler number similar to Ocampo et al. (2006), Zarnetske et al. (2012), Gomez-Velez et al. (2015), Pinay et al. (2015)).

2.2 Methods

2.2.1 Conceptual model

We use a simple conceptualization to explore the role of flow dynamics on the characteristics of bedform-induced hyporheic exchange. For simplicity, we assume that the bedforms are stationary and their shape and hydraulic properties are unaffected by changes in river discharge. Our modeling domain (Ω in Figure 2.2) represents stream sediments with a sinusoidal sediment-water interface (SWI; $\partial\Omega_{SWI}$) as the idealized small-scale topography is often represented by sinusoidal structure in the downstream direction (Stonedahl et al. 2010). The functional form of the SWI is given by $Z_{SWI} = (\Delta/2)\sin(2\pi x/\lambda)$, where Δ [L] and λ [L] are the characteristic amplitude and wavelength of the bedforms (e.g., ripple, dune, and riffle-pool sequences), respectively. The total streamwise length and depth of the modeling domain are $L = 3\,\lambda$ and d_b [L], respectively, and were selected to avoid boundary effects in the numerical simulations (see Table 4.1 for the values used in the model).

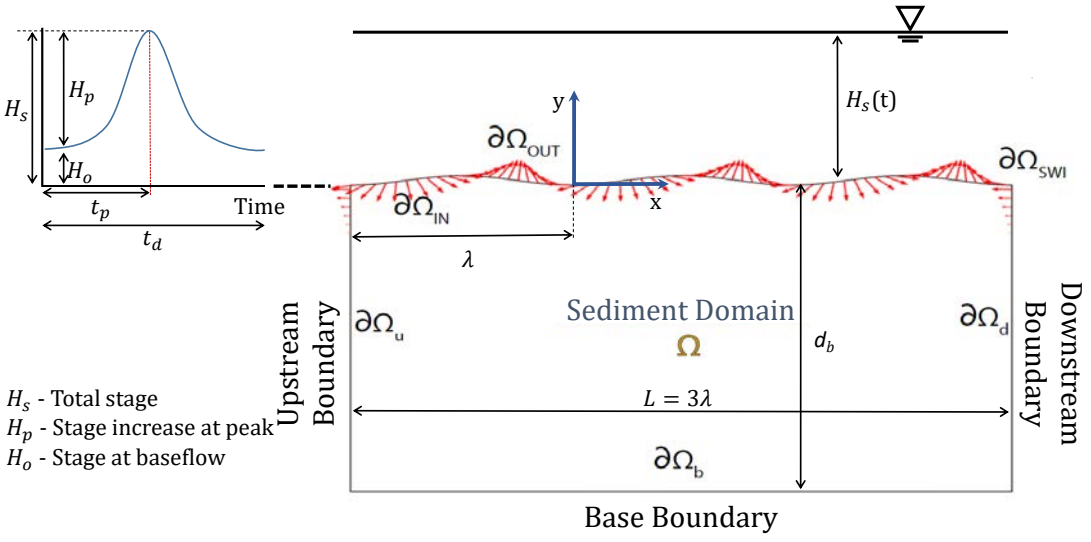

FIGURE 2.2: Depiction of the reduced-order model. Hyporheic exchange is induced by the interaction of stage variations with the bedform topography. The sediment domain (Ω) is assumed homogeneous and isotropic. A prescribed head distribution is imposed along the SWI ($\partial\Omega_{SWI}$) which can be further discretized into inflow ($\partial\Omega_{IN}$) and outflow boundaries ($\partial\Omega_{OUT}$) (red arrows). Periodic boundary conditions are assumed for the lateral boundaries ($\partial\Omega_u$ and $\partial\Omega_d$), horizontal ambient flow is assumed proportional to the channel slope, and the base of the model domain ($\partial\Omega_b$) is assumed impervious.

Within this domain, we implemented a detailed flow and transport model using COMSOL Multiphysics. The finite element mesh consists of triangular elements with a maximum size of 0.05λ and with telescopic refinement of 0.0125λ along the sediment-water interface ($\partial\Omega_{SWI}$) and lateral boundaries ($\partial\Omega_u$ and $\partial\Omega_d$), resulting in a total of about 56,500 elements. This level of refinement is needed for mesh-independent simulations and to capture the effect of local, fast-flowing hyporheic circulation cells and calculate accurate boundary fluxes.

2.2.2 Flow model

Neglecting the storage term, a reasonable assumption for submerged channel sediments, flow within the domain is described by the following version of the groundwater flow equation and Darcy's law

$$\nabla \cdot \left[\rho \frac{\kappa}{\mu} \big(\nabla p + \rho g \nabla z \big) \right] = 0 \tag{2.1}$$

where $\mathbf{x} = (x, y)$ is the spatial location vector [L], $p(\mathbf{x}, t)$ is pressure [$\mathrm{ML^{-1}T^{-2}}$], g is the acceleration due to gravity [$\mathrm{LT^{-2}}$], κ is the permeability [$\mathrm{L^2}$], ρ is fluid density [$\mathrm{ML^{-3}}$], μ_d is fluid dynamic viscosity [$\mathrm{ML^{-1}T^{-1}}$], $h = \dfrac{p}{\rho g} + z$ is hydraulic head [L], and Darcy velocity is $\mathbf{q} = -\dfrac{\kappa}{\mu}(\nabla p + \rho g \nabla z)$ [$\mathrm{LT^{-1}}$].

Flow is driven by pressure gradients at the sediment-water interface ($\partial\Omega_{SWI}$). For simplicity, we use a prescribed head distribution that assumes a linear combination of head fluctuations induced by large- and small-scale bed topography (Wörman et al. 2006, Stonedahl et al. 2010):

$$h_{\mathrm{SWI}}(x, t) = -Sx + H_s(t) + \frac{2h_d(t)}{\Delta} Z_{\mathrm{SWI}}\left(x + \frac{\lambda}{4} \right) \tag{2.2}$$

TABLE 2.1: Parameterisation of the numerical model for the analysis.

Parameters	Value	Description
Constant model parameters		
λ	1 m	Bedform wavelength
d_b	5 m	Depth of the domain
B	5 m	Channel width
M	0.05	Manning's coefficient
α_L	0.05 m	Longitudinal dispersivity
α_T	0.005 m	Transverse dispersivity
κ	10^{-10} m^2	Permeability
ρ	1000 kg m^{-3}	Fluid density
μ	1.002×10^{-3} Pa s	Fluid dynamic viscosity
g	9.81 ms^{-2}	Acceleration due to gravity
d_{bkf}	$10^2\times\Delta$ m	Bankfull depth
H_0	$0.1\times d_{\mathrm{bkf}}$	Reference stage
Varied model parameters		
Δ/λ	0.1, 0.01, 0.001	Bedform aspect ratio
S	0.1, 0.01, 0.001, 0.0001	Channel slope
H_p	$50\%\times d_{\mathrm{bkf}}$, $100\%\times d_{\mathrm{bkf}}$	Peak stage
t_d	1 and 10 days	Duration of the peak-flow event
t_p/t_d	0.25, 0.5	Flow skewness
τ_{o_2}	0.5, 1 and 10 hours	Timescale for oxygen consumption

where S is channel slope, $H_s(t)$ [L] is the time-varying river stage, $Z_{SWI}(x)$ is the function describing the bed topography, and $h_d(t)$ is the intensity of the dynamic head fluctuations (Elliott & Brooks 1997)

$$h_d(t) = 0.28\frac{U_s(t)^2}{2g}\begin{cases}\left(\dfrac{\Delta}{0.34\,H_s(t)}\right)^{3/8} & \text{for}\dfrac{\Delta}{H_s(t)} \leqslant 0.34;\\ \left(\dfrac{\Delta}{0.34\,H_s(t)}\right)^{3/2} & \text{for}\dfrac{\Delta}{H_s(t)} > 0.34,\end{cases} \tag{2.3}$$

where the mean velocity is estimated with the Chezy equation for a rectangular channel as $U_s(t) = M^{-1}H_s(t)^{2/3}S^{1/2}$ with M is the Manning coefficient [$\mathrm{L}^{-1/3}\mathrm{T}$] (Dingman 2009). Notice that the pressure distribution at the sediment-water interface is the function of both space x and time t, where the temporal fluctuations are induced by the peak-flow event (see Section 2.2.1).

Assuming that bedforms repeat periodically along the channel, we implemented a periodic boundary condition for the lateral boundaries ($\partial\Omega_u$ and $\partial\Omega_d$; $p(x = -L, y, t) = p(x = 2L, y, t) + \rho g[h_{SWI}(x = -L, t) - h_{SWI}(x = 2L, t)]$). Under neutral groundwater conditions (*i.e.* without gaining and losing groundwater conditions), the only groundwater flow constraining the hyporheic zone is the ambient groundwater flow driven by the channel gradient (*i.e.* horizontal under-flow component), and therefore no-flow is assumed for lower boundary ($\partial\Omega_b$). The depth of this boundary (d_b) was selected to minimize boundary effects. Finally, the solution under steady state (*i.e.* , baseflow conditions) is used as the initial condition for the transient simulations (*i.e.* , during the peak-flow event). This method of calculating pressure distribution at the SWI reproduces reasonable observations. It also allows the exploration of large number of scenarios with fewer complexities when implemented in the model , and with reduced computational demands.

The sediment-water interface ($\partial\Omega_{SWI}$) can be discretized into inflow ($\partial\Omega_{IN} = \{\mathbf{x} \mid (\mathbf{n}\cdot\mathbf{q} < 0) \wedge (\mathbf{x} \in \partial\Omega_{SWI})\}$ and outflow sub-boundaries ($\partial\Omega_{OUT} = \{\mathbf{x} \mid (\mathbf{n}\cdot\mathbf{q} > 0) \wedge (\mathbf{x} \in \partial\Omega_{SWI})\}$ such that $\partial\Omega_{SWI} = \partial\Omega_{IN} \cup \partial\Omega_{OUT}$ (see Figure 2.2) with $\mathbf{n}$ an outward vector normal to the boundary. Notice that these boundaries are dynamic in nature, contracting and expanding with variations in the forcing.

2.2.2.1 Hydrograph generation

A single peak-flow pulse is used to mimic the dynamic nature of river discharge (Figure 2.2). This transient hydrologic forcing changes the hyporheic zone's flow field, spatial extent (area, depth) and residence times (Wondzell & Swanson 1999, McCallum & Shanafield 2016, Gomez-Velez et al. 2017), having potentially important implications for biogeochemical transformations. The deterministic stage hydrograph was modeled with an asymmetric curve previously proposed by Cooper & Rorabaugh (1963):

$$H_s(t) = \begin{cases} H_0 + H_p\, e^{-\delta(t-t_p)}\, \dfrac{[1-\cos(wt)]}{[1-\cos(wt_p)]} & \text{if} t \in [0, t_d] \\ H_0 & \text{otherwise} \end{cases} \tag{2.4}$$

where H_0 is the stage at baseflow conditions [L], H_p is the maximum rise of stream stage [L], t_p is the time-to-peak of the event [T], t_d is the duration of the peak-flow event [T], $w = 2\pi/t_d$ is the frequency of the event [T^{-1}], and $\delta = w\cot(wt_p/2)$ is a constant that determines the degree of asymmetry [T^{-1}].

2.2.3 Solute transport model and delineation of the hyporheic zone

The advection-dispersion equation (ADE) is used to model the transport of conservative solutes within the sediments

$$\theta \frac{\partial C}{\partial t} = \nabla \cdot (\mathbf{D} \nabla C) - \nabla \cdot (\mathbf{q} C) \tag{2.5}$$

where C is concentration [ML^{-3}], $\mathbf{q}$ is the Darcy flux [LT^{-1}], and $\mathbf{D} = \{D_{ij}\}$ is the dispersion-diffusion tensor defined as Bear (1972):

$$D_{ij} = \alpha_T |\mathbf{q}| \delta_{ij} + (\alpha_L - \alpha_T) \frac{q_i \, q_j}{|\mathbf{q}|} + \frac{\theta}{\xi_m} D_m \tag{2.6}$$

with α_T and α_L the transverse and longitudinal dispersivities [L], D_m the effective molecular self-diffusion coefficient, $\xi_m = \theta^{-1/3}$ is the fluid tortuosity (defined here with the Millington and Quirk model (Millington & Quirk 1961)), and δ_{ij} is the Kronecker delta function.

Modeling the transport of a conservative tracer allows us to explore the mixing and extend of the HZ. We assume that the concentration of the tracer in the stream water column is C_s, and therefore a prescribed boundary condition $C(\mathbf{x}, t) = C_s$ is used along the SWI's inflow areas ($\partial\Omega_{IN}$). Outflow areas ($\partial\Omega_{OUT}$) along the SWI are advective boundaries where $\mathbf{n} \cdot (\mathbf{D} \nabla C) = 0$. Lateral boundaries ($\partial\Omega_u$ and $\partial\Omega_d$) are periodic boundaries $C(x = -L, y) = C(x = 2L, y)$ and the bottom boundary ($\partial\Omega_b$) is a no-flow boundary $\mathbf{n} \cdot (\mathbf{q} C - \mathbf{D} \nabla C) = 0$. An initial condition for the concentration field is obtained from a steady-state simulation of the transport model

(Eq. (5.4)) under baseflow conditions (*i.e.* $H_s = H_0$). In this case, the hyporheic zone is defined as the zone with at least 90% of the pore water originated from the stream (*i.e.* $C \geq 0.9C_s$). This definition is similar to the one proposed by Triska et al. (1989) and Gomez-Velez et al. (2014, 2017). Through the manuscript, we refer to this definition as the *biogeochemical definition of the hyporheic zone*.

2.2.4 Residence time model

The hyporheic zone residence time describes the time that water and solutes are exposed to the stream sediment biogeochemical conditions. Here, we evaluate the impacts of transient flow, driven by a peak-flow event, on the moments of the HZ's residence time distribution. To this end, we use the approach outlined in Gomez-Velez et al. (2012) Gomez-Velez & Wilson (2013), and Gomez-Velez et al. (2017) where the moments of the residence time distribution are described by an ADE of the form

$$\frac{\partial(\theta a_n)}{\partial t} = \nabla \cdot (\theta \mathbf{D} \nabla a_n) - \nabla \cdot (\mathbf{v} \theta a_n) + n\theta a_{n-1} \tag{2.7a}$$

$$a_n(\mathbf{x}, t) = 0 \quad \text{on } \partial\Omega_{IN} \tag{2.7b}$$

$$\mathbf{n} \cdot (\theta \mathbf{D} \nabla a_n) = 0 \quad \text{on } \partial\Omega_{OUT} \tag{2.7c}$$

$$a_n(x = -L, y) = a_n(x = 2L, y) \text{ for } \partial\Omega_u \text{ and } \partial\Omega_d \tag{2.7d}$$

$$\mathbf{n} \cdot (\mathbf{q} a_n - \mathbf{D} \nabla a_n) = 0 \quad \text{on } \partial\Omega_b \tag{2.7e}$$

$$a_n(\mathbf{x}, t = t_0) = a_{n0} = \int_0^\infty \xi^n \Psi_0(\mathbf{x}, \xi) \, \mathrm{d}\xi \tag{2.7f}$$

where $a_n(\mathbf{x}, t)$ [T] ($n = 1, 2, ...$ and $a_0(\mathbf{x}, t) = 1$) is the n-th moment of the residence time distribution $\Psi(\mathbf{x}, t, \tau)$ [T^{-1}], which is defined as

$$a_n(\mathbf{x}, t) = \int_0^\infty \xi^n \Psi(\mathbf{x}, t, \xi)\ \mathrm{d}\xi, \text{ for } n = 1, 2, \ldots. \tag{2.8}$$

Initial and boundary conditions are defined following the approach in Gomez-Velez & Wilson (2013) and Gomez-Velez et al. (2017). Similar to the conservative transport model, the initial distribution of the first (mean residence time) and second (variance of residence time) moments were estimated under steady baseflow conditions.

2.2.5 Peak-flow event scenarios

Typical geomorphic length scales for ripples, dunes, and alternating bars in a broad range river sizes and hydraulic conditions were estimated with the methodology proposed by Gomez-Velez & Harvey (2014*b*) and Gomez-Velez et al. (2015).This approach uses the best available empirical equations for length scales and a Monte Carlo approach to generate plausible scenarios that represent variations along a real Mississippi river network (Gomez-Velez & Harvey 2014*b*). Our simulations explore three different values of bedform aspect ratio: ripples ($AR = 0.1$), dunes($AR = 0.01$) and alternating bars ($AR = 0.001$) (Dingman 2009, Bridge 2009). For each of these bedforms we also explore (i) two flow skewness values (t_p/t_d): 0.25 and 0.5, where the latter value is typically observed in regulated systems, e.g., reservoirs and sewage discharge (Sawyer et al. 2009), (ii) two peak-flow intensities: 50% and 100% of typical bankfull depth (d_{bkf}), (iii) two values of event duration: 1 day and 10 days, and (iv) four values of channel slope: 0.1, 0.01, 0.001, 0.0001. This results in 96 scenarios;

however, we focus our discussion on a handful of peak-flow event scenarios, as shown in Table 2.2 and Figure 2.3). These scenarios allow us to systematically explore the effects of flow dynamics in the hyporheic exchange process.

2.2.6 Metrics

We use multiple metrics to quantify the impact of transient forcing in hyporheic exchange. In the following, we briefly define and describe each of them.

2.2.6.1 Hyporheic zone area and penetration

Dynamic changes in the pressure distribution along the SWI induce changes in the sediment flow field, and therefore in the extent (area and penetration depth) of the hyporheic zone, that is, the area of the sediment exposed to water originating from the stream. We estimate the boundary of the hyporheic zone using both a hydrodynamic and a biogeochemical criteria (Gooseff 2010).

First, the hydrodynamic definition assumes that the hyporheic zone boundary corresponds to the deepest streamline originating and terminating in the SWI. The flow field, and therefore this boundary and area of the HZ, is highly sensitive to dynamic changes in hydrologic forcing. The high sensitivity is explained by the negligible porous media storage of the stream sediments, which results in a fast propagation of pressure fluctuations at the sediment-water interface (*i.e.* , the response time is negligible). Second, the biogeochemical definition, similar to the one used by Gomez-Velez et al. (2014), assumes that the boundary of the hyporheic zones corresponds to the contour defining porewaters with 90% stream water. The

TABLE 2.2: Description of the peak-flow event scenarios used for the analysis (FD - Peak-flow event duration, Sk - Peak-flow skewness, FI - Peak-flow intensity, d_{bkf} - Bankfull depth).

No.	Scenario	Event Duration [d]	Skewness	Peak-flow Intensity (% of d_{bkf})
1	$FD_{low}Sk_{low}FI_{low}$	1	0.25	50%
2	$FD_{low}Sk_{low}FI_{high}$	1	0.25	100%
3	$FD_{low}Sk_{high}FI_{low}$	1	0.5	50%
4	$FD_{low}Sk_{high}FI_{high}$	1	0.5	100%
5	$FD_{high}Sk_{low}FI_{low}$	10	0.25	50%
6	$FD_{high}Sk_{low}FI_{high}$	10	0.25	100%
7	$FD_{high}Sk_{high}FI_{low}$	10	0.5	50%
8	$FD_{high}Sk_{high}FI_{high}$	10	0.5	100%

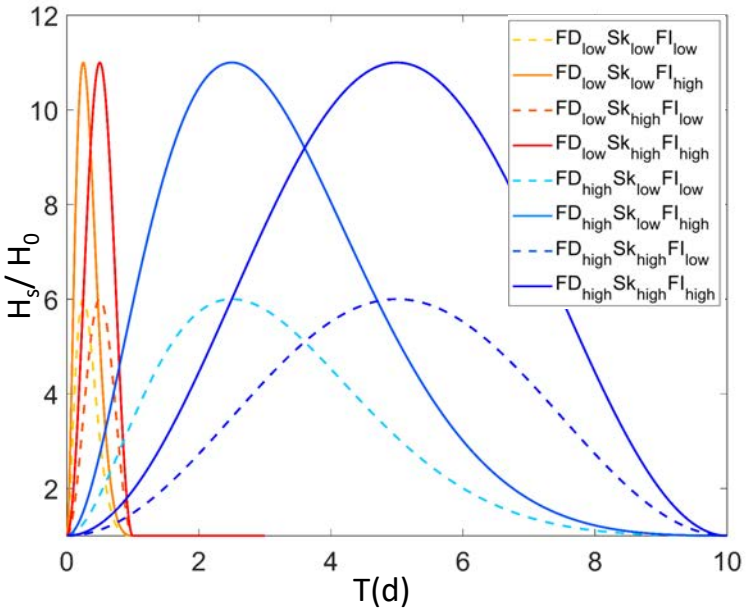

FIGURE 2.3: Depiction of the stage hydrographs produced by the Equation 2.4 and associated with the scenarios shown in the Table 2.2.

other metrics below use the biogeochemical definition of the HZ in order to define the boundaries of integration.

2.2.6.2 Hyporheic exchange flux

The hyporheic exchange flux (HEF) corresponds to the integral of the Darcy flux along the sections of the SWI discharging hyporheic water into the stream:

$$Q_{hz,out} = \frac{\int_{\partial\Omega_{out,hz}} nq \, \mathrm{d}x}{\int_{\partial\Omega_{SWI}} \mathrm{d}x} \tag{2.9}$$

where $\partial\Omega_{out,hz}$ is the outflow boundary discharging hyporheic water, defined by the biogeochemical definition.

2.2.6.3 Residence times

Similarly, a representative value of residence time for the exchange process is estimated by flux-weighting the modeled mean residence time, standard deviation of residence time (SD), and coefficient of variation of residence time (CV) along the sections of the SWI discharging hyporheic water into the stream. See section 5.2.3.4 for a detailed description of the residence time model). The mean residence time (μ) corresponds to the first central moment (a_1), the standard deviation of residence time is calculated as $\sigma = \sqrt{a_2 - \mu^2}$, with a_2 the second central moment, and finally CV is calculated as $\frac{\sigma}{\mu}$.

2.2.6.4 Hyporheic zone efficiency

Likely locations and size of the oxic-anoxic zones have been described by using the Damköhler number, DN = a_1/τ_{o_2}, where τ_{o_2} is the biogeochemical timescale for oxygen consumption and its typical value varies from 0.5 to 10h (Gomez-Velez et al. 2015). DN allows us to explore and compare the role of reaction and transport processes within the system (Ocampo et al. 2006, Pinay et al. 2015). in particular, DN for O_2 is an important indicator of the potential for net nitrification or denitrification in the hyporheic zone (Zarnetske et al. 2012).

To evaluate the biogeochemical potential of hyporheic zones and how it changes as a function of time, we assume that the stream water column is dominant source of oxygen entering the sediments. Similar to Gomez-Velez et al. (2015), we assume that DN = 4.6 corresponds to a 99% reduction in the oxygen concentration, and therefore the sediment area where DN$\geq$ 4.6 is essentially anoxic and a likely location where denitrication takes place. Similarly the locations with DN$<$ 4.6 are oxic zones where the presence of oxygen is likely to promote nitrification. In this work, we explore τ_{o_2} = 0.5, 1 and 10 hours. To emphasize on the quantification of anoxic waters discharged from the HZ, we also calculate Q_{anoxic}. This is defined as the amount of anoxic waters discharged from the hyporheic zones with respect to different timescales for oxygen comsumption. As an example, for the τ_{o_2} = 10 hours, Q_{anoxic} will be the anoxic waters discharged from the hyporheic zones with residence times of over 10 hours.

Finally, we define the HZ efficiency as the ratio of the HEF discharging anoxic water (Q_{anoxic}) and the total HEF ($Q_{hz,out}$)

$$HZ_{eff} = \frac{Q_{anoxic}}{Q_{hz,out}} \tag{2.10}$$

2.3 Results

2.3.1 Hyporheic flow patterns and geometry of the hyporheic zone

The flow field (magnitude and direction) changes dynamically as the peak-flow event moves along the SWI. Figure 2.4 illustrates the temporal evolution of these changes by comparing the fields before the event (*i.e.* , baseflow at $t \leq 0$) and during the event ($t \leq t_d$). The hyporheic zone initially expands during the rising limb of the event, and then contracts during the recession returning to the initial baseflow conditions (columns 2-5 in Figure 2.4). The shape of the peak-flow event determines the impact in the flow field, and at the same time the magnitude of the changes are controlled by the bedform aspect ratio.

Under baseflow conditions ($t \leq 0$), the hyporheic zone for alternating bars ($AR = 0.001$, Figure 2.4) is very small, almost completely absent. This is explained by the compressing effect of the ambient flow (proportional to the channel slope). However, the peak-flow event overcomes the moderating effect of the ambient flow and results in the emergence of a HZ that drastically penetrates into the sediments (Figure 2.4). On the other hand, morphologies with higher aspect ratios such as dunes

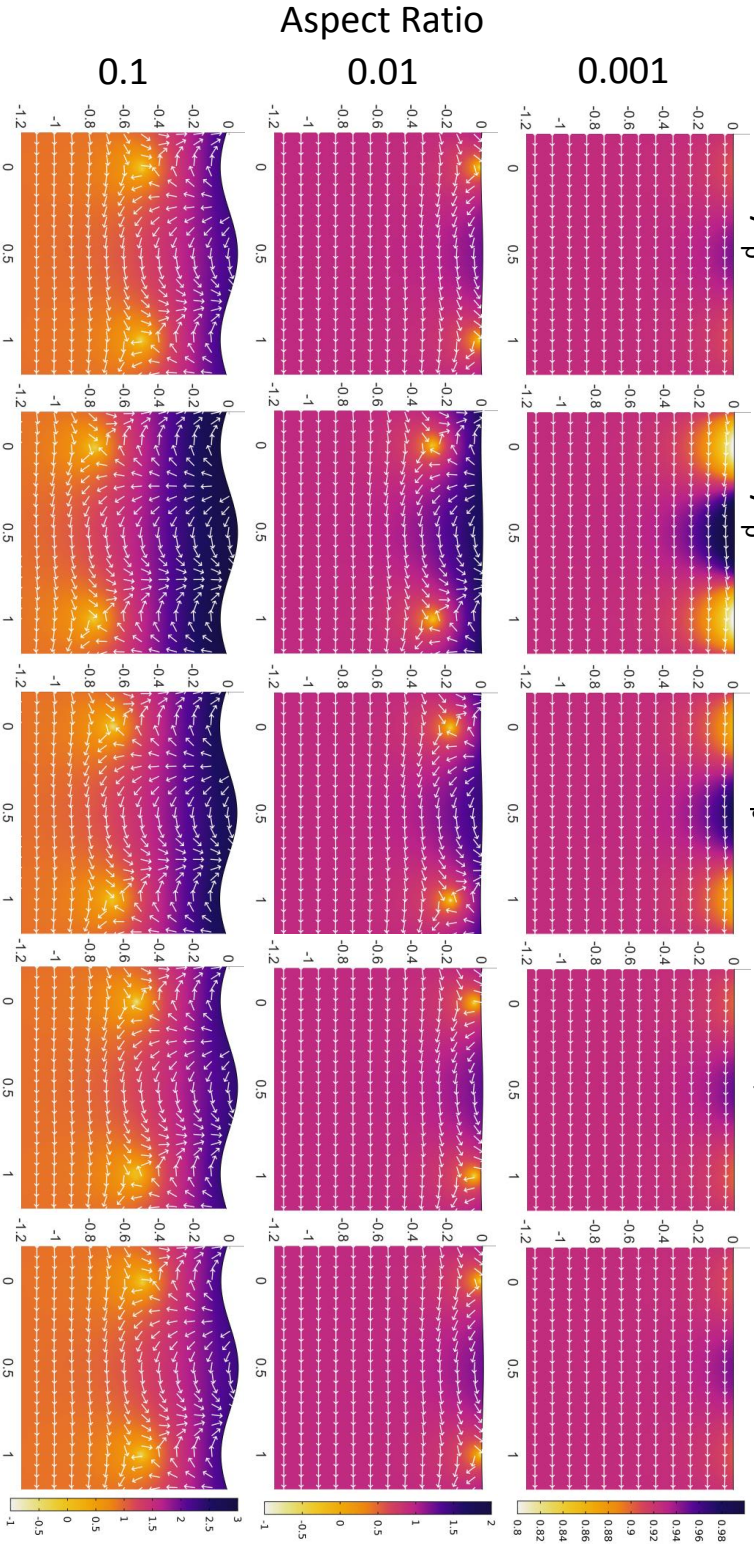

FIGURE 2.4: Snapshots of the flow field (white arrows represent direction and not proportional to magnitude) within the sediment at different times t/t_p. Coloured surface represents the magnitude of Darcy flux vector in log scale m/d (white is low and black is high). Rows correspond to different bedform aspect ratios: $AR = 0.001$ is typical for alternating bars, $AR = 0.01$ is typical for dunes and $AR = 0.1$ typical for ripples. The scenarios include peak-flow intensity of 50% of d_{bkf}. For all panels, the channel slope is 10^{-1} and the hydraulic conductivity is 9.8×10^{-4} m/s. Vertical and horizontal axis are scaled by the bedform wavelength.

($AR = 0.01$) and ripples ($AR = 0.1$) consistently have a larger and more persistent HZ during the course of the event as illustrated in Figure 2.4.

These results highlight the importance of ambient groundwater flow (proportional to channel slope) and its moderating role under both steady and transient flow conditions. Figure 2.4 illustrates the case where the pressure gradient induced by bedform topography are not enough to overcome the modulating effect of the ambient flow. The magnitude of such gradients progressively increases during the event and eventually the hydrodynamic forcing overcomes the ambient groundwater flow, resulting in the development of a HZ (Figs. 2.4b-e). Moreover, higher peak-flow intensities (FI_{high}) lead to an increase in vertical flow velocities, which produce a larger HZ and advect more mass into the streambed. This, at the same time, changes the location and size of stagnation zones, which oscillate in depth and size during the flow event, resulting in potential emergence of highly reactive environments purely driven by hydrodynamic changes. This is in line with the findings of Gomez-Velez & Wilson (2013). Note that the maximum extent of the HZ is always at peak flow; however, the evolution of the expansion and contraction strongly depends on the peak-flow skewness (t_p/t_d) and peak-flow magnitude.

2.3.1.1 Difference between hydrodynamic and biogeochemical extent of hyporheic zone under dynamic flow conditions

As discussed in section 4.2, hyporheic zone extent can be defined from a hydrodynamic and biogeochemical perspective. Each of these definitions represents different flow and transport processes and can have different sensitivities to transience. Our simulations show that these two definitions are not consistent under transient flow conditions. The relative change (to baseflow conditions) in hydrodynamic area [%]

is considerably higher than the biogeochemical area [%] in response to different flow conditions (Figure 2.5). Notice that for the left panel, the curves associated with FD_{low} scenarios are coinciding with FD_{high} scenarios due to the scaling of time to the time-to-peak of the event. For scenarios with high peak-flow intensity, the simulated hyporheic area based on the hydrodynamic definition increased by up to 200% whereas the HZ area based on the respective biogeochemical definition is limited to 45% (for the slope value 10^{-1}). Note that both definitions result in the same area for steady flow, but the dynamic nature of the flow affects them differently. In particular, the biogeochemical definition, which is closely linked with transport and potential for biogeochemical transformations, tends to be more stable and relatively insensitive to transient forcing. In the case of the HZ's hydrodynamic area, the boundary used to estimate the area corresponds to the the deepest streamline that begins and ends at the SWI, which instantaneously mimics the pressure fluctuations at the interference. This area definition does not take into account the predominant mass transport and retention process within the HZ. The results shown here confirm that under dynamic flow conditions, the residence time and the length of hyporheic flow path may not be coupled (e.g., Schmadel et al. 2016, Ward et al. 2017). Furthermore, our simulations indicate that after the peak-flow-induced expansion of the HZ area, there is a faster contraction of the hydrodynamically defined HZ; however, biogeochemically defined HZ takes longer time to return back to pre-event conditions.

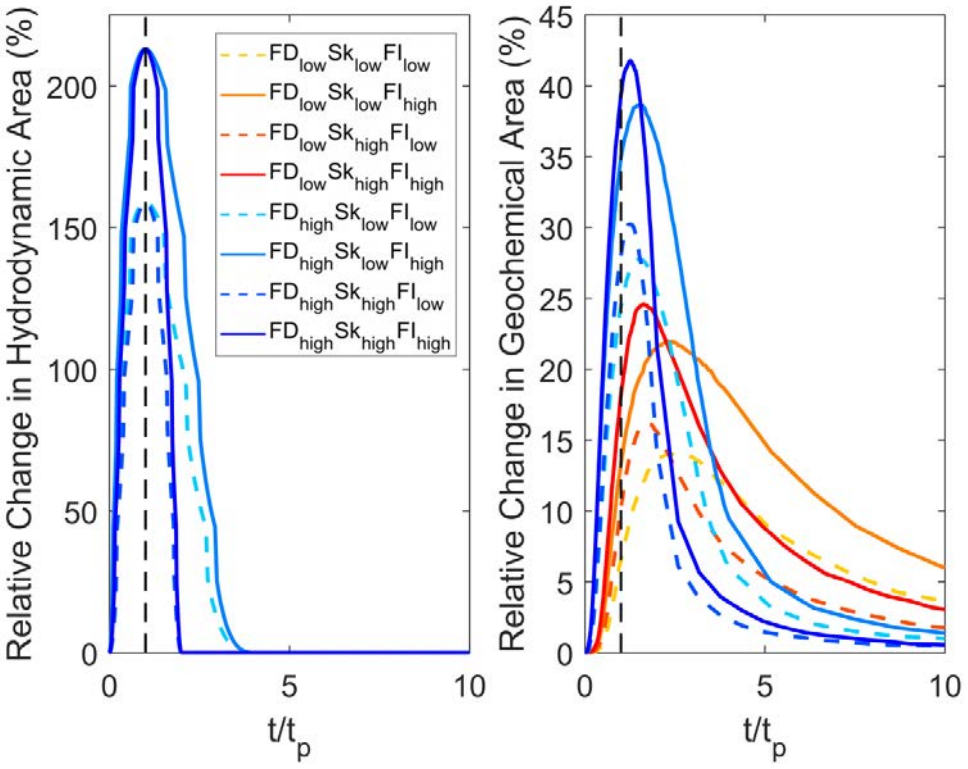

FIGURE 2.5: Relative change (to baseflow conditions) in hydrodynamic and biogeochemical hyporheic zone area [%] as a function of dimensionless time (t/t_p) for 8 scenarios listed in Table 2.2. Channel slope and bedform aspect ratio are 10^{-1} and 0.01, respectively. Note that the curves associated with FD_{low} scenarios are coinciding with FD_{high} scenarios for the case of hydrodynamic area as it shows relative change.

2.3.2 Impact of transient forcing on net hyporheic exchange flux and residence time

2.3.2.1 Net HEF

We quantify the change in net hyporheic exchange flux (HEF), relative to baseflow conditions, for different scenarios and channel slopes (see Figure 2.6). Given the instantaneous hydraulic response time (Boano et al. 2007) of submerged sediments (implicit in Eq. 5.3), the exchange flux and hydrograph are concurrent, resulting in the highest exchange differences at peak flow (t_p). Relative differences are notable, reaching values between 450 and 900 % during peak flow, with the smaller differences for high channel slopes, as expected given the modulating effect of ambient groundwater flow.

Although the relative change (to baseflow conditions) in HEF (%) is invariant for both the scenarios *i.e.* for slope values 10^{-1} and 10^{-4}, the absolute numbers differ. Notice that for both the panels the curves associated with FD_{low} scenarios are coincident with FD_{high} scenarios due to the scaling of time-to-peak of the event and hence subsets depict evolution of exchange flux (in m/s) as a function of time. For channel slopes of 10^{-1}, the absolute HEF is 3.27×10^{-4} m/s whereas for slopes 10^{-4} is 3.27×10^{-7} m/s. These results highlight the impact of slope *i.e.* the channel gradient which drives the ambient flow in the streambed. HEF is generally greater in magnitude for slope value 10^{-1} as the channel gradient drives the horizontal flow with higher velocities resulting in higher rates of hyporheic waters discharged to the surface water.

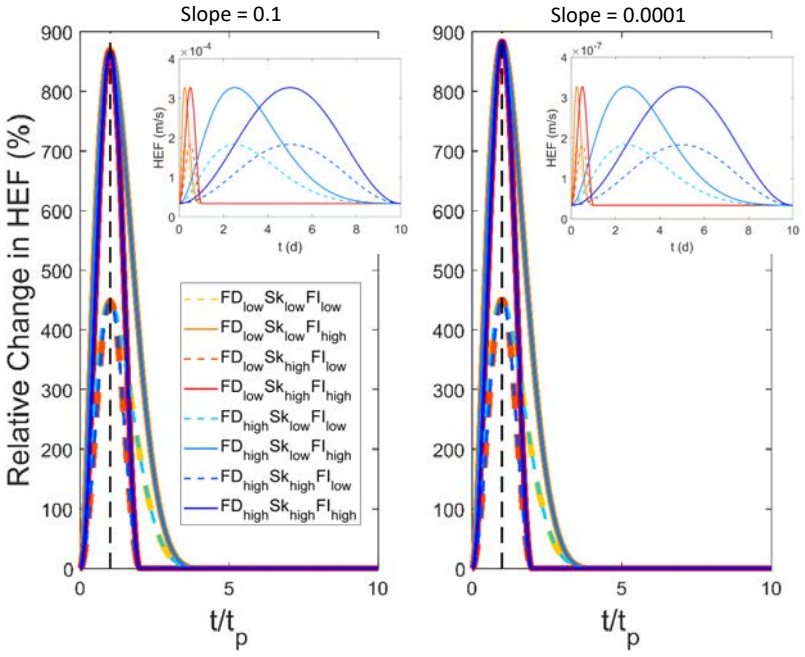

FIGURE 2.6: Relative change (to baseflow conditions) in net hyporheic exchange flux [%] as a function of dimensionless time (t/t_p) for 8 scenarios listed in Table 2.2. The bedform aspect ratio is $AR = 0.01$ and the channel slopes are 10^{-1} and 10^{-4} for the left and right panels, respectively. Note that the curves associated with FD_{low} scenarios are coinciding with FD_{high} scenarios due to the scaling of time-to-peak of the event. For further clarification, insets in each panel show the evolution of exchange flux (in m/s) as a function of time.

2.3.2.2 Moments of the residence time distributions

Ambient groundwater flow, which is proportional to the channel slope S, strongly modulates the residence time distributions for all bedform aspect ratios and forcing scenarios. First, systems with high channel slopes are strongly modulated by the ambient groundwater flow, and therefore the hyporheic zone cannot expand considerably during the peak-flow event, forcing all the flow through relatively shallow flow paths and resulting in residence times with younger waters and less variability (see columns 1, 3, and 5 in Figure 2.7). On the other hand, low channel slopes allow the hyporheic zone to expand, penetrating deeper and discharging waters progressively older and with more variable residence times initially, reaching a maximum after the event's time-to-peak, and then switching to younger waters over the long term, where eventually the system returns to the original state (see columns 2, 4, and 6 in Figure 2.7). This is consistent with previous findings by Gomez-Velez et al. (2017) in the context of alluvial aquifers. Notice that this oscillatory behavior on the moments of the residence time distribution is attenuated for the events with low duration (FD_{low}, yellow, orange, and red lines in Figure 2.7). Note that unlike the exchange fluxes, the differences in the moments of the residence time distribution are lagged relative to the peak-flow event (*i.e.* , peak-flow intensity and peak differences are reached at different times) and the return to baseflow conditions is relatively slow, specially as the flow duration is smaller and the skewness is higher. This is important from the perspective of solute retention within the reactive environment and the enhancement of transformations or slow release of contaminants.

Simulation results for bedform aspect ratio of 0.01 reveal that for shorter event durations larger quantities of older water is released out of the SWI for higher slopes

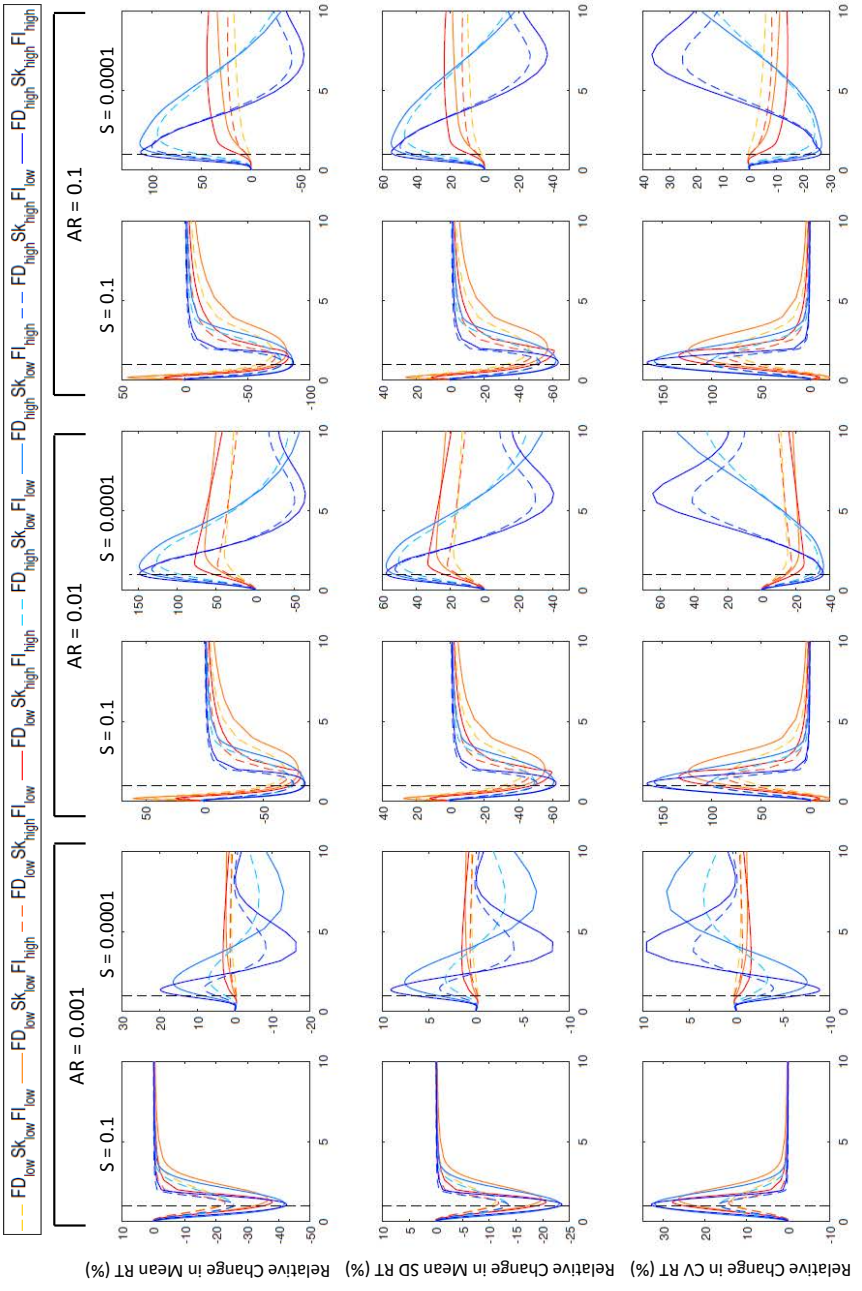

FIGURE 2.7: Relative Change [%] (to baseflow conditions) in mean residence time (RT), standard deviation of residence time (SD RT) and coefficient of variation of residence time (CV RT) as a function of dimensionless time (t/t_p) for 8 scenarios listed in Table 2.2. Columns correspond to different bedform aspect ratios (0.001, 0.01 and 0.1) and channel slope values (10^{-1} and 10^{-4}).

i.e. 10^{-1} (column 3 Figure 2.7). This indicates that sudden penetration of larger quantities of surface water into deeper subsurface flow paths causes more discharge of older water even though for very short period of time. Moreover, for all the peak-flow scenarios we observe discharge of younger hyporheic waters since steep slopes promote stronger ambient groundwater flow and hence causing compressing of HEF cells. In contrast, for low slopes (10^{-4}), the relative change (to baseflow conditions) in mean residence time (%) shows more discharge of older water during the event for all eight considered peak-flow scenarios (highest $\approx 150\%$). This is due to the slow horizontal velocities of the ambient groundwater flow observed for low slopes, allowing HEF to penetrate the streambed at greater depths. These deeper and hence longer flow paths lead to broader residence time distributions.

Streambed topography also plays a dominant role in modulating the residence time of the water and the solutes in the streambed. For different bedform aspect ratios of the streambed the spatial distribution of the hydraulic head vary at the SWI. In the case of the aspect ratios of 0.001, due to the shallow fast flowing subsurface flow paths, there is particularly higher discharge of younger water as the stream stage rises and progresses back to initial conditions relatively quickly. Notice that, this is the case for all bedform aspect ratios but for the scenarios associated with shorter duration of the event and higher slope values (see columns 1, 3, 5 Figure 2.7). However if the event duration is longer, for the higher aspect ratios (see columns 3 and 5 Figure 2.7), we observe relatively higher discharge of older waters after the sudden increase in the stream stage. However, for lower slope values, we observe long-term memory effects due to the slow horizontal ambient groundwater flows in the sediment domain. As presented in Figure 2.4, higher aspect ratios enlarges the HZ and elongates the subsurface flow paths in the streambed leading

to higher discharge of older water. This indicates long term release of older water post-flow event, particularly for the events with longer duration, which implies that if there's a second peak (or multiple peaks) before the system has recovered to baseflow conditions, system will result with additional older waters, potentially providing more time for reactions and transformations.

For all the considered scenarios, we observe that the higher peak-flow intensities (FI_{high}) intensify the impacts for the three metrics (Figure 2.7) *i.e.* in contrast to lower peak-flow intensities (FI_{low}). For example, focussing on bedform aspect ratio of 0.01, slope value of 10^{-4}, and shorter event duration, relative change (to baseflow conditions) in mean residence time (%) rises by $\approx 70\%$ for FI_{high} and only $\approx 40\%$ for FI_{low} , indicating more discharge of older water for higher peak-flow intensities. A similar trend is observed for the shorter duration of the event (FD_{low}). This demonstrates the importance of peak-flow intensity and event duration on the mean residence time (μ) of the water being discharged out of the SWI during and after a event. Therefore, each of the parameters involved in the simulations play a crucial role in determining the systems potential to discharge older or younger waters.

2.3.3 Hyporheic zone efficiency

We use the Damköhler number to delineate oxic and anoxic zones for various peak-flow event and geomorphic scenarios – a proxy for the oxygen consumption and denitrification potential. The vertical penetration of both the hyporheic zone and the oxic-anoxic zone increases with bedform aspect ratio (Figure 2.8), highlighting the impact of channel topography in the transport of water and solutes within the streambed.

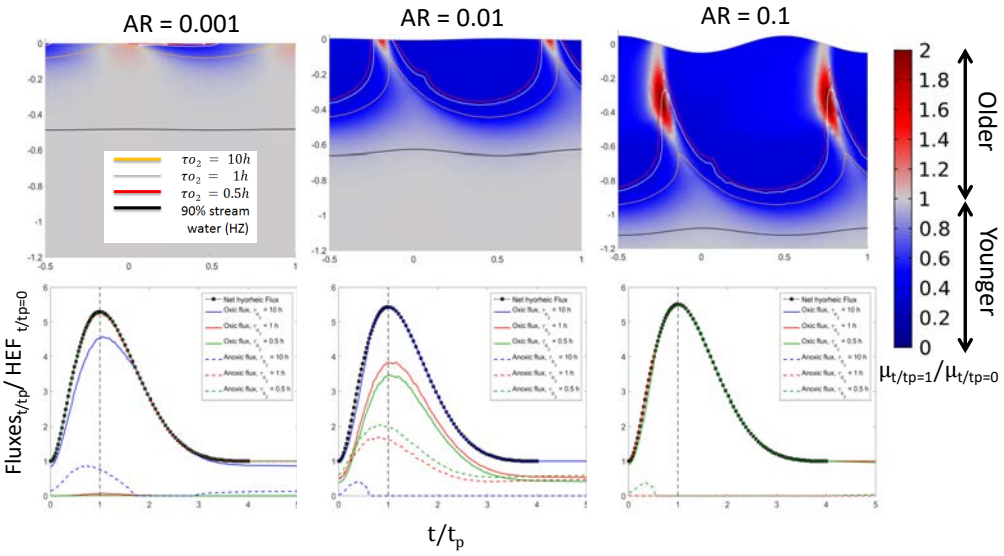

FIGURE 2.8: Snapshots for the ratio of mean RT and the base flow mean RT at $t/t_p = 1$ (1st row) and ratio of evolution of fluxes (net hyporheic exchange flux, oxic and anoxic) and net hyporheic flux at $t/t_p = 0$ as a function dimensionless time (t/t_p) (2nd row) for bedform aspect ratios 0.001, 0.01 and 0.1 (columns). Contours and curves correspond to the oxic-anoxic transition boundary for oxygen consumption time scales $\tau_{o_2} = 10, 1, 0.5$ [h]. Extent of the hyporheic zone is based on the biogeochemical definition. Channel slope is 10^{-1} in all cases and the vertical and horizontal axis are scaled by the bedform wavelength.

For bedform aspect ratio of $AR = 0.001$ cause only shallow oxic zones *i.e.* close to the SWI indicating occurrence of aerobic respiration only at the shallow regions of the streambed. However, during peak flow events there will be discharge of anoxic hyporheic waters from the streambed for all τ_{o_2} values (Figure 2.8). This indicates existence of favourable conditions for denitrification in the deepest hyporheic flow-paths which also relies on the availability of Dissolved Organic Carbon (DOC) as an electron donor deep in the streambed. Whereas, for $AR = 0.01$, with a timescale for oxygen consumption being 10 h, predominantly oxic hyporheic water is released from the SWI. This can be explained by the high flow velocities along the shallow subsurface flow paths resulting in younger water closer to the SWI. However, we also found that comparatively more anoxic water is released for lower τ_{o_2} values (*i.e.* 0.5h and 1h) for aspect ratio of 0.01 during the event. Moreover, for $AR = 0.1$, aerobic conditions extend deeper into the streambed during peak flows (Figure 2.8). It indicates that the anoxic hyporheic waters would remain in the streambed during the peak flows and eventually discharged after the recession of the event. It's important to notice that these results represent the higher channel slope value (10^{-1}) and that the interplay between the channel gradient and morphology varies the transport of oxygen into the streambed.

An analysis of potential memory effects of post-event (based on the metric - HZ efficiency) on the biogeochemical characteristics of the HZ and streambed environment has been performed using the example of nitrogen cycling. The time to reach the initial state of the system after a peak-flow event increases with the duration of the event (see FD_{high} scenarios in Figure 2.9). This implies that conditions favouring denitrification are prevalent for longer time, hence the nitrate removal efficiency of the system could be potentially higher. During longer events, reaction times would

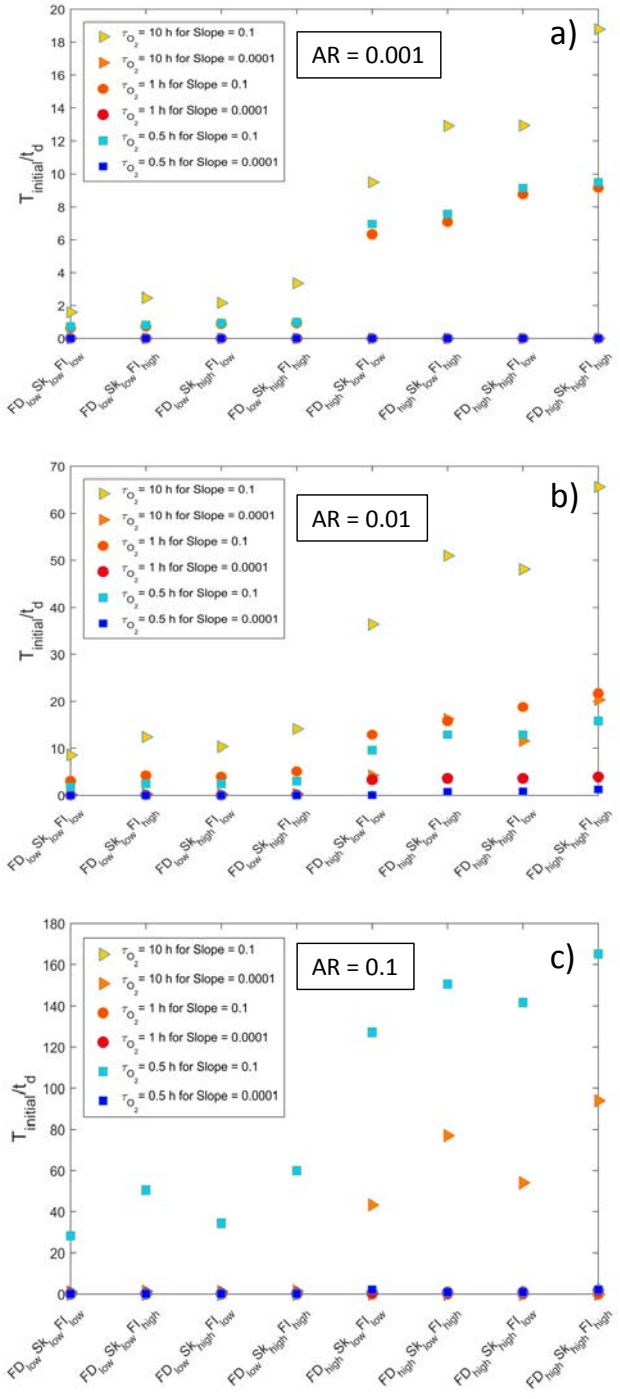

FIGURE 2.9: HZ Efficiency: Time to reach to the initial state of the system (*i.e.* to baseflow conditions) scaled to the duration of the peak-flow event (t_d) for eight scenarios listed in Table 2.2 and three biogeochemical time scales for oxygen consumption (τ_{o_2} values $= 10, 1$ and $0.5(h)$) and two channel slope values ($S = 10^{-1}$ and 10^{-4} for the bedform aspect ratios a) 0.001 b) 0.01 and c) 0.1

be substantially enhanced primarily for $AR = 0.01$ and $AR = 0.1$ (see Figure 2.9 b) and c)). Furthermore, event characteristics such as skewness of flow-peaks and intensities have substantial impact on the simulated HZ efficiency. For instance, we observe that the FI_{high} scenarios result in higher $T_{initial}/t_d$ than FI_{low} scenarios. Moreover, higher peak-flow skewness causes higher $T_{initial}/t_d$ even though the impact of peak-flow skewness is not as pronounced as seen for event duration and peak-flow intensity (Figure 2.9).

2.4 Discussion

2.4.1 Dynamic hyporheic zone expansion, contraction and exchange fluxes

Recent studies have recognized the need for comprehensive studies on the drivers and controls of hypoheic exchange (McCallum & Shanafield 2016, Schmadel et al. 2016, Malzone, Lowry & Ward 2016), hence we have attempted to present an integrated, comprehensive and systematic approach that incorporates a wide range of parametric combinations. This study combined both geomorphic (streambed topography, channel gradient) and hydrological controls (different peak-flow event characteristics like intensity and skewness of the peak and duration of the event) to gain mechanistic understanding of flow patterns and exchange fluxes between groundwater-surface water interfaces.

The study showed that the increased pressure gradient at the SWI due to a peak-flow event cause HZ appearance and then expansion which was maximum at the peak

flows indicating the dominance of transient driver on hypoheic exchange. However, on the basis of our further findings, it is evident that pressure distribution caused by the transient forcings is majorly counteracted by the ambient groundwater flow. Primarily, steeper channel slopes exert stronger underflow and compress the HZs. The importance of slopes of streambed on hyporheic exchange has been highlighted for steady state discharge conditions by Cardenas & Wilson (2006) and Tonina & Buffington (2009).

Under transient discharge conditions, the HZ extent based on hydrodynamic and biogeochemical definitions varied drastically. We observed rapid changes in gradients during the course of the flood event whereas the penetration of surface water solutes was decelerated by the counter-directional nature of the local flow patterns. This in turn leads to the development of dynamic stagnation zones (*i.e.* zones with extremely low or zero velocities) where solutes might accumulate and develop regions of *biogeochemical hotspot* in the streambed (Gomez-Velez & Wilson 2013).

2.4.2 Potential impacts of transient forcing on biogeochemical processes

During high discharge conditions, the transport of surface water into the streambed accelerates (Malcolm et al. 2004, Gu et al. 2008), hence leading to increased accumulation of solutes deeper into the streambed. Previous research has demonstrated that the nutrient cycling at the river-aquifer system is strongly controlled by, and often proportional to the residence times of surface water in the hyporheic zone (Wondzell & Swanson 1999, Zarnetske et al. 2011, 2012, McCallum & Shanafield 2016) and are

good indicators of biogeochemoical processes (Sanz-Prat et al. 2015, 2016). The results indicate that peak-flow event characteristics like magnitude, skewness of peaks and duration of the event can have a considerable impact on HEF and the mean residence time of water in the hyporheic zone. Stormflow induced variability in HEF control the transport of water, solutes (and even contaminants) deeper in the alluvium and alter its residence times in the streambed, and hence may also impact rates of biogeochemical transformations (as shown by the results of Gomez-Velez & Wilson (2013) and Trauth & Fleckenstein (2017)).

The various parametric combinations of streambed height, channel gradient, duration of the event, intensity and skewness of the peak-flows revealed interesting results. For example, in the cases of hydropeaking ($t_p/t_d = 0.5$) observed in dam operations or discharge from wastewater treatment plant (Casas-Mulet et al. 2015, Sawyer et al. 2009, Zhou et al. 2018), the results showed relatively higher discharge of older water and for a longer period of time when compared to lower t_p/t_d ratio. This was observed for all the bedform aspect ratios of streambed but only for lower slope values. The direct impact of hydropeaking which may cause thermalpeaking as well is observed in water chemistry and hence also hyporheic invertebrates as highlighted in the results by Bruno et al. (2009, 2013), Jones (2014). Moreover, the results indicated that for the same event duration and peak-flow intensity, hyporheic zones relatively release higher discharge of older water for bedforms like dunes and ripples when compared to alternating bars.

Using the framework of Damköhler number, we found that the HZ efficiency may increase during the peak-flow event. The HZ efficiency metric relates the anoxic hyporheic waters with the total hyporheic exchange flux, hence the conditions with

anaerobic respiration. Here, the efficiency was seen as the potential for anaerobic respiration, hence was correlated to potential nitrification and denitrification in the streambed. During the peak flow events, the aerobic and anaerobic respiration increased (not with the same factor) with respect to the initial conditions. The formation of longest and deepest flowpath was highly dependent on the local pressure gradient caused by the streambed topography, flow intensity and ambient groundwater flow. Zarnetske et al. (2011) showed that the denitrification in anaerobic zones of the HZ is limited by the supply of labile Dissolved Organic Carbon (DOC). Additionally, the authors also suggested that only estimates of residence times and timescales for oxygen consumption are crucial to predict the locations of nitrification and denitrification (Zarnetske et al. 2012). Moreover, previous studies by Hinton et al. (1997), Inamdar et al. (2004) have suggested higher and faster transport of DOC into deeper parts of HZ during an event, hence acting as an electron donor when oxygen is depleted in the deeper parts of the streambed. Results indicated potential development of larger areas of anoxic zones *i.e.* favourable for denitrification during the peak flow events. Assuming higher influx of labile DOC into the streambed during an event, the river-aquifer system can be highly efficient in removing nitrates post-event, especially for the bedforms like ripples and dunes. As the regions of anoxic zones are formed deeper into the streambed during the event, transported labile DOC would help the denitrifying bacteria to complete the process of denitrification. These findings are similar to Trauth & Fleckenstein (2017) where there simulation results for an in-stream gravel bar showed higher rates of aerobic respiration and denitrification for higher peak-flow intensities and longer durations of the event.

The mechanistic understanding of the dynamic hyporheic exchange presented in

this manuscript is the preliminary step to predict the regional-scale water quality outcomes. The attenuation of nutrients and efficiency of transformation processes is moderated by the intensity of surface water exchange in the HZ as it determines the contact time of the water and solutes in the buffer zone (*i.e.* the HZ). As this exchange is highly dependent on the local conditions of the sites, the accurate quantification of HEF beginning from the small-scale is essential to translate to the regional-scale.

2.4.3 Limitations and future work

In this study, we have used a reduced-order numerical model of an idealized, uniform and single type of bedform essentially to gain a deeper mechanistic understanding of the dynamic exchange processes occurring in hyporheic zones in result of peak-flow events. While, for the systematic analyses, we considered a broad range of different scenario conditions (with regards to bedform topography, channel gradient, peak-flow event characteristics), there remain further variables and potentially impactful drivers that have not been analysed in this study such as variability in streambed structural properties (Gomez-Velez et al. 2014) or the impacts of critical flows with the potential to mobilize the streambed materials (Simpson & Meixner 2012, Wu et al. 2015). Combination of several bedform morphologies with topographic structure of the catchment determines the overall HEF (Caruso et al. 2016, Schmadel et al. 2017, Ward et al. 2018). This includes nested flow paths, however in this manuscript we have only taken into consideration the shorter and local flow paths. Furthermore, we assumed only conditions without gaining or losing groundwater conditions. The analysis of potential additional impacts of net gains and losses of water and the resulting interference with peak-flow event driven hyporheic

exchange remain as the focus of future investigations. Moreover, the simulations assume no temperature induced effects with the impact of temporal fluctuations of water temperatures on resulting HEF (*i.e.* induced by diurnal surface water temperature oscillations). Considering earlier work on temperature effects on hyporheic exchange flow (Cardenas & Wilson 2007*a*), it appears promising to extend investigations towards potential temperature effects on HEF and temperature-dependent chemical reaction rates during transient flow conditions.

2.5 Conclusions

Interactions between bedform topography, channel gradient and hydrodynamic forcings result in complex exchange of water and solute fluxes between the water column and underlying hyporheic zones. The simulation results systematically explored the complex impacts of various peak-flow events and geomorphic conditions on hyporheic exchange flow patterns and dynamics for a comprehensive range of scenarios for an idealized, uniform and single-type of bedform. The results indicated dynamic expansion and contraction of the HZs during the event, however in several cases this expansion was counteracted by strong ambient horizontal flow induced by larger slope values of the stream channel. Although the relative change (to baseflow conditions) in HEF (%) was unaffected by different values of channel slopes, absolute magnitudes varied substantially. The primary impact of peak-flow events was observed on the residence time of the water in hyporheic zones. Intensification of discharge of younger and older water out of the SWI was evident at high intensities and longer durations of the event. Primarily, for streambed profiles with low slopes, events caused more discharge of older water for the higher bedform aspect ratios (i.e

for dunes and ripples). The direct influence of alterations in residence time distributions was observed in the efficiency of the hyporheic zones in developing larger areas of potential nitrification and denitrification.

Chapter 3
EFFECTS OF THE SUPERIMPOSED AND REPEATED FLOW EVENTS ON FLOW AND RESIDENCE TIMES OF DYNAMIC HYPORHEIC ZONES

Hyporheic exchange flow is a key control of the type and rates of streambed biogeochemical processes, including metabolism, respiration, nutrient turnover and the transformation of pollutants. High stream flow enhances surface-water down-welling and transports water rich in oxygen, dissolved organic matter and nutrients into the hyporheic zone—and thus increasing biogeochemical turnover. Repeated and potentially superimposed peak-flow events in the river-aquifer system have the potential to either decelerate or facilitate such processes. Herein, we use a process-based two-dimensional model to explore the role of superimposed and repeated peak-flow events on flow and transport characteristics of hyporheic zones (HZs). We conduct systematic analyses of the event-specific impacts of time lags between two flow events as well as the magnitude and the duration of the events. We use a simple but robust conceptualization of two peak-flow events for a series of sinusoidal idealized bedforms. Using the model we estimate the vertical expansion of the HZ, the total amount of exchange and residence times of discharged hyporheic waters. In addition, we present numerical breakthrough curves to estimate the relative contribution of individual events to the transport of conservative solutes from the sediment-water interface to the streams. The results indicate that an increase in the separation between the time-to-peak of the two events shows higher variability compared to peak-flow events which are superimposed i.e. with shorter separation time. Furthermore, with increasing time lag between two flow events, the maxima of first central moment i.e. mean age slowly reaches the plateau where for any further increase, the value remains constant. Flatter numerical breakthrough curves were observed for events with increased separation and longer duration of the events. Observations demonstrate the importance of the dynamic nature of HZs especially for the river-aquifer systems that are exposed to successive peak-flow events, that has implications for biogeochemical transformations and fate of contaminants in river-corridors.

3.1 Introduction

Repeated peak-flow events are ubiquitous in river-aquifer systems. These can occur due to the anthropogenic interference (such as artificial discharges from waste water treatment plants or dam operations) or natural hydrological conditions (increased snow melting and intense precipitation events). River stage fluctuations are highly responsive to these events (Sawyer et al. 2009, Bernard-Jannin et al. 2016, Salazar et al. 2014, Trauth & Fleckenstein 2017, Vivoni et al. 2006) and in many cases, a single event can generate large magnitude of change to the river stage. Perturbations in river stage, often the principal driver of hyporheic exchange (Jung et al. 2004) —alters the pressure distributions at the interface between the water column and the streambed, and thus leading to flux velocities several orders of magnitude higher than the base flow conditions (Wu et al. 2018, Singh et al. 2019, Gomez-Velez et al. 2017). Apart from river stage fluctuations, continuous exchange of water, solutes and energy between the water column and hyporheic zones (HZs) is also associated with the interplay between various drivers and controls such as geomorphological settings, channel gradient, hydraulic conductivity, sediment heterogeneity and spatial variability in heads at the sediment-water interface (SWI) (Gomez-Velez et al. 2014, Gomez-Velez & Harvey 2014*a*, Marzadri et al. 2016, Tonina & Buffington 2011). Interactions between these driving forces determine the overall volume of hyporheic exchange, retention time of water and solutes, subsurface flow paths and velocities at different depths within the HZ.

Repeated peak-flow events can cause variability in physio-chemical characteristics of the streambed. Advantages and disadvantages of the repeated peak-flow events can be found in literature (Fritz & Arntzen 2007, Bruno et al. 2009, Hinton

et al. 1997, Inamdar et al. 2004, Krause, Hannah, Fleckenstein, Heppell, Kaeser, Pickup, Pinay, Robertson & Wood 2011). The main advantages of peak-flow events relate to the activation of deeper subsurface flow paths, enhanced reactivity owing to the faster transport of solutes into the reactive zones and contaminant attenuation. For example, when denitrification in anaerobic zones of the HZ is limited by the supply of labile dissolved organic carbon (DOC) (Zarnetske et al. 2011), peak-flow events can facilitate higher and faster transport of DOC into the streambed to complete the nitrogen cycling (Hinton et al. 1997, Inamdar et al. 2004). In another study by Fritz & Arntzen (2007), the higher influx of river water due to increased river stage was shown to cause lower uranium concentrations as a result of dilution. On the contrary, disadvantages highlighted by Bruno et al. (2009) showed that peak-event induced disturbance for hyporheic invertebrates. This is mainly because sharp discharges can lead to scouring, disturbing the benthic invertebrates and salmonid eggs and eventually impacting overall ecosystem functioning.

Numerical models enable a mechanistic understanding of the dynamic behavior of the HZs and possibly provide explanations for the implications of superimposed and repeated peak-flow events on biogeochemical cycling and hyporheic invertebrates. It can act as a tool to predict the regional-scale water quality outcomes by the accurate quantification of hyporheic exchange flows beginning from the small scale and then translating to the regional and catchment scales. Previous modelling studies have shown the importance of the dynamic nature of river corridors (Boano et al. 2013, Ward et al. 2013, Dudley-Southern & Binley 2015, Malzone, Anseeuw, Lowry & Allen-King 2016, Malzone, Lowry & Ward 2016, Schmadel et al. 2016, McCallum & Shanafield 2016, Ward et al. 2018), and few studies have primarily focused on the effect of single discharge events on hyporheic exchange processes

(Trauth & Fleckenstein 2017, Singh et al. 2019, Wu et al. 2018, Gomez-Velez et al. 2017, Liang et al. 2018). Dominant drivers and controls of hyporheic exchange flows during transient stream flow conditions have been identified by these studies. For example, Harvey et al. (2012) found that larger magnitude and longer-lasting events have higher potential to activate the hyporheic flow paths and engage in solute and fine particulate transportation. The modelling of dynamic HZ by Malzone, Lowry & Ward (2016) showed that the volume of HZ and fluxes is controlled by annual and storm-induced groundwater fluctuations and Schmadel et al. (2016) investigated the importance of diel hydrologic fluctuation and controls such as hillslope lag, amplitude of the hillslope and cross-valley and down-valley slopes on hyporheic flow path and residence times. McCallum & Shanafield (2016) found alterations in the residence time distributions of bank inflows and outflows for different flow events. Gomez-Velez et al. (2017) demonstrated that dimensionless framework can be used to explore the role of high discharge events on the spatial and temporal evolution of river bank storage and sinuosity-driven hyporheic exchange. In addition, a field-based study incorporating successive storm events by Dudley-Southern & Binley (2015) showed that these events can lead to a reversal of vertical hydraulic gradient and can enhance mixing up to 30 cm in the streambed. To the authors' knowledge, none of the modelling studies incorporated the effects of successive hydrological events, therefore mechanistic understanding of the impacts of superimposed and repeated peak-flow events remains elusive. Moreover, the effect of the interaction between two successive events on water and solute transportation also mostly remains largely unaccounted in these studies.

The objective of this multi-parametric study is to (1) examine and quantify the hydrodynamic variations in the HZ behaviour; (2) investigate the dependency

of first peak-flow event on the event followed using solute transport and residence time models; and (3) estimate the contribution of each event on the transfer of conservative solutes in the HZs. We provide a systematic approach to decipher the potential impacts of superimposed and repeated peak-flow events on hyporheic exchange flows, using reduced-order models of idealized, uniform and single type of bedform-induced hyporheic exchange. The term *reduced-order* indicates that the model formulation assumes and captures first-order drivers and controls of the exchange process, ignoring some of higher-order complexities such as heterogeneity in the sediments. These assumptions allow us to gain comprehensive understanding from many simulations owing to the reduced computational effort. We evaluate the impacts by studying the effects of three different parameters, namely (i) lag between two peak-flow events (t_{lag}); (ii) magnitude (H_{p_2}); and (iii) duration of second event (t_{d_2}). These results can help us to unravel the biogeochemical signature of the surface and groundwater, hence when explored, can be effectively employed in designing field experiments involving dynamic studies and explaining the results from the tracer experiments.

3.2 Methodology

The process-based model was developed in six main steps (1) set-up of the sediment geometry and defining its properties; (2) superimposed hydrograph generation; (3) inclusion of flow model; (4) solute transport model to track the hyporheic zone; (5) Residence time model; and finally (6) model for numerical breakthrough curves.

3.2.1 Conceptual model

We use a simplified conceptualization of a streambed-river interface to systematically explore the impact of superimposed and repeated peak-flow events on bedform-driven hyporehic exchange. For this purpose, we implement a detailed flow, transport and residence time models in the model domain. The modeling domain (Ω); represents homogeneous and isotropic stream sediments. It is bounded at the top by the SWI ($\partial\Omega_{SWI}$), which is assumed sinusoidal $Z_{\mathrm{SWI}} = \frac{\Delta}{2}\sin(\frac{2\pi x}{\lambda})$ where Δ [L] and λ [L] are the characteristic amplitude and wavelength of the bedform, respectively. The total length and depth of the modeling domain are $L = 3\,\lambda$ and d_b [L], respectively. At the bottom, the 0.model domain is bounded by a horizontal boundary ($\partial\Omega_b$) and at sides by the lateral boundaries ($\partial\Omega_u$ and $\partial\Omega_d$) These dimensions are selected to avoid boundary effects in the numerical simulations.

COMSOL Multiphysics is used for the numerical solution of the proposed model. Mesh independent solutions are achieved with a the resultant mesh of approximately forty-thousand triangular elements with telescopic refinement closer to the sediment-water interface. This is needed in order to capture the effect of local, fast-flowing hyporheic circulation cells and have accurate flux integrals along the boundaries.

3.2.2 Superimposed hydrograph generation

A single peak-flow pulse is used to mimic the dynamic nature of river discharge. The deterministic stage hydrograph is modeled with an asymmetric curve as proposed

by Cooper & Rorabaugh (1963):

$$H_{\text{generic}}(t) = \begin{cases} H_0 + H_p \; e^{-\delta(t-t_{lag})} \; \dfrac{[1-\cos(wt)]}{[1-\cos(wt_p)]} & \text{if} \quad t > t_{lag}, \quad \& \quad t < t_d + t_{lag} \\ H_0 & \text{otherwise} \end{cases} \tag{3.1}$$

where H_0 is the stage at baseflow conditions [L], H_p is the maximum rise of stream stage [L], t_p is the time-to-peak of the event [T], t_{lag} is the time when the peak-flow event commences [T], t_d is the duration of the peak-flow event [T], $w = 2\pi/t_d$ is the frequency of the event [T^{-1}], and $\delta = w\cot(wt_p/2)$ is a constant that determines the degree of asymmetry [T^{-1}].

We use the $H_{\text{generic}}(t)$ to create hydrographs with two superimposed/repeated peak-flow events

$$H_{sup}(t) = H_{\text{generic}}(t, H_{p1}, t_{p1}, t_{d1}, 0) + H_{\text{generic}}(t, H_{p2}, t_{p2}, t_{d2}, t_{lag}) - H_0 \tag{3.2}$$

where H_{p1}, t_{p1} and t_{d1} describe the first peak-flow event and H_{p2}, t_{p2}, t_{d2} and t_{lag} describe the second peak-flow event. Note that $t_{lag} = 0$ for the first event, hence for all the scenarios commence at $t = 0$. For convenience, from here t_{lag} is used to define the lag between two peak-flow events and the time at which second event commences, t_{d2} is used to describe the time at which duration of the second event ends (*i.e.* at $t_{lag} + t_{d2}$) and t_{p2} for the time at which peak for the second event occurs (*i.e.* at $t_{lag} + t_{p2}$).

With estimated $H_{sup}(t)$ [L] i.e the time-varying river stage, we describe the pressure distribution at the sediment-water interface ($\partial\Omega_{SWI}$). For simplicity, we use an expression for prescribed head distribution that assumes a linear combination

of head fluctuations induced by large- and small-scale bed topography (Wörman et al. 2006, Stonedahl et al. 2010):

$$h_{SWI}(x,t) = -S\,x + H_{sup}(t) + \frac{2\,h_d(t)}{\Delta}\,Z_{SWI}\left(x + \frac{\lambda}{4}\right) \tag{3.3}$$

where S is channel slope, $H_{sup}(t)$ [L] is the time-varying river stage, $Z_{SWI}(x)$ is the function describing the bed topography, and $h_d(t)$ is the intensity of the dynamic head fluctuations (Elliott & Brooks 1997),

$$h_d(t) = 0.28\frac{U_s(t)^2}{2g}\begin{cases}\left(\dfrac{\Delta}{0.34\,H_{sup}(t)}\right)^{3/8} & \text{for} \quad \dfrac{\Delta}{H_{sup}(t)} \leqslant 0.34, \\ \left(\dfrac{\Delta}{0.34\,H_{sup}(t)}\right)^{3/2} & \text{for} \quad \dfrac{\Delta}{H_{sup}(t)} > 0.34, \end{cases} \tag{3.4}$$

where the mean velocity is estimated with the Chezy equation for a rectangular channel as $U_s(t) = M^{-1}H_s(t)^{2/3}S^{1/2}$ with M is the Manning coefficient [$\mathrm{L}^{-1/3}\mathrm{T}$] (Dingman 2009). Notice that the pressure distribution at the sediment-water interface is the function of both space x and time t, where the temporal fluctuations are induced by the peak-flow event (see Section 2.2.1).

3.2.3 Flow model

Flow within the domain is driven by pressure gradients at the sediment-water interface ($\partial\Omega_{SWI}$). Neglecting the storage term, a reasonable assumption for submerged channel sediments, flow within the domain is described by the following version of

the groundwater flow equation and Darcy's law

$$\nabla \cdot \left[\rho \frac{\kappa}{\mu} \big(\nabla p + \rho g \nabla z \big) \right] = 0 \tag{3.5}$$

where $\mathbf{x} = (x, y$ is the spatial location vector [L], $p(\mathbf{x}, t)$ is pressure [$\mathrm{ML^{-1}T^{-2}}$], g is the acceleration due to gravity [$\mathrm{LT^{-2}}$], κ is the permeability [$\mathrm{L^2}$], ρ is fluid density [$\mathrm{ML^{-3}}$], μ_d is fluid dynamic viscosity [$\mathrm{ML^{-1}T^{-1}}$], $h = \dfrac{p}{\rho g} + z$ is hydraulic head [L], and Darcy velocity is $\mathbf{q} = -\dfrac{\kappa}{\mu}(\nabla p + \rho g \nabla z))$ [$\mathrm{LT^{-1}}$].

Assuming that bedforms repeat periodically along the channel, we implemented a periodic boundary condition for the lateral boundaries ($\partial\Omega_u$ and $\partial\Omega_d$; $p(x = -L, y, t) = p(x = 2L, y, t) + \rho g[h_{SWI}(x = -L, t) - h_{SWI}(x = 2L, t)]$). Under neutral groundwater conditions (*i.e.* without gaining and losing groundwater conditions), the only groundwater flow constraining the hyporheic zone is the ambient groundwater flow driven by the channel gradient (*i.e.* horizontal under-flow component), and therefore no-flow is assumed for lower boundary ($\partial\Omega_b$). The depth of this boundary (d_b) was selected to minimize boundary effects. Finally, the solution under steady state (*i.e.* , baseflow conditions) is used as the initial condition for the transient simulations (*i.e.* , during the peak-flow event). This method of calculating pressure distribution at the SWI reproduces reasonable observations. It also allows the exploration of large number of scenarios with fewer complexities when implemented in the model , and with reduced computational demands.

The sediment-water interface ($\partial\Omega_{SWI}$) can be discretized into inflow ($\partial\Omega_{IN} = \{\mathbf{x} \mid (\mathbf{n} \cdot \mathbf{q} < 0) \wedge (\mathbf{x} \in \partial\Omega_{SWI})$) and outflow sub-boundaries ($\partial\Omega_{OUT} = \{\mathbf{x} \mid (\mathbf{n} \cdot \mathbf{q} > 0) \wedge (\mathbf{x} \in \partial\Omega_{SWI})$) such that $\partial\Omega_{SWI} = \partial\Omega_{IN} \cup \partial\Omega_{OUT}$ with $\mathbf{n}$ an outward vector

normal to the boundary. Notice that these boundaries are dynamic in nature, contracting and expanding with variations in the the time-varying river stage , $H_{sup}(t)$.

3.2.4 Solute transport model and delineation of the hyporheic zone

The *advection-dispersion equation* (ADE) is used to model the transport of conservative solutes within the sediments

$$\theta \frac{\partial C}{\partial t} = \nabla \cdot (\mathbf{D} \nabla C) - \nabla \cdot (\mathbf{q} C) \tag{3.6}$$

where C is concentration [ML^{-3}], $\mathbf{q}$ is the Darcy flux [LT^{-1}], and $\mathbf{D} = \{D_{ij}\}$ is the dispersion-diffusion tensor defined as Bear (1972):

$$D_{ij} = \alpha_T |\mathbf{q}| \delta_{ij} + (\alpha_L - \alpha_T) \frac{q_i \, q_j}{|\mathbf{q}|} + \frac{\theta}{\xi_m} D_m \tag{3.7}$$

with α_T and α_L the transverse and longitudinal dispersivities [L], D_m the effective molecular self-diffusion coefficient, $\xi_m = \theta^{-1/3}$ is the fluid tortuosity (defined here with the Millington and Quirk model (Millington & Quirk 1961)), and δ_{ij} is the Kronecker delta function.

Modelling the transport of a conservative tracer allows us to explore the mixing and extent of the HZ. We assume that the concentration of the tracer in the stream water column is C_s, and therefore a prescribed boundary condition $C(\mathbf{x}, t) = C_s$ is used along the SWI's inflow areas ($\partial\Omega_{IN}$). Outflow areas ($\partial\Omega_{OUT}$) along the SWI are advective boundaries where $\mathbf{n} \cdot (\mathbf{D} \nabla C) = 0$. Lateral boundaries ($\partial\Omega_u$ and $\partial\Omega_d$) are periodic boundaries $C(x = -L, y) = C(x = 2L, y)$ and the bottom boundary ($\partial\Omega_b$)

is a no-flow boundary $\mathbf{n}\cdot(\mathbf{q}C-\mathbf{D}\nabla C)=0$. An initial condition for the concentration field is obtained from a steady-state simulation of the transport model (Eq. (5.4)) under baseflow conditions (*i.e.* , $H_s = H_0$). In this case, the hyporheic zone is defined as the zone with at least 90% of the pore water originated from the stream (*i.e.* , $C \geq 0.9C_s$). This definition is similar to the one proposed by Triska et al. (1989) and Gomez-Velez et al. (2014, 2017). Through the manuscript, we refer to this definition as the *biogeochemical definition of the hyporheic zone*.

3.2.5 Residence time model

The hyporheic zone residence time describes the time that water and solutes are exposed to the stream sediment biogeochemical conditions. Here, we evaluate the impacts of transient flow, driven by a peak-flow event, on the first moment of the HZ's residence time distribution. To this end, we use the approach outlined in Gomez-Velez et al. (2012), Gomez-Velez & Wilson (2013), and Gomez-Velez et al. (2017) where the moment of the residence time distribution are described by an ADE of the form

$$\frac{\partial(\theta a_1)}{\partial t} = \nabla\cdot(\theta\mathbf{D}\nabla a_1) - \nabla\cdot(\mathbf{v}\theta a_1) + \theta a_0 \tag{3.8a}$$

$$a_1(\mathbf{x},t) = 0 \quad \text{on } \partial\Omega_{IN} \tag{3.8b}$$

$$\mathbf{n}\cdot(\theta\mathbf{D}\nabla a_1) = 0 \quad \text{on } \partial\Omega_{OUT} \tag{3.8c}$$

$$a_1(x=-L,y) = a_1(x=2L,y) \text{ for } \partial\Omega_u \text{ and } \partial\Omega_d \tag{3.8d}$$

$$\mathbf{n}\cdot(\mathbf{q}a_1 - \mathbf{D}\nabla a_1) = 0 \quad \text{on } \partial\Omega_b \tag{3.8e}$$

$$a_1(\mathbf{x},t=t_0) = a_{10} = \int_0^\infty \tau\Psi_0(\mathbf{x},\tau)\ \mathrm{d}\tau \tag{3.8f}$$

where $a_1(\mathbf{x}, t)$ [T] is the first moment of the residence time distribution $\Psi(\mathbf{x}, t, \tau)$ [T^{-1}] which is defined as

$$a_1(\mathbf{x}, t) = \int_0^\infty \tau \Psi(\mathbf{x}, t, \tau)\ \mathrm{d}\tau, \text{ for } n = 1, 2, ... \tag{3.9}$$

Initial and boundary conditions are defined following the approach in Gomez-Velez & Wilson (2013) and Gomez-Velez et al. (2017). Similar to the conservative transport model, the initial distribution of the first moment of the residence time distribution (mean residence time) were estimated under steady baseflow conditions.

3.2.6 Numerical breakthrough curves and scenarios

To model the breakthrough curves, firstly the advection-dispersion equation is used on multiple conservative tracers. Multiple conservative tracers are used to potentially estimate relative contributions by not only first and second events individually but also when the events are superimposed. We define the time of the occurrence of the second event (t_{lag}) by the equation

$$t_{lag} = t_{p1} + \eta(t_{d1} - t_{p1}) \tag{3.10}$$

where $\eta = 1/4$, $2/4$, $3/4$, $4/4$, $5/4$ and $6/4$. Depending on the values of η describing the lag between the two events, tracking of the mixing between the two events would need deployment of two or three conservative tracers. Following are the formulated cases (See Figure 3.1):

Case I: $\eta < 1$, $t_{lag} < t_{d1}$, $t_{d1} \geq t_{lag} + t_{d2}$

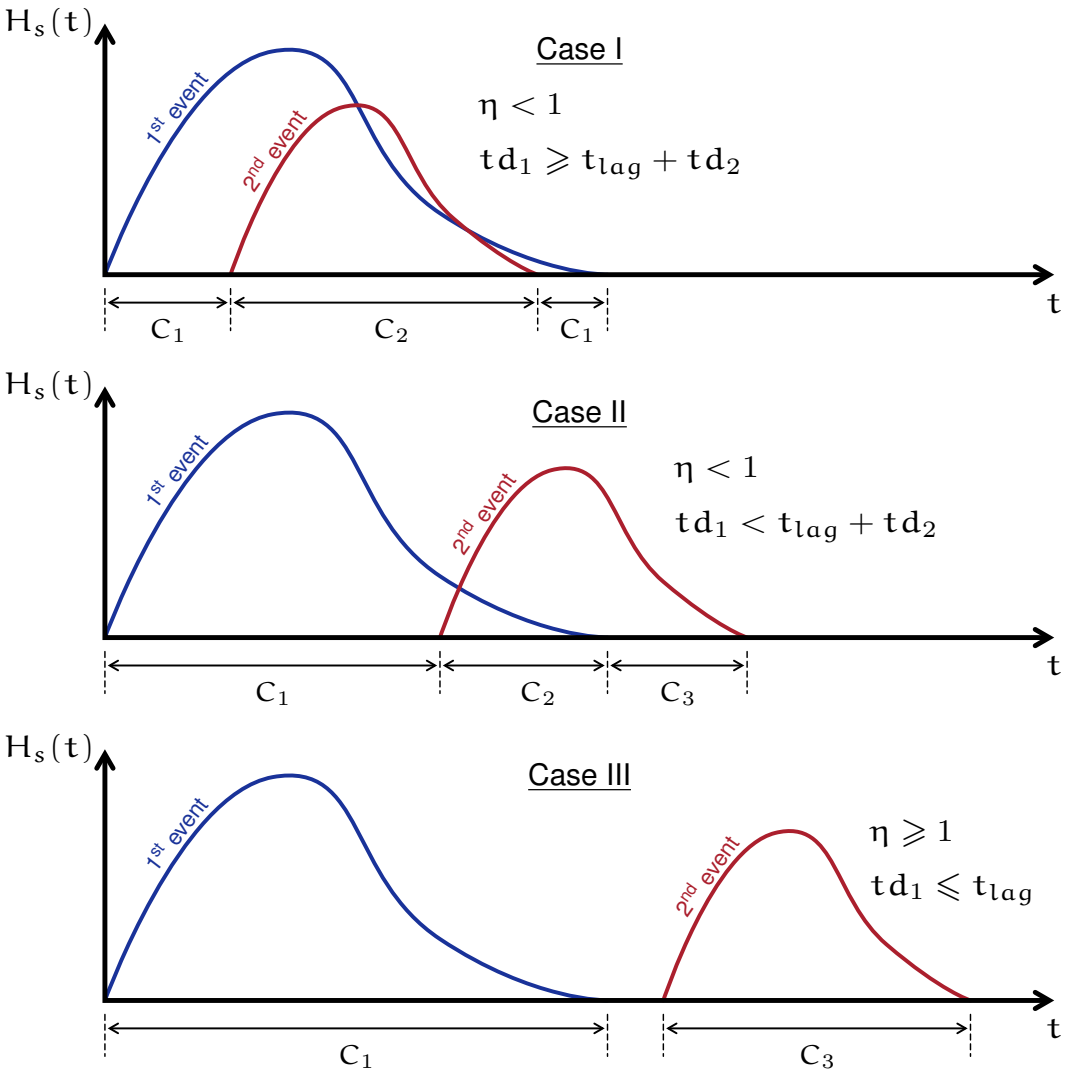

FIGURE 3.1: Depiction of the deployment of conservative tracers depending on the lag between two events t_{lag} (See Equation 3.10). Cases I and II constitute the scenarios with superimposition or overlapping of two events whereas Case III represents scenarios with no overlapping of the two peak-flow events.

Case II: $\eta < 1$, $t_{lag} < t_{d1}$, $t_{d1} < t_{lag} + t_{d2}$

Case III: $\eta \geq 1$, $t_{lag} \geq t_{d1}$

Cases I and II represent the scenarios when there is overlapping between the two events and Case III represents the scenarios with no overlapping. To track the mixing for Case I, two tracers are injected namely c_1 and c_2. The tracers are described by the piece-wise function where $c_1 = 1$ when first event is active or the rise in stage is due to the first event, $c_2 = 1$ when both the events are active i.e the stage rise is due to combined effect of the two events and finally we use $c_3 = 1$ for stage rise due to the second event only (see Figure 3.1 for further clarification).

For the tracer entering the sediment-water interface *i.e.* $\partial\Omega_{IN}$, the total mass that entered the system is estimated as

$$M_{in} = \int_a^b \left[\int_{\partial\Omega_{IN}} (\mathbf{n}.\mathbf{q}) c \, \mathrm{d}x \right] \mathrm{d}t \tag{3.11}$$

where $\partial\Omega_{IN}$ is the inflow boundary at the sediment-water interface. The mass leaving the hyporheic zone is given by

$$m_{out} = \int_{\partial\Omega_{OUT}} (\mathbf{n}.\mathbf{q}) c \, \mathrm{d}x \tag{3.12}$$

Finally the cumulative mass (or recovery) gives the breakthrough curve (BTC) estimated by the following mathematical statement

$$BTC(t) = \frac{\int_0^t m_{out} \, \mathrm{d}t}{M_{in}} \tag{3.13}$$

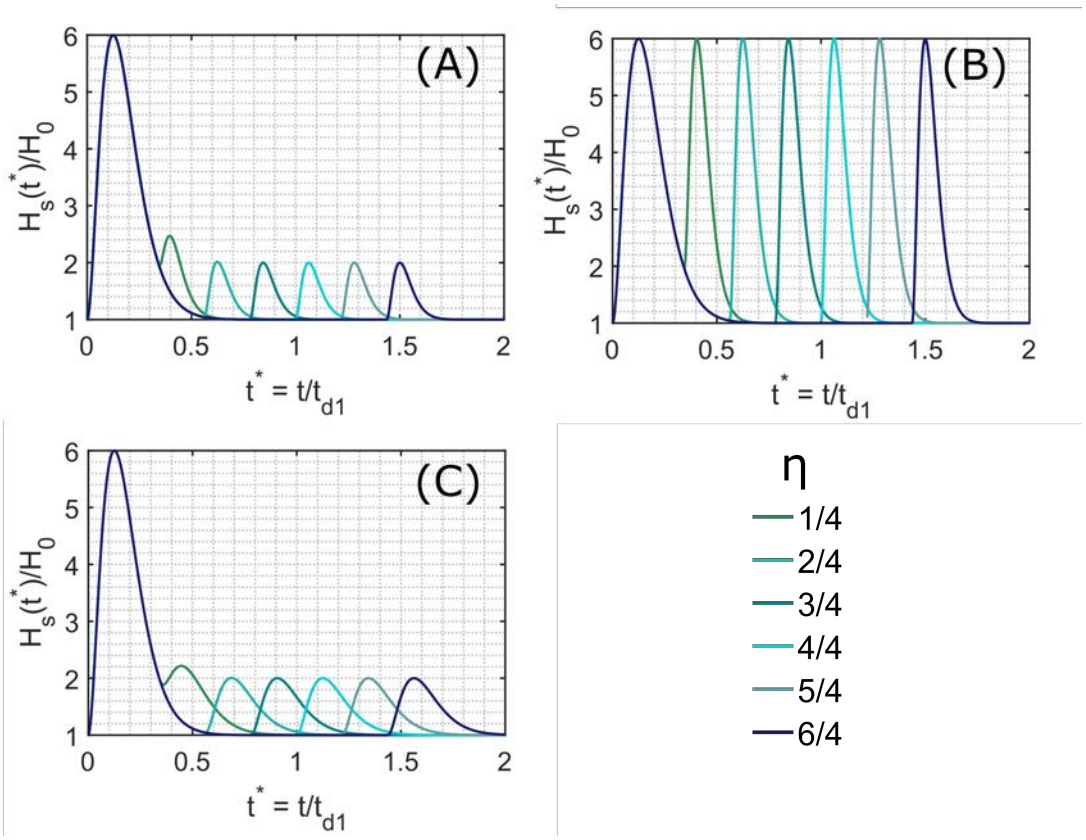

FIGURE 3.2: Depiction of dimensionless stage hydrographs. The first peak-peak flow event is of higher magnitude and is identical for all the scenarios. For (A) *i.e.* Category 1, the second peak-flow event is of shorter magnitude and occurs at t_{lag} defined by Equation 1. As shown, scenarios with $\eta = 1/4$, $2/4$ and $3/4$ the two events are superimposed. For the scenarios with $\eta = 4/4$, $5/4$ and $6/4$, the second event occurs after the duration of the first event. For (B) *i.e.* Category 2, $H_{p_1} = H_{p_2}$ and $t_{d_1} > t_{d_2}$ and for (C) *i.e.* Category 3, $H_{p_1} > H_{p_2}$ and $t_{d_1} = t_{d_2}$

All the scenarios used for the simulations have same duration (t_{d_1}) and magnitude of the first event (H_{p_2}; see Figure 3.2). Time to peak of the first event t_{p_1}) $= Sk_1 \times t_{d_1}$ and time to peak for the second event $t_{p_2} = Sk_1 \times t_{d_2}$, where $Sk_1 = 1/8$. Category 1 represent the scenarios with magnitude of the second event (H_{p_2}) less than the magnitude of the first event (H_{p_1}) and duration of the second event (t_{d_2}) is less than the duration of the first event (t_{d_1}) (Figure 3.2 (A)). Category 2 corresponds to scenarios with magnitude of the second event (H_{p_2}) equal to the magnitude of the first event (H_{p_1}) (Figure 3.2 (B)) and duration of the second event (t_{d_2}) is equal to the duration of the first event for Category 3 scenarios (t_{d_1}) (Figure 3.2 (C)).

3.3 Results and Discussion

3.3.1 Hyporheic Flow Field and Extent

Peak-flow event induced pressure distribution along the sediment-water interface varies dynamically. Temporal evolution of flow field are illustrated in Figure 3.3. $t \leq 0$ represents the base flow conditions and $t \leq t_{d_2}$ represents the dynamics during the superimposed event for the scenario $\eta = 3/4$. HZ dynamically expands and contracts during the events, with maximum expansion at $t = t_{p_1}$ due to the large magnitude of the first event. In addition, HZ expands at $t = t_{p_2}$, however relatively less compared to at $t = t_{p_1}$ due to smaller magnitude of the second even in the illustrated example. The magnitude and duration of the events determines the dynamic changes in the flow field.

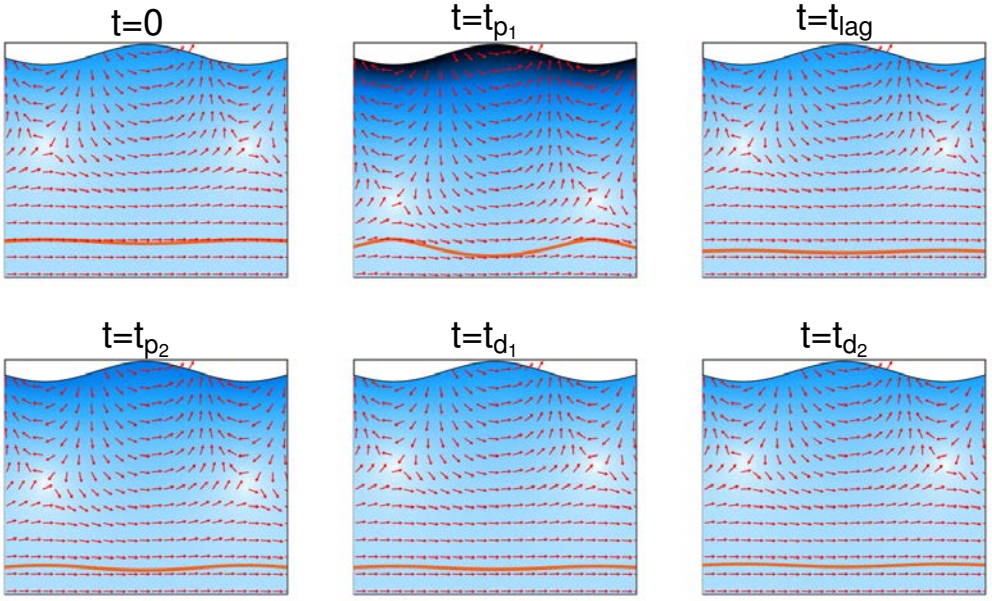

FIGURE 3.3: Snapshots of the flow field (red arrows represent direction and not proportional to magnitude) and HZ extent using the biogeochemical definition (orange line) within the sediment domain. Surface represents the magnitude of Darcy flux vector (white is low and black is high) for time at $t = 0$, $t = t_{p_1}$, $t = t_{lag}$, $t = t_{p_2}$, $t = t_{d_1}$ and $t = t_{d_2}$ for the scenario with $\eta = 3/4$ within Category 1 simulations. ($\Delta/\lambda = 0.1$, $S = 0.001$)

We also use the biogeochemical definition to define and illustrate the HZ (see the orange line in Figure 3.3). This can be numerically achieved by introduction of a conservative tracer and tracking its transportation in the streambed. The delineation is characterized by the contour where at least 90% of the water originates from the stream. HZ shape and size varies considerably for different times, however this tends to be more stable compared to the variations in flow field. This is explained flow field instantaneously propagates with pressure fluctuations at the sediment-water interface. On the other hand, HZ extent based on biogeochemical definition takes into consideration transport and retention processes within the HZ. Observations demonstrate the variability in the HZ extent showing significant change for $t = t_{p_1}$, followed by $t = t_{p_2}$, both linked to maximum rise in stage.

Another prominent characteristic observed is the horizontal and longitudinal movement of stagnation zones (in each subplot of Figure 3.3). These are the regions or locations where the absolute Darcy velocity is zero or near-zero to form stagnant zones. Presence of stagnation zones is dependent on the existence of the counter-directional local flow systems (Jiang et al. 2011). Dynamic stagnation zones are usually characterised as reactive hotspots, playing a primary role in types and rates biogeochemical transformations. For example, reduction of nitrates and nitrites in nitrogen cycling.

3.3.2 Flux-weighted mean residence time

A representative value of residence time for the exchange process is estimated by flux-weighting the modeled mean residence time along the sections of the SWI discharging hyporheic water into the stream (described in the residence time model). The mean

residence time, μ corresponds to the first central moment, a_1. Here we estimate flux-weighted mean residence time, μ_τ^* with respect to baseflow conditions ($t = 0$).

Temporal evolution of flux-weighted mean residence time (μ_τ^*) increases with the first peak-flow event (Figure 3.4, 3.5 and 3.6). This is because first high flush in all the scenarios expand the hyporheic zones, penetrating deeper and discharging older hyporheic waters, reaching its maximum before event's time to peak. Increased mean residence time of water discharged from the hyporheic zones for a short period of time and this is followed by, progressive discharge of younger hyporheic waters due to activation of short flow paths closer to the sediment-water interface. This is in line with findings of Singh et al. (2019) and Gomez-Velez et al. (2017).

The first peak-flow event is followed by the low magnitude (Figures 3.4 and 3.6) and high magnitude second peak-flow event (Figure 3.5) which is superimposed for the cases with $\eta = 1/4, 2/4$ and $3/4$ (first row of Figure 3.4 and 3.5) and separated for $\eta = 4/4, 5/4$ and $6/4$ (second row of Figure 3.4). This event disturbs the system causing variability, preventing the system to attain base-flow conditions for a certain period of time depending on the values on η, magnitude and duration of the second peak-flow event. This variability leads to discharge of relatively older water (compared to reference conditions; see gray lines in Figures 3.4, 3.5 and 3.6) for a short duration of the event which eventually starts declining shortly after the second peak is attained.

Variations in different scenarios is observed for different values of η. The results indicate that consecutively increasing the separation between the time-to-peak of the two events, t_{lag}, exhibits higher variability of μ_τ^*. The hyporheic waters discharged from the sediment-water interface is older, compared to the μ_τ^* for reference scenario

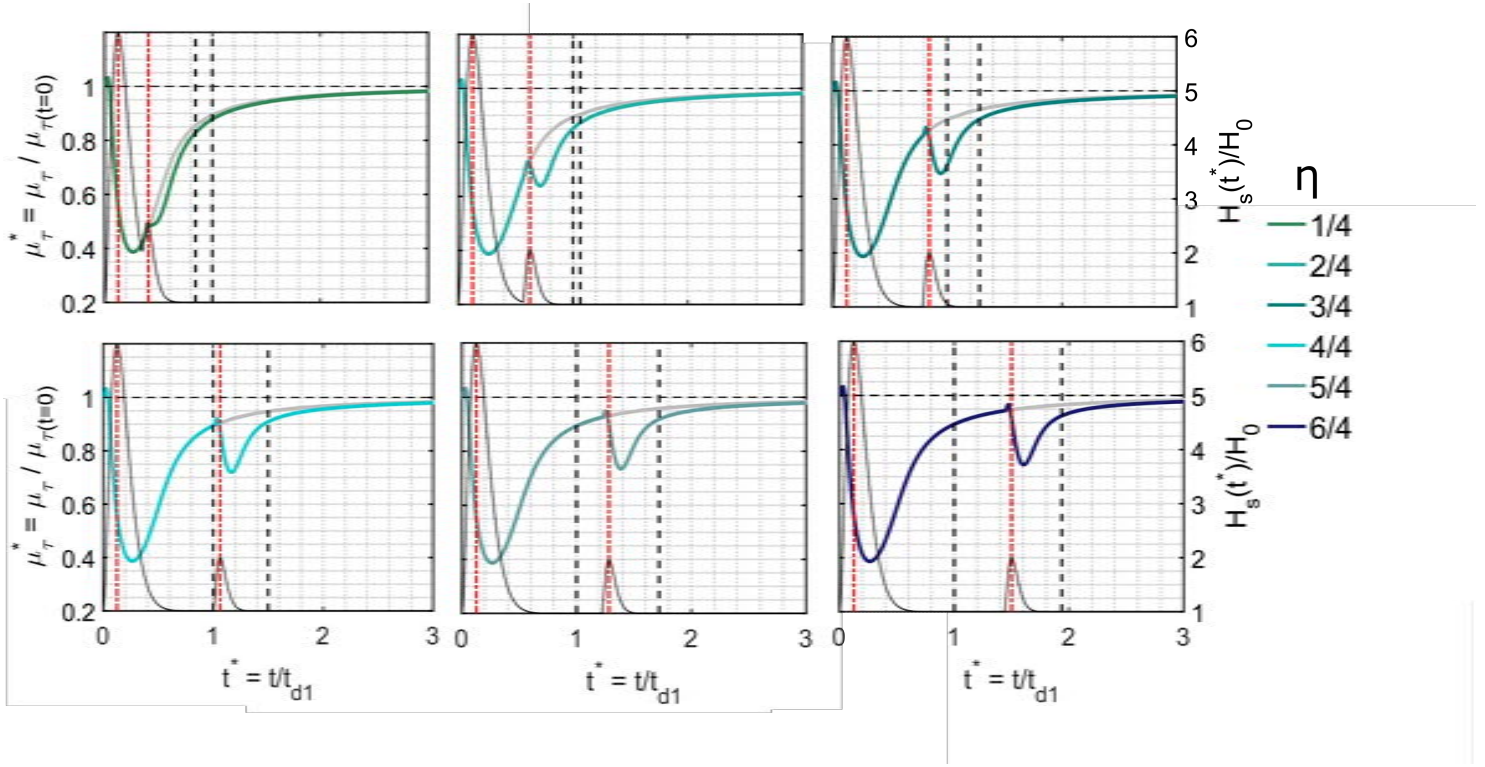

FIGURE 3.4: Temporal evolution of flux-weighted residence time μ^*_τ of hyporheic waters leaving the sediment-water interface, as a function of dimensionless time. Category 1 scenarios are shown where $H_{p_1} > H_{p_2}$ and $t_{d_1} > t_{d_2}$. Vertical red lines and black lines correspond to time-to-peak and duration of the events respectively. Different colours represents different *eta* values. Black horizontal dotted line represents the baseflow conditions where $\mu^*_\tau = 1$. Balck solid curve correspond to the shape of the hydrograph and gray line to the μ^*_τ for the reference scenario.

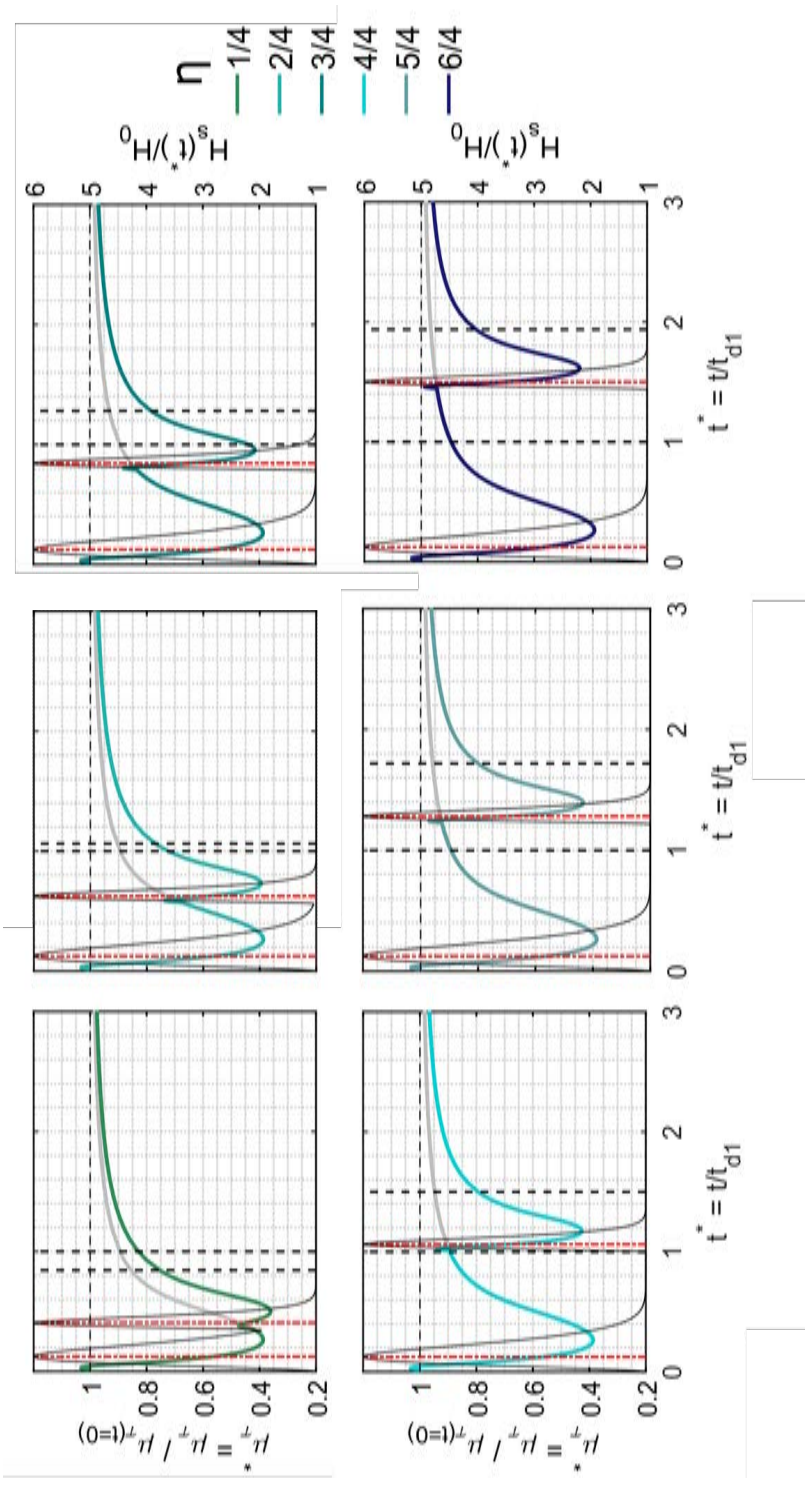

FIGURE 3.5: Temporal evolution of flux-weighted residence time μ_τ^* of hyporheic waters leaving the sediment-water interface, as a function of dimensionless time. Category 2 scenarios are shown where $H_{p_1} = H_{p_2}$ and $t_{d_1} > t_{d_2}$. Vertical red lines and black lines correspond to time-to-peak and duration of the events respectively. Different colours represents different *eta* values. Black horizontal dotted line represents the baseflow conditions where $\mu_\tau^* = 1$. Black solid curve correspond to the shape of the hydrograph and gray line to the μ_τ^* for the reference scenario.

(*i.e.* when the second peak-flow event does not exist) for the scenarios with $\eta = 3/4, 4/4, 5/4$ and $6/4$. On the other hand, two events with a short interval of time in between causes lesser variability primarily because of activation of shorter subsurface flow paths with high flow velocities, leading to mixing of younger water in the hyporheic zone and decreasing μ^*_τ. Increased duration of the second event deviates the system from the reference scenario for a longer period of time (Figures 3.4 and 3.6). Moreover, increased magnitude of the second-peak flow event leads to discharge of hyporheic waters with higher values μ^*_τ, when compared to scenarios with low magnitude second event (Figures 3.4 and 3.5). It is important to note that the analysis presented here is for the slope value 0.001. If the slope is decreased by an order of magnitude, more oscillatory behaviour in the residence times can be observed (as shown in Figure 2.7 for a single peak-flow event). Low channel slopes allow the hyporheic zone to expand, penetrating deeper and discharging waters progressively older and with more variable residence times.

Further analysis of maxima of the first central moment of flux-weighted mean residence time for the second peak, μ_{max} shows interesting results (Figure 3.7). When two peak-flow events occur with shorter separation time (t_{lag}), mean age of the hyporheic waters leaving the streambed is relatively younger. Consecutively, increasing the value of t_{lag}, μ_{max} increases. When the η is 5/4 and 6/4, the maxima of central moment (μ_{max}) slowly reaches the plateau where for any further increase μ_{max} become constant. This is an indication that the two events are completely independent with no memory effects from the first peak-flow event is carried forward to the second event and hence any response of the system is solely due to the second event. Second peak-flow event with larger magnitude increased the peaked mean RT (μ_{max}) due to its impact (red curve in Figure 3.7). Also note that for $\eta = 1/4$,

scenarios associated with category 2 and 3 do not exhibit a μ_{max} (see black and gray curve in Figure 3.7, instead there is a slight deviations from attaining reference scenario conditions.

3.3.3 Numerical breakthrough curves

Conservative solute tracer retention was determined by estimating and comparing the integrated mass fluxes for different case-defined concentrations tracers. Mass entering and leaving the system was computed by multiplying the discharge by the concentration of conservative solute tracer entering the streambed and leaving the hyporheic zones (*i.e.* $c \geq 0.9$) respectively. Breakthrough curves of tracers were determined by comparing the integrated mass fluxes leaving the system to the total mass injected.

Observations from the numerical tracer tests and its response to superimposed and repeated peak-flow events provided insights into the complex retention and transport behavior of conservative solute tracers within a sediment domain. For the scenario with $\eta = 1/4$ in Figure 3.8, the breakthrough curve for c_1 is steeper, due to higher mass-transfer rate owing to shorter lag between the two events. As the concentration of c_2 emerges, the c_1 is pressed out of the hyporheic zones at a faster rate. c_2 tracer corresponds to the concentrations which is the combination or mixing of first and the second peak-flow events which exhibits broader breakthrough curve for $\eta = 1/4$. Another spike in c_1 indicates activation of the first peak-flow event after cessation of the second-peak flow event. Longest mass transfer, i.e flatter breakthrough curve for the c_1 is observed for the scenarios with $\eta = 4/4, 5/4$ and

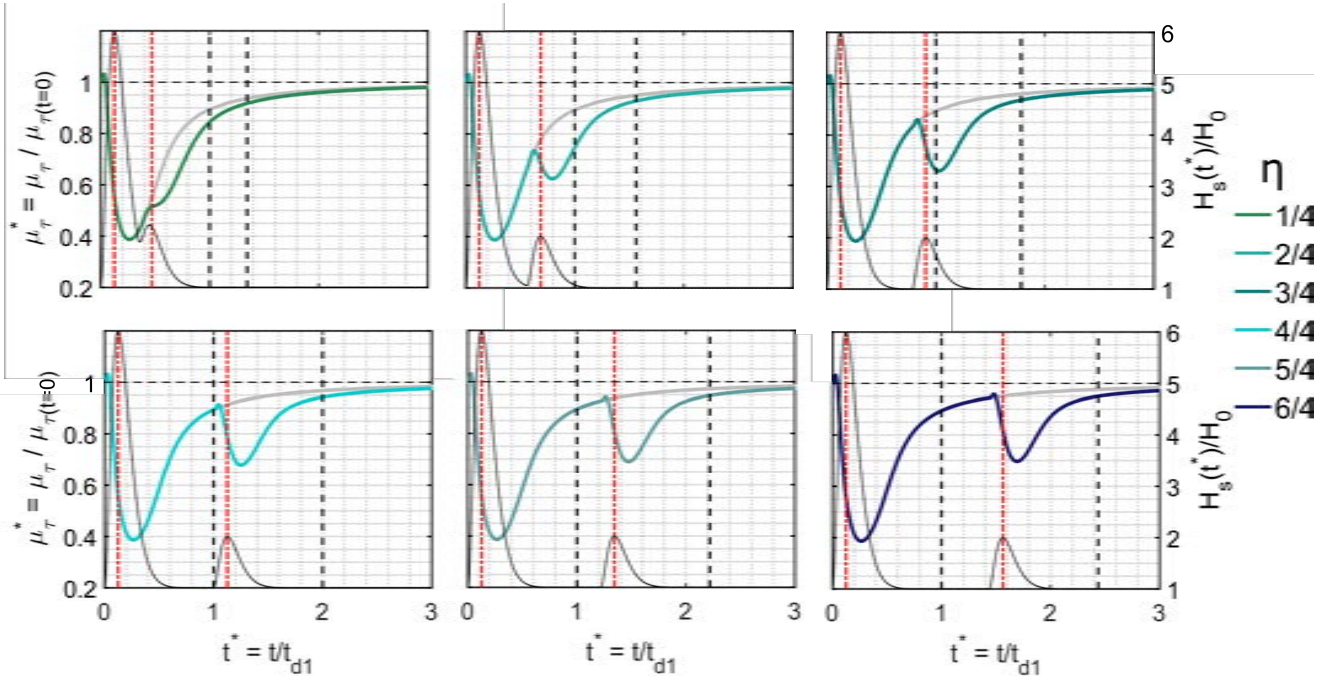

FIGURE 3.6: Temporal evolution of flux-weighted residence time μ^*_τ of hyporheic waters leaving the sediment-water interface, as a function of dimensionless time. Category 3 scenarios are shown where $H_{p_1} > H_{p_2}$ and $t_{d_1} = t_{d_2}$. Vertical red lines and black lines correspond to time-to-peak and duration of the events respectively. Different colours represents different *eta* values. Black horizontal dotted line represents the baseflow conditions where $\mu^*_\tau = 1$. Black solid curve correspond to the shape of the hydrograph and gray line to the μ^*_τ for the reference scenario.

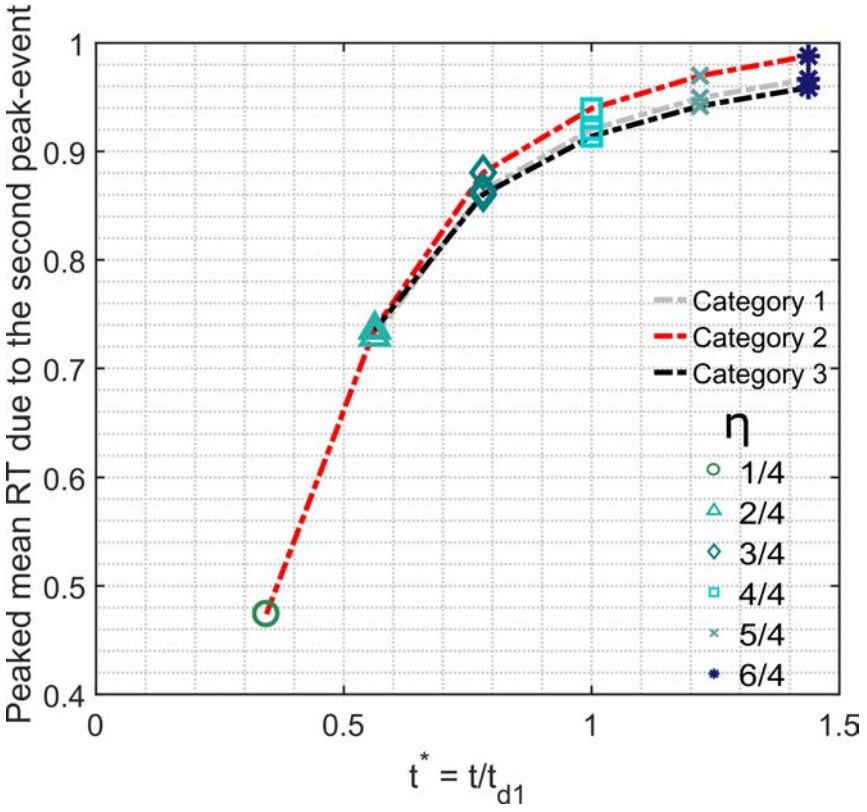

FIGURE 3.7: Peak flux-weighted mean residence time of water leaving the HZ. Values are plotted as a function of time, *i.e.* the time when second peak event commences (t_{lag}). Colours and symbols correspond to different values of η. Gray, red and black curves represent Category 1, 2 and 3 scenarios respectively.

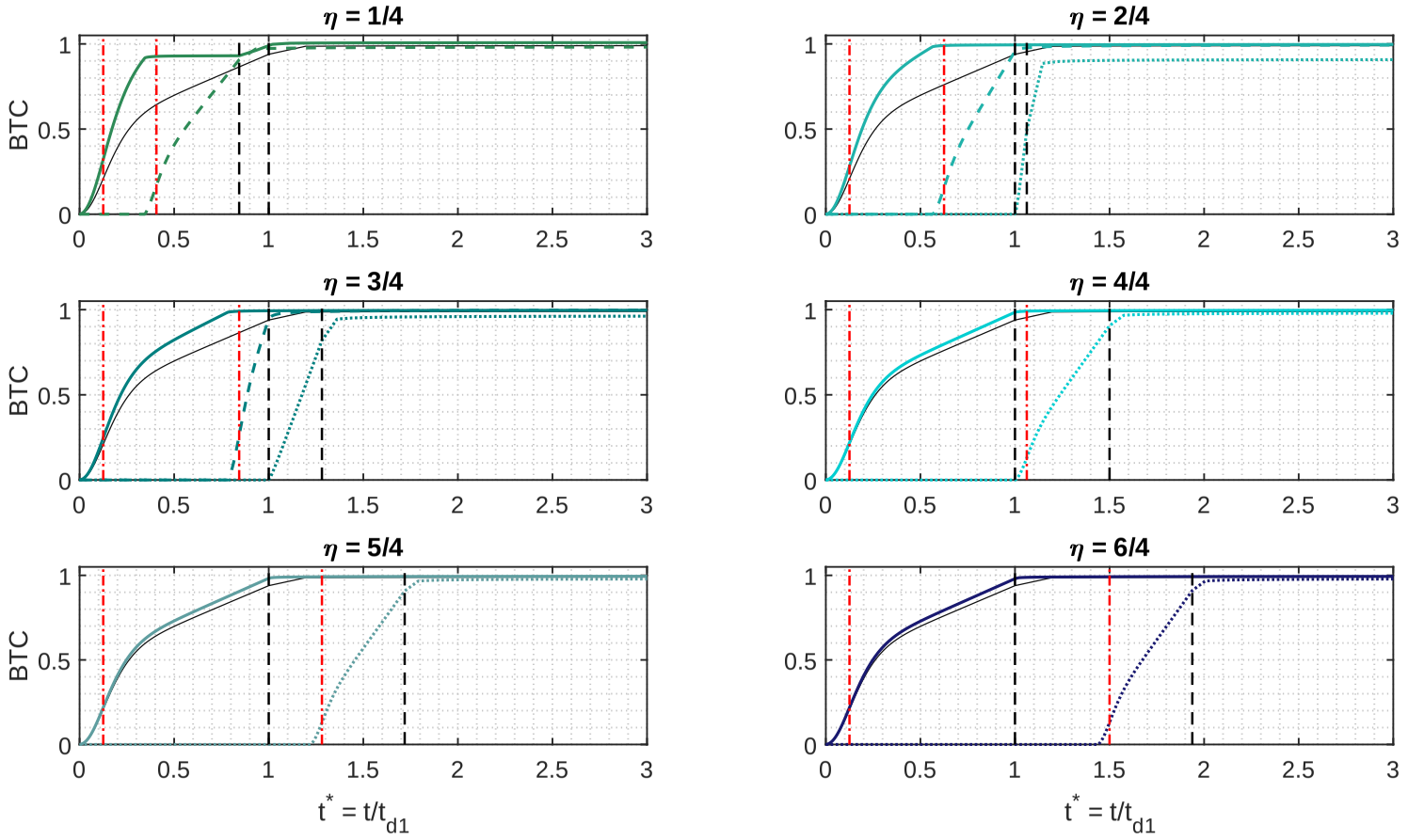

FIGURE 3.8: Modeled breakthrough curve as a function of dimensionless time. Category 1 scenarios are shown where $H_{p_1} > H_{p_2}$ and $t_{d_1} = t_{d_2}$. Solid coloured lines correspond to c_1 (i.e when 1st event is active), dashed coloured lines for c_2 (i.e when both the events are active at the same time) and dotted lines is for c_3 (i.e when only 2nd event is active). Vertical red lines and black lines correspond to time-to-peak and duration of the events respectively. Gray line represents breakthrough curves for the reference scenario. Different colours represents different η values.

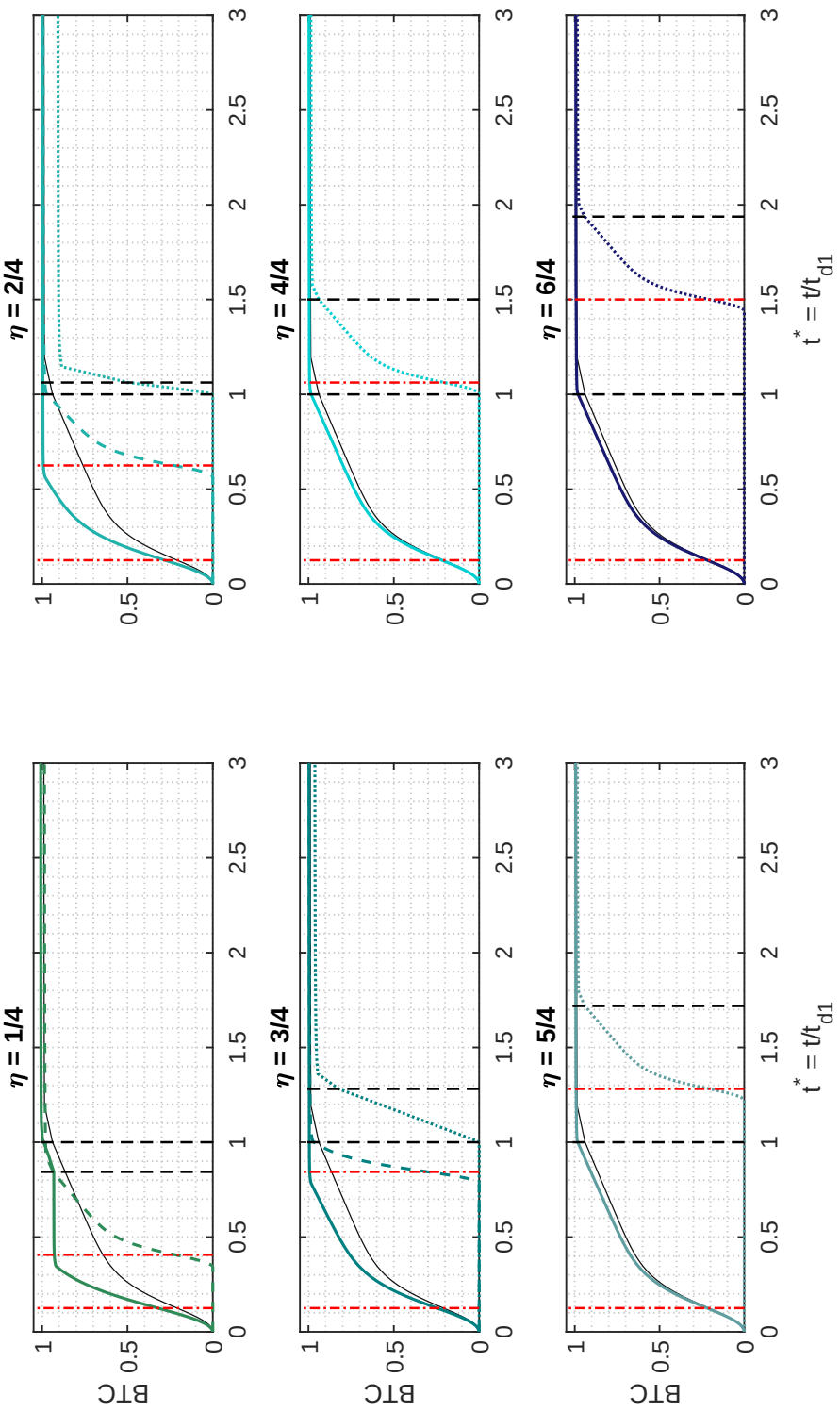

FIGURE 3.9: Modeled breakthrough curve as a function of dimensionless time. Category 1 scenarios are shown where $H_{p_1} = H_{p_2}$ and $t_{d_1} > t_{d_2}$. Solid coloured lines correspond to c_1 (i.e when 1st event is active), dashed coloured lines for c_2 (i.e when both the events are active at the same time) and dotted lines is for c_3 (i.e when only 2nd event is active). Vertical red lines and black lines correspond to time-to-peak and duration of the events respectively. Gray line represents breakthrough curves for the reference scenario. Different colours represents different η values.

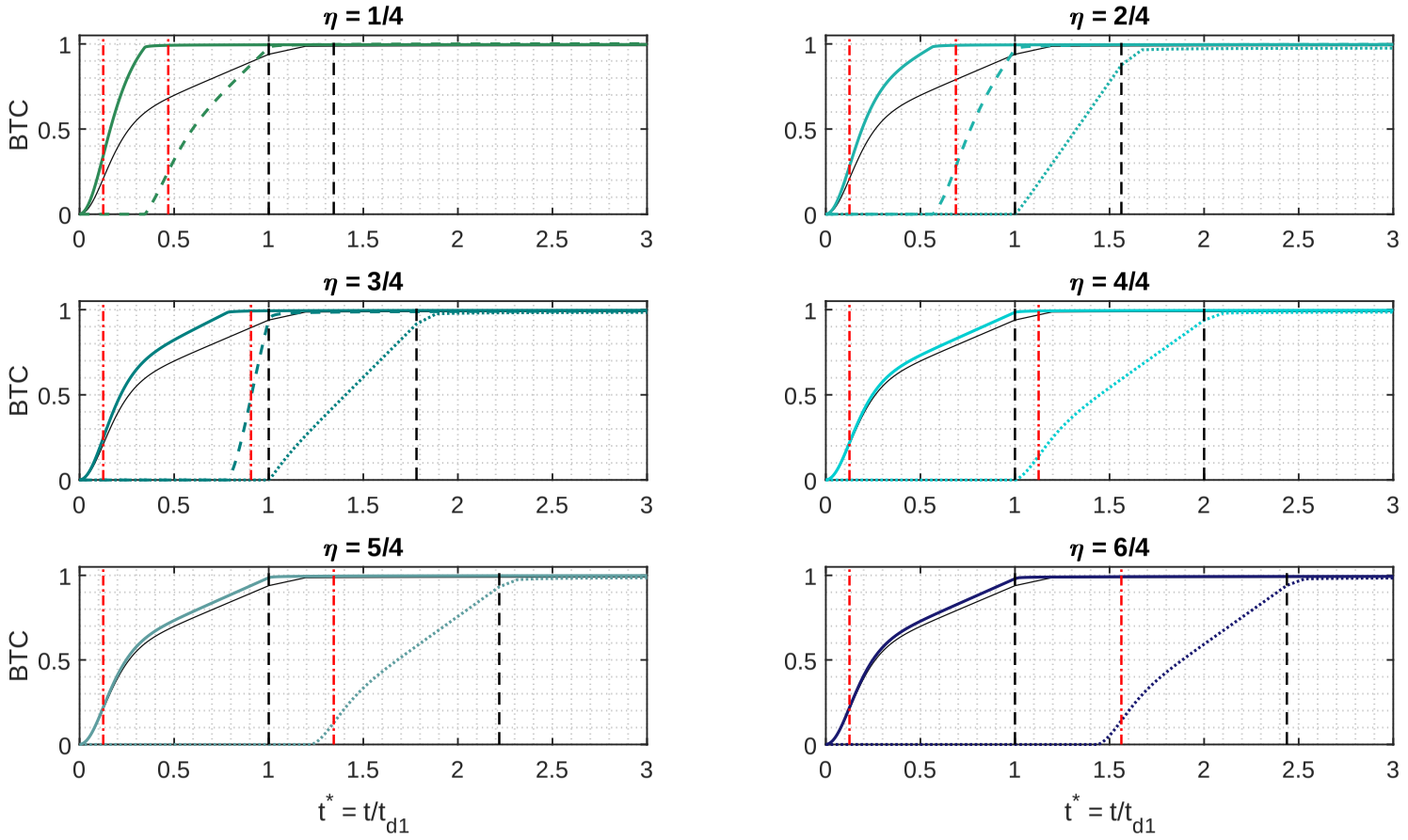

FIGURE 3.10: Modeled breakthrough curve as a function of dimensionless time. Category 1 scenarios are shown where $H_{p_1} > H_{p_2}$ and $t_{d_1} = t_{d_2}$. Solid coloured lines correspond to c_1 (i.e when 1st event is active), dashed coloured lines for c_2 (i.e when both the events are active at the same time) and dotted lines is for c_3 (i.e when only 2nd event is active). Vertical red lines and black lines correspond to time-to-peak and duration of the events respectively. Gray line represents breakthrough curves for the reference scenario. Different colours represents different η values.

6/4, primarily due to non-interference and non-superimposition of second peak-flow event. Similar behavior is observed for the second peak-flow event *i.e.* for c_3. Shape of the breakthrough curve is dependent on the flow rate and diffusion characteristics. When the lag between the two events is shorter, the solutes are relatively less retained in the system and transported at a faster rate, potentially from the shorter flow paths. In addition, it is also observed that as t_{lag} increases, the first event's behavior becomes similar to the reference concentration which represents the scenario with a single peak-flow event *i.e.* c_1 for $\eta = 6/4$ nearly coincided with reference concentration (black solid curve). Furthermore, increase in the magnitude of the second peak-flow event causes the concentration to increase at a faster rate (see Figure 3.9).

A prominent observation in breakthrough curves for scenarios with longer duration of the second event (Figure 3.10) is that the curves are much flatter when compared to scenarios with shorter duration. This can be explained by the slower mass transfer due to the longer spread of the event. Moreover, for $\eta = 1/4$, c_3 tracer is also injected as the longer duration of the second event causes partial over lapping of the events and not complete as for the same condition in Category 1 scenario (Figure 3.8).

3.3.4 Solute transport retention and dynamics during the two peak-flow events

Observations of the flux-weighted mean age and breakthrough curves unravelled interesting results detailing the impact of repeated and superimposed peak-flow events

on water and solutes' residence times and transport. The increased transient pressure gradient due to the peak-flow events induce hyporheic flows that are primarily an instantaneous response to changes in the river stage. This instantaneous increase enlarges the hyporheic zones, elongates the subsurface flow paths and increase the hyporheic fluxes. However, the solute transport remains a gradual process. Sudden rise in stage induces newly activated deeper and elongated subsurface flow paths that increases the transport timescale for the water and solutes.The results indicated that the duration of the impact in the residence times caused by the first event is highly determined by the flow characteristics of the second-peak flow event. For example, if the second peak-flow event with a shorter magnitude occurs immediately after the first event, there is only minor deviation in the change in residence times. The intensity, time of occurrence and duration of the second peak-flow event determines the magnitude of variations in the residence times over the course of events. Primarily, when the second peak-event is of a large magnitude, the changes can be considerable and can exhibit long term change in the system. As also illustrated by Harvey et al. (2012), streams with longer duration and larger magnitude will potentially completely flush deeper and longer flow paths.

Solute tracers results demonstrated that the peak flow events can lead to prolonged storage and delayed release of solute tracers, for the scenarios where the two peak flow events are not superimposed and occur for a longer duration of time. This is mainly because of the slower mass transfer due to the longer spread of the event. This is also indicated in the study by Harvey et al. (2012). The results indicate that separation between two-peak flow events (t_{lag}) is a crucial determinant of water and solutes retention time in the hyporheic zones. However, other geomorphological parameters such as channel gradient, bedform amplitude, wavelength (Elliott &

Brooks 1997, Singh et al. 2019, Wu et al. 2018) and flood characteristics like intensity, duration and skewness of the event also determine the transport and retention behaviour of water and solutes.

3.3.5 Biogeochemical and ecological implications

Herein we use numerical tracer tests to investigate the impacts of superimposed and repeated peak flow events on water and solute retention and transport in sediment domain. This research mainly focuses on variations in hyporheic flux velocities, residence times and transport of conservative solutes under dynamic flow conditions. Results indicated that high-flow events caused expansion of the hyporheic zones and increase the hyporheic fluxes indicating that events have the potential to enhance surface water downwelling rich in oxygen, dissolved organic matter, and other nutrients, getting delivered at high concentrations into greater depths and larger streambed areas. Findings by Drummond et al. (2017) suggested that storm event can mobilize or remobilize solutes and fine particles within the streambed and therefore further fuelling biogeochemical transformations That said, successive events occurring within a short duration of time *i.e.* when system is unable to recover from first event may not enhance stream metabolism, owing to the larger amount of water pressed from shorter subsurface flow paths. Dissolved organic carbon, dissolved oxygen, contaminants and microbes are affected by the transience in the streams, hence dynamics studies must be considered to study stream-aquifer metabolism.

During superimposed and repeated peak flow events, the altered hydraulic conditions affect the solute transport and retention. Increased residence times with increase in the separation between the two events suggests that high discharge events

when occurred after certain period of time has the potential to positively contribute to processes such as nitrification and denitrification. The results suggests that depending on the magnitude of the events, increased hyporheic flow paths due to repeated peak-flow events may enhance the stream metabolism. The results presented by Trauth & Fleckenstein (2017) demonstrated that the single discharge events increased the reactive efficiency of the hyporheic zone. However, the findings show that this is only true for the cases if the first event is not immediately followed by the second event. As the biogeochemical timescales for oxygen consumption is an important determinant for shifting the respiration from aerobic to anaerobic conditions in the streambed, elongated subsurface flow paths can promote biogeochemical transformations in deeper parts of the streambed (Kennedy et al. 2009, Hinton et al. 1997, Krause et al. 2013, Inamdar et al. 2004, Malcolm et al. 2004, Gu et al. 2008). In addition, transience variability in hydraulic conditions and stream chemistry can have cascading influence on diversity and productivity of hyporheic organisms (Bruno et al. 2009).

3.4 Conclusions

This research highlights the importance of consideration of the impacts of superimposed and repeated peak-flow events on hydrodynamics of hyporheic zones, and transport and retention of water within the streambed. We deployed a two-dimensional model consisting of sinusoidal bedforms and implemented flow, transport and residence time models. Systematically, we designed hydrograph scenarios with variations in lag between the occurrence of two events, magnitude and duration of the events. Time-lag between two events covered scenarios with complete overlapping

i.e. superimposition of two events, partial overlapping and scenarios with no overlapping *i.e.* representing repeated peak-flow events. Furthermore we systematically introduced three conservative tracers depending on the contribution and mixing of the events in order to comprehend solute retention in the hyporheic zones.

During peak-flow events, instantaneous change in temporally variable hyporheic flow field was observed due to rapid pressure wave propagation within the streambed, however the expansion based on geochemical definition was relatively more stable. The results demonstrated that longer the lag or separation between two events, higher the variability in the flux-weighted mean residence times, hence has the potential to discharge more older hyporheic waters. Numerical breakthrough curves were found to be flatter for the events with increased separation and longer duration of the following event. Higher magnitude of the second event caused the breakthrough curves to become steeper, when compared to low magnitude and longer duration of the second event. Exploration of the impacts of two successive flow events using reduced-order models demonstrated the importance of consideration of dynamic behaviour of HZs. Breakthrough curves for such events can unravel the biogeochemical signature of the water that is being transported in and out of the hyporheic zones. This implies that depending on the event characteristics, the potential of the water with different chemical properties to retain in the hyporheic zones may determine the types and rates of redox reactions and therefore overall water quality and chemistry.

Chapter 4
PROPAGATION OF DIURNAL SURFACE WATER TEMPERATURE OSCILLATIONS IN RIPPLES AND IMPACTS ON HYPORHEIC EXCHANGE FLUXES

The physical, chemical and biological processes occurring in the hyporheic zone are often temperature-dependent. Temperature has a direct impact on microbial activity and the degradation of organic matter, nutrient cycling, and the attenuation of contaminants. The propagation of heat and its distribution within streambed sediments is affected by sediment thermal properties and exchange fluxes across the sediment-water interface that are dependent on hydraulic parameters such as hydraulic conductivity and channel slopes. Hitherto, there has been no systematic analysis of the interplay of bedform geometry (such as ripples), channel gradient, hydraulic conductivity and their impact on heat propagation within streambeds. To understand the interactions of this phenomena, we conducted numerical simulations of the propagation of diurnal surface temperature oscillation under steady flow conditions. Diurnal temperature fluctuations in the water column were imposed at the sediment-water interface. Our results show the propagation of diurnal oscillations in surface water temperature in ripples depends on the magnitude of the change in temperature. Variations in dynamic viscosity are seen to generate significant changes in hyporheic exchange flux, flux-weighted temperature leaving the hyporheic zone and temperature-dependent reaction rates (using Arrhenius equation). In addition, hyporheic temperature signals leaving the stream were strongly modulated by hydraulic conductivity and ambient groundwater flow (proportional to channel slope) i.e. the parameters that determine the heat transport timescales. Our simulations revealed differences in the propagation of diurnal temperature oscillations at ranges relevant for biogeochemical reaction rates.

4.1 Introduction

Streambed areas associated with hyporheic exchange flows have been shown to be biogeochemically active regions (Krause, Hannah, Fleckenstein, Heppell, Kaeser, Pickup, Pinay, Robertson & Wood 2011, Zarnetske et al. 2011, 2012, Gomez-Velez et al. 2014, Zheng et al. 2016), often representing hotspots of microbial metabolic activity (Krause et al. 2014). Biogeochemical processing in streambed environments is not only affected by the conditions prevailing in the streambed but also in the overlying water column. Literature has revealed that diurnal fluctuations in water column temperature propagate into the streambed, impact stream ecological functioning and biogeochemical transformations (Brown et al. 2006, Webb et al. 2008, Mouw et al. 2009, Krause, Hannah, Fleckenstein, Heppell, Kaeser, Pickup, Pinay, Robertson & Wood 2011, Comer-Warner et al. 2018). Streambed temperatures have a critical impact on biogeochemical cycling rates (Westrich & Berner 1988, Boulton et al. 2008), mainly due to its effect on sediment microbial activity which is strongly temperature sensitive (Kaplan & Bott 1989, Fenchel et al. 2012). In addition, adverse impacts of sudden stream warming have been demonstrated for aquatic ecological functioning, such as the hatching of salmonid and invertebrate eggs (Malcolm et al. 2002, 2004, Burkholder et al. 2008). Furthermore, abiotic processes such as sorption and desorption processes are also temperature-dependent (Nimick et al. 2003, Kleineidam et al. 2004). Therefore, thermal conditions can considerably impact water quality and ecological functioning in the river-aquifer system (Webb et al. 2008).

Heat transfer processes within the streambed are complex and can vary considerably across spatial and temporal scales. In the field based studies, temperature

measurements have been used as an important tracer to detect and measure hyporheic exchange (Anderson 2005, Constantz 2008). This is due to the response of streambed thermal patterns to heat convection advected by water flow. Previous studies have emphasized the complexity of heat exchange in the hyporheic zones (HZs) owing to continuous upwelling and downwelling of hyporheic water. This exchange phenomenon is determined by bedform features (such as pools and riffles (Evans & Petts 1997, Hannah et al. 2009)), streambed lithology, streambed permeability, porosity (Malcolm et al. 2002, Constantz 2008), flow fluctuations (Gomez-Velez et al. 2017, Singh et al. 2019, Wu et al. 2018) and biological factors such as macrophyte cover and algal cover over the streambed (Conant 2004).

Water temperature variability can occur naturally or as a result of anthropogenic perturbations (Caissie 2006) such as thermal pollution, flow dynamics, climate change. This results in complex thermal dynamics which is driven and controlled by the interplay of several factors such as tree shading, groundwater inflows and outflows, hyporheic exchange, additional discharge due to precipitation, dam operations, thermal pollution, etc (Evans et al. 1995, Evans & Petts 1997, Acornley & Sear 1999, Malcolm et al. 2002, Story et al. 2003, Brown et al. 2006). Thus, heat propagation combined with hyporheic hydrology may be highly dynamic considering complex processes involved in local bedform-driven hyporheic exchange and broader patterns of groundwater inflows/outflows, including potential flow exchange between alluvial and bedrock aquifers (Malcolm et al. 2004, Cardenas & Wilson 2007*a*, Krause, Hannah, Fleckenstein, Heppell, Kaeser, Pickup, Pinay, Robertson & Wood 2011).

The published literature has highlighted the importance of water column temperature in moderating streambed temperature and also its influence on provision

of thermal refugia (Evans & Petts 1997, Lenk & Saenger 2000, Malard et al. 2001, Hannah et al. 2009, Norman & Cardenas 2014), including a number of numerical modelling attempts (Cardenas & Wilson 2007*a*, Zheng et al. 2016, Zheng & Cardenas 2018). Marzadri et al. (2012) and Zheng et al. (2016), Zheng & Cardenas (2018) considered constant and diurnal temperature oscillations of surface water, respectively, to study the thermal effects on biogeochemical cycling for single-type of bedform features. The study of heat transport using flume experiments by Norman & Cardenas (2014) demonstrated that increased permeability and channel flow rates increased the convective heat transport in the HZs. Arrigoni et al. (2008) highlighted the complex thermal dynamics in the HZs and showed that hyporheic temperatures leaving the stream was not simply cooled or warmed but buffered and lagged as well. However, to our knowledge no study has performed systematic analysis on the interplay of surface water temperature amplitudes and parameters such as hydraulic conductivity and channel slopes that effect the heat transport timescales, on the thermal dynamics and hyporheic characteristics in ripple-like bedforms.

In this work, we perform systematic analysis of the impacts of different values of hydraulic conductivity and channel gradients on the thermal dynamics within streambed sediments. We focus on the propagation of diurnal surface water temperature oscillations within and below ripples through fully coupled reduced-order models of Darcy flow and heat-transport in the sediments using a temperature-dependent relationship of viscosity and density of water. For the systematic analyses we vary the peak amplitude of water column temperature (T_{amp}), hydraulic conductivity and channel slopes, and estimate hyporheic exchange fluxes, flux-weighted temperature leaving the HZs, temporal variations of dynamic viscosity and density of water. Moreover, we quantify the relative contributions of convective and conductive heat

transfer in the sediment bed using *Peclet number*. Furthermore, in order to analyze the impact of diurnal temperature fluctuation on the spatial distribution of reaction rates in streambed sediments, we evaluate temperature-dependent reaction rate [%] using the Arrhenius equation.

4.2 Methods

4.2.1 Conceptual model

We use a simplified conceptualization of a streambed-river interface to systematically explore the impact of diurnal surface water temperature oscillations on streambed thermal patterns and hyporheic exchange flow under the influence of different temperature amplitude, hydraulic conductivity and channel gradients (See Figure 4.1). We therefore implemented a detailed flow, heat and transport model for the stream sediments and impose diurnal fluctuations in water column at the sediment-water interface (SWI). Our modeling domain (Ω); represents homogeneous and isotropic stream sediments. See Figure 4.2. This domain is bounded at the top by the SWI ($\partial\Omega_{SWI}$), which is assumed sinusoidal $Z_{\mathrm{SWI}} = \frac{\Delta}{2}\sin(\frac{2\pi x}{\lambda})$ where Δ [L] and λ [L] are the characteristic amplitude and wavelength of the ripple. The total length and depth of the modeling domain are $L = 3\,\lambda$ and d_b [L], respectively. These dimensions are selected to avoid boundary effects in the numerical simulations. COMSOL Multiphysics is used for the numerical solution of the proposed model.

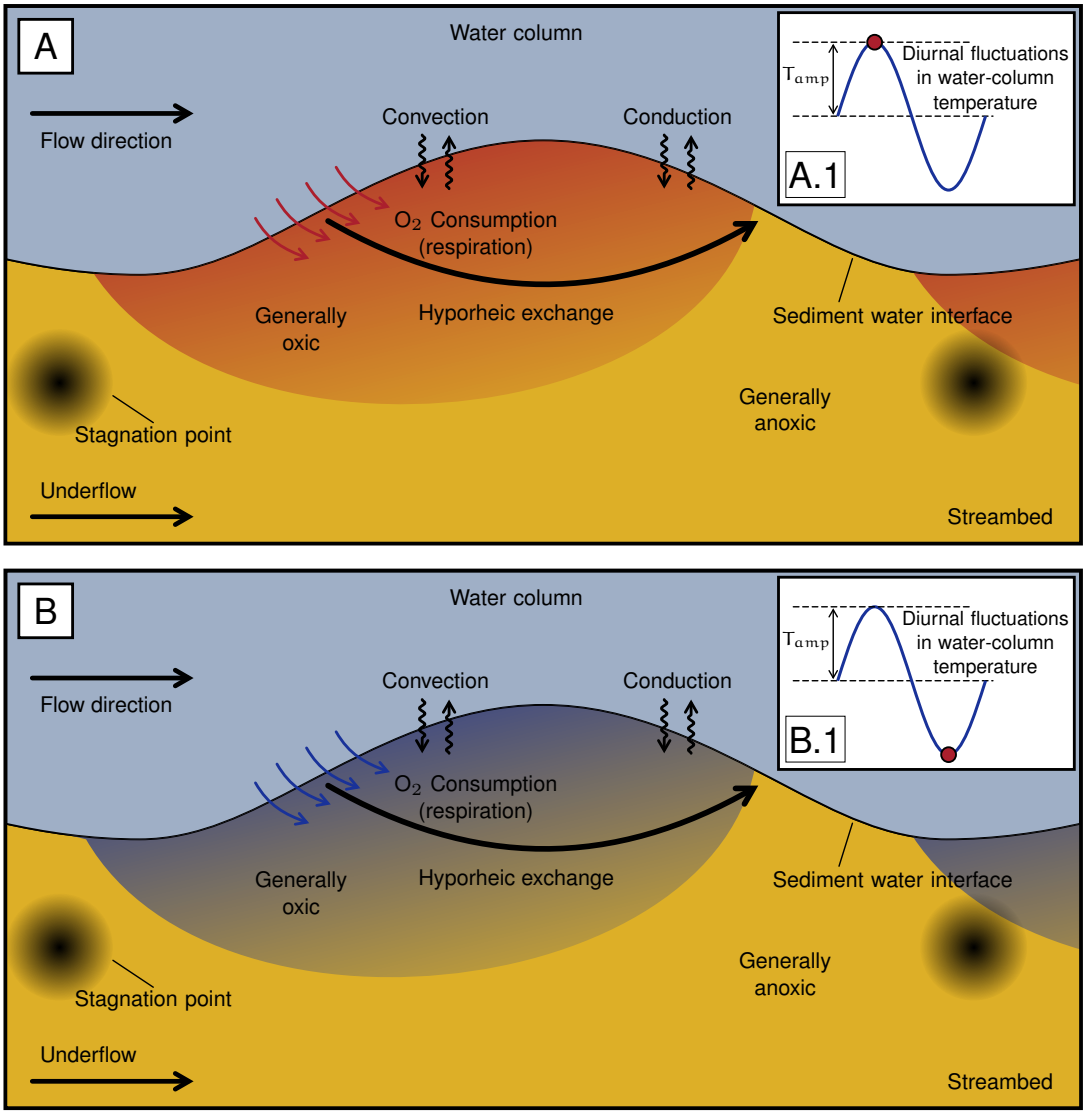

FIGURE 4.1: Conceptualisation of heat transport and hyporheic exchange within the streambed. A: Heat propagation at times of maximum water column temperatures (A.1) and B: Heat flow during during the coldest point of a diurnal temperature oscillation (B.1). Stream flow direction is from left to right.Relationship of heat transport and hyporheic exchange could be more complex than depicted in the figure.

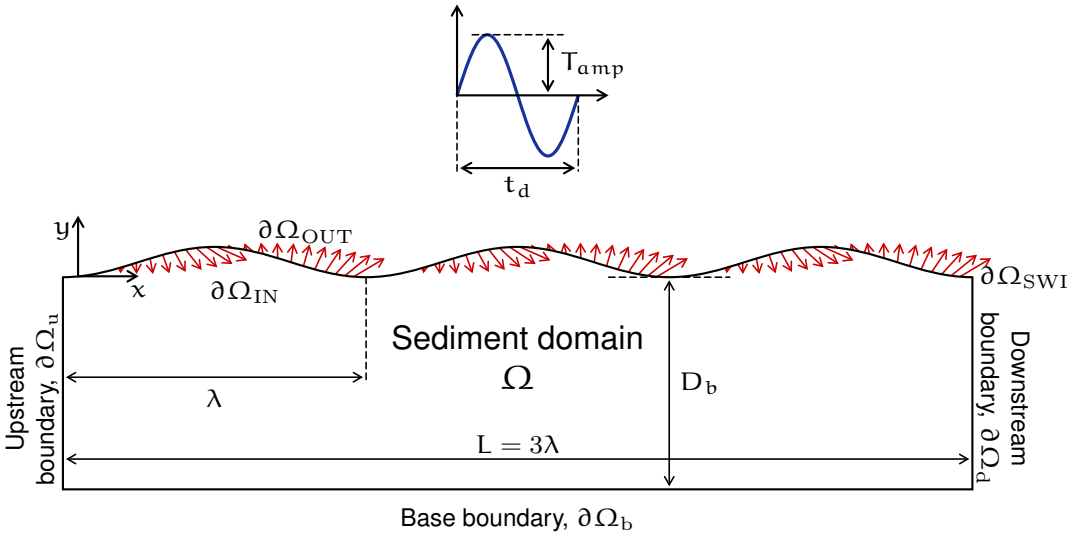

FIGURE 4.2: Schematic representation of the reduced-order model. Hyporheic exchange is affected by hydraulic conductivity, channel gradient and temperature variations in the surface water column. Flow direction is from left to right.

4.2.2 Flow model

Flow within the stream sediments is modeled as a fully saturated homogeneous and isotropic porous media using the groundwater flow equation and Darcy's law (Bear 1972).

$$\nabla \cdot \left[\rho \frac{\kappa}{\mu} \big(\nabla p + \rho g \nabla z \big) \right] = 0 \tag{4.1}$$

where $\mathbf{x} = (x, y)$ is the spatial location vector of dimension [L], $p(\mathbf{x}, t)$ is pressure [$\mathrm{ML^{-1}T^{-2}}$], g is the acceleration due to gravity [$\mathrm{LT^{-2}}$], κ is the permeability [$\mathrm{L^2}$], ρ is fluid density [$\mathrm{ML^{-3}}$], μ is fluid dynamic viscosity [$\mathrm{ML^{-1}T^{-1}}$], hydraulic head is $h = \frac{p}{\rho g} + z$, and Darcy velocity is $\mathbf{q} = -\frac{\kappa}{\mu}(\nabla p + \rho g \nabla z)$. The storage term is considered negligible and hence hyporheic exchange with adjacent banks is not considered. Temperature-dependency of the dynamic viscosity and density is described in the next section.

Flow is driven by pressure gradients at the SWI ($\partial\Omega_{SWI}$). In this case, a prescribed head distribution with a linear combination of head fluctuations induced by large- and small-scale bed topography has been assumed (Wörman et al. 2006, Stonedahl et al. 2010).

$$h_{SWI}(x) = H_0 - Z_{bed}(x) + \frac{2\,h_d}{\Delta}\, Z_{bed}\bigg(x + \phi \bigg) \tag{4.2}$$

where H_0 is the river stage, $Z_{SWI}(x)$ is the function describing the bed topography. Dynamic head follows the bed topography with a phase shift of ϕ. $h_d(t)$ is the

intensity of the dynamic head fluctuations (Elliott & Brooks 1997) defined by

$$h_d = 0.28\frac{U_s^2}{2g}\begin{cases}\left(\dfrac{\Delta}{0.34\,H_0}\right)^{3/8} & \text{for } \dfrac{\Delta}{H_0} \leqslant 0.34 \\ \left(\dfrac{\Delta}{0.34\,H_0}\right)^{3/2} & \text{for } \dfrac{\Delta}{H_0} > 0.34\end{cases} \tag{4.3}$$

where the mean velocity is estimated with the Chezy equation for a rectangular channel as $U_s = M^{-1}H_0^{2/3}S^{1/2}$ with M is the Manning coefficient [$\mathrm{L}^{-1/3}\mathrm{T}$] (Dingman 2009).

Assuming that bedforms repeat periodically along the channel, we implemented a periodic boundary condition for the lateral boundaries ($\partial\Omega_u$ and $\partial\Omega_d$; $p(x = -L, y, t) = p(x = 2L, y, t) + \rho g[h_{SWI}(x = -L, t) + h_{SWI}(x = 2L, t)]$). Under neutral groundwater conditions, the only groundwater flow constraining the HZ is the ambient flow driven by the channel gradient, and therefore no-flow is assumed for the lower boundary, $\partial\Omega_b$. The depth of this boundary, d_b was chosen to minimize any potential boundary effects.

The SWI ($\partial\Omega_{SWI}$) can be discretized into inflow ($\partial\Omega_{in,SWI} = \{\mathbf{x} \mid (\mathbf{n}\cdot\mathbf{q} < 0) \wedge (\mathbf{x} \in \partial\Omega_{SWI})\}$) and outflow sub-boundaries ($\partial\Omega_{out,SWI} = \{\mathbf{x} \mid (\mathbf{n}\cdot\mathbf{q} > 0) \wedge (\mathbf{x} \in \partial\Omega_{SWI})\}$) such that $\partial\Omega_{SWI} = \partial\Omega_{in,SWI} \cup \partial\Omega_{out,SWI}$. Here, $\mathbf{n}$ is an outward vector normal to the boundary. Notice that these boundaries are dynamic in nature owing to the variations in the temperature of the water column.

4.2.3 Heat transport model

Heat transport in porous media is described by the *heat transport equation* (HTE) (Bejan 1993, Nield & Bejan 2013)

$$\frac{\partial T}{\partial t} = \nabla \cdot (\mathbf{D_T}\, \nabla T) - \nabla \cdot (\mathbf{v_T}\, T) \tag{4.4}$$

where T is temperature [Θ], $\mathbf{v_T} = (\rho_f\, c_f)/(\rho\, c)\mathbf{q}$ is the thermal front velocity [LT^{-1}],$\mathbf{D_T}$ is the hydrodynamic thermal dispersion tensor [$\mathrm{L}^2\mathrm{T}^{-1}$], and $\rho\, c$ is the specific volumetric heat capacity [$\mathrm{ML}^{-1}\mathrm{T}^{-2}\Theta^{-1}$]

$$\rho\, c = \theta\, \rho_f\, c_f + (1-\theta)\, \rho_s\, c_s, \tag{4.5}$$

$\rho_f\, c_f$ specific volumetric heat capacity of the fluid [$\mathrm{ML}^{-1}\mathrm{T}^{-2}\Theta^{-1}$], and $\rho_s\, c_s$ specific volumetric heat capacity of the solids [$\mathrm{ML}^{-1}\mathrm{T}^{-2}\Theta^{-1}$]. The longitudinal (subscript l) and transversal (subscript t) components of the hydrodynamic thermal dispersion tensor are given by (Bear 1972, De Marsily 1986)

$$D_{l,t} = \frac{\kappa_T}{\rho\, c} + \beta_{l,t} |\mathbf{v_T}| \tag{4.6}$$

where β_l and β_t are the longitudinal and transverse thermal dispersivity coefficients [L], respectively, and κ_T is the bulk thermal conductivity [$\mathrm{MLT}^{-3}\Theta^{-1}$] (Woodside & Messmer 1961, Rau et al. 2014)

$$\kappa_T = \kappa_f^{\theta} \cdot \kappa_s^{1-\theta} \tag{4.7}$$

with κ_f and κ_s is the thermal conductivity of the fluid and solids, respectively.

Boundary conditions at the SWI ($\partial\Omega_{SWI}$) and lateral boundaries ($\partial\Omega_u$ and $\partial\Omega_d$) are given by

$$T(\mathbf{x}, t) = T_s \quad \text{on } \partial\Omega_{in,SWI} \tag{4.8a}$$

$$\mathbf{n} \cdot (\mathbf{D_T} \nabla T) = 0 \quad \text{on } \partial\Omega_{out,SWI} \tag{4.8b}$$

$$T(x = -L, y) = T(x = 2L, y) \text{ for } \partial\Omega_u \text{ and } \partial\Omega_d \tag{4.8c}$$

where T_s is the temperature of the water column [Θ], which is assumed to vary diurnally ($t_d = 1\,\text{day}$) as a periodic function

$$T_s(t) = T_{sm} + T_{amp} \sin\left(\frac{2\pi}{P} t\right) \tag{4.9}$$

where T_{sm} is the mean diurnal temperature and T_{amp} is the amplitude of temperature fluctuations over one day.

Boundary conditions at the bottom ($\partial\Omega_b$) depend on the magnitude of the basal flow. In this manuscript we only take into account neutral (neither gaining nor losing) conditions ($q_s = 0$) and hence,

$$\mathbf{n} \cdot (\mathbf{v_T} T - \mathbf{D_T} \nabla T) = 0 \quad \text{on } \partial\Omega_b \tag{4.10}$$

The viscosity and density of water are sensitive to temperature and thereby we couple flow and heat transport with the equation of state used by Cardenas et al. (2012). Dynamic viscosity is given by

$$\mu(T) = m_5 T^5 + m_4 T^4 + m_3 T^3 + m_2 T^2 + m_1 T + m_0 \tag{4.11}$$

where viscosity is in Pa·s, temperature is in °C and $m_5 = -3.916 \times 10^{-13}$, $m_4 = 1.300 \times 10^{-10}$, $m_3 = -1.756 \times 10^{-8}$, $m_2 = 1.286 \times 10^{-6}$, $m_1 = -5.895 \times 10^{-5}$, and $m_0 = 1.786 \times 10^{-3}$.

Density is given by

$$\rho(T) = \rho_0 - \rho_0\,\alpha(T - T_0) \tag{4.12}$$

where the reference density and temperature are $\rho_0 = 991.1\,\mathrm{kg/m^3}$ and $T_0 = 20^\circ\,\mathrm{C}$, respectively, and the thermal expansion coefficient is $\alpha = 2.067 \times 10^{-4\circ}\,\mathrm{C}^{-1}$.

4.2.3.1 Thermal peclet number

The Peclet number Pe_T is a dimensionless number used in calculations involving convective and conductive heat transfer. To study the relative contributions of convective and conductive heat transfer processes on the hyporheic exchange, we use the following equation

$$Pe_T = \frac{\rho_f\, c_f}{\kappa_{T0}} |\mathbf{q}| L \tag{4.13}$$

where L is a characteristic length for the heat transport problem being considered. When $Pe_T > 1$, convection dominates and when $Pe_T < 1$ conduction dominates.

4.2.3.2 Temperature-dependent reaction rates

The Arrhenius' rate law describes how variations in temperature affect reaction rates (Langmuir 1915)

$$r_T = r_R \exp\left[\frac{E_a(T - T_R)}{R_u\, T\, T_R}\right] \tag{4.14}$$

where T is the current absolute temperature [°K], T_R is the reference absolute temperature [°K], E_a is the activation energy, and R_u is the universal gas constant and r_R is the pre-exponential factor. The above version of Arrhenius equation accounts for the temperature distribution within the streambed.

4.2.4 Solute transport model and tracking of the hyporheic zone

The *advection-dispersion equation* (ADE) is used to model the transport of conservative solutes within the porous media domain (Bear 1972)

$$\theta \frac{\partial C}{\partial t} = \nabla \cdot (\mathbf{D} \nabla C) - \nabla \cdot (\mathbf{q} C) \tag{4.15}$$

where C is concentration [ML^{-3}], $\mathbf{q}$ is the Darcy flux [LT^{-1}], and $\mathbf{D} = \{D_{ij}\}$ is the dispersion-diffusion tensor defined as (Bear 1972):

$$D_{ij} = \alpha_T |\mathbf{q}| \delta_{ij} + (\alpha_L - \alpha_T) \frac{q_i \, q_j}{|\mathbf{q}|} + \frac{\theta}{\xi_m} D_m \tag{4.16}$$

with α_T and α_L the transverse and longitudinal dispersivities, D_m the effective molecular self-diffusion coefficient, $\xi_m = \theta^{-1/3}$ is the fluid tortuosity (defined here with the Millington and Quirk model (Millington & Quirk 1961)), and δ_{ij} is the Kronecker delta function.

Modelling the transport of a conservative tracer allows us to explore the mixing and extend of the HZ. We assume that the concentration of the tracer in the stream water column is C_s, and therefore a prescribed boundary condition $C(\mathbf{x}, t) = C_s$ is used along the SWI's inflow areas ($\partial\Omega_{in,SWI}$). Outflow areas ($\partial\Omega_{out,SWI}$) along

the SWI are advective boundaries where $\mathbf{n} \cdot (\mathbf{D}\nabla C) = 0$. Lateral boundaries ($\partial\Omega_u$ and $\partial\Omega_d$) are periodic boundaries $C(x = -L, y) = C(x = 2L, y)$ and the bottom boundary ($\partial\Omega_b$) is a no-flow boundary $\mathbf{n} \cdot (\mathbf{q}C - \mathbf{D}\nabla C) = 0$. In this case, the HZ is defined as the zone with at least 95% of the pore water originated from the stream (*i.e.* , $C \geq 0.95C_s$).

4.2.5 Characteristic scales, Monte-Carlo analysis and scenarios

Using the scaling analysis on the heat transport equation (Bejan 1993, Nield & Bejan 2013), the time scale for heat transport is described and estimated by the following equation

$$t_c = \frac{\lambda^2}{(\mathbf{D_T} + \mathbf{v_c}\lambda)} \tag{4.17}$$

and characteristic q_c is the similar as calculated previously (Wu et al. 2018)

$$q_c = K_c \frac{SH_0\Delta^{1/3}}{2gM^2\lambda} \tag{4.18}$$

Monte-Carlo approach was adopted to generate histograms of characteristic time scale for heat transport and ratio between hyporheic exchange and the ambient flow within the streambed (See Figure 4.3). In order to explore a consistent range of scenarios, we compiled hydraulic variables and then used typical values to parameterise the model (Gomez-Velez & Harvey 2014*a*, Bridge 2009, Buffington & Tonina 2009). Hydraulic conductivity was constrained and estimated based on typical grain-size for each morphology and Kozeny-Carman equation. Ranges of typical grain sizes (D_{50} : 10^{-4} to 10^{0} mm for ripples were used (Gomez-Velez & Harvey 2014*a*, Bridge

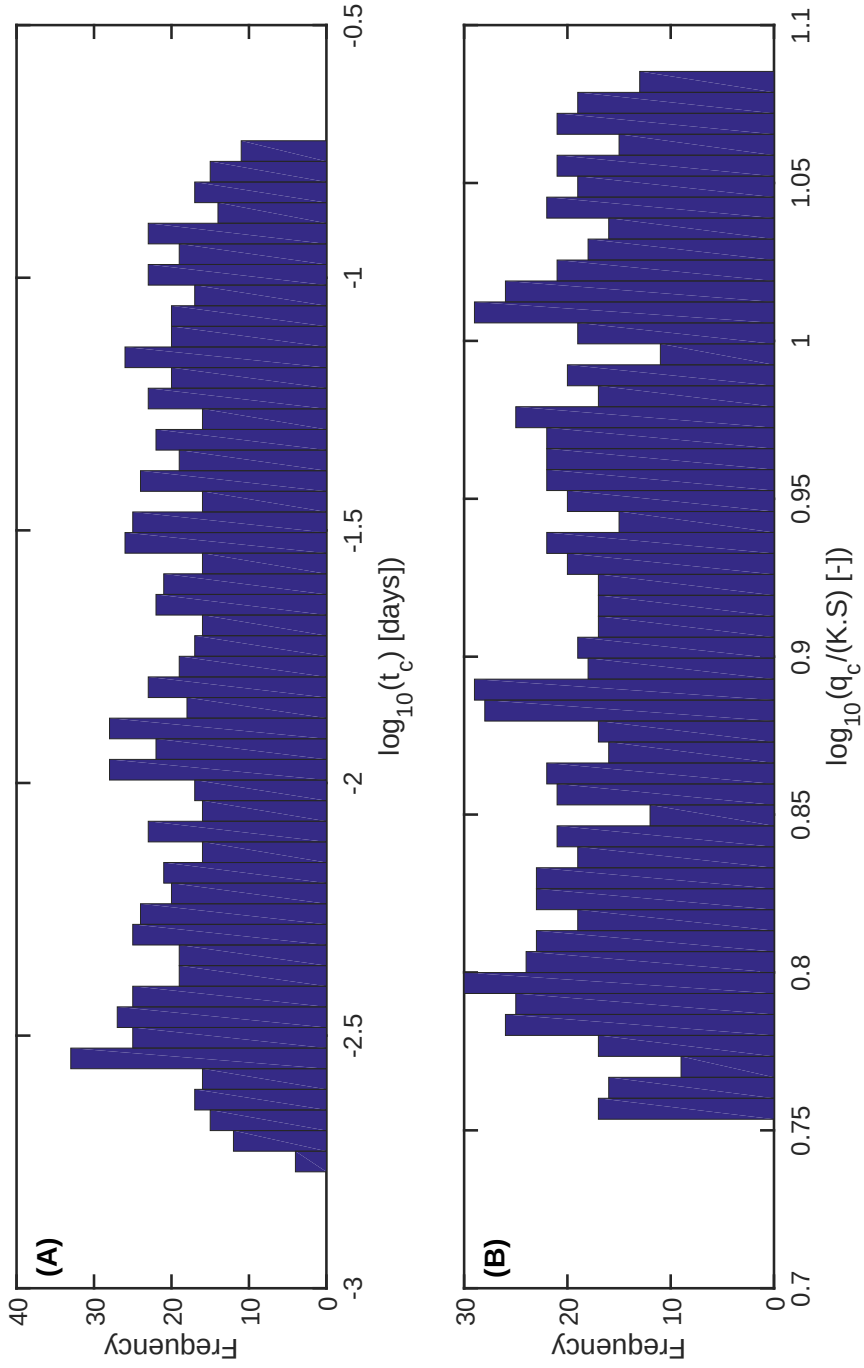

FIGURE 4.3: Monte Carlo analysis for the characteristic time scale for heat transport (t_c) for ripples (A) and ratio between hyporheic exchange and ambient groundwater flow (q_c/KS) for ripples (B).

TABLE 4.1: Parameterisation of the numerical model

Parameters	Value	Description
Constant model parameters		
Δ/λ	0.1	Bedform aspect ratio
M	0.03	Manning's coefficient
θ	0.3	Porosity
α_L	0.05 m	Longitudinal dispersivity
α_T	0.005 m	Transverse dispersivity
ρ_f	991.102 kgm^{-3}	Fluid density (at 15 °C)
ρ_s	1905 kgm^{-3}	Density of solid
μ_d	0.0011373 Pa s	Fluid dynamic viscosity (at 15 °C)
c_f	4185.5 J/kg.K	Specific heat capacity of fluid
c_s	780 J/kg.K	Specific heat capacity of solid
k_f	0.591 W/mK	Thermal conductivity of fluid
k_s	2 W/mK	Thermal conductivity of solids
g	9.81 ms^{-2}	Acceleration due to gravity
T_{sm}	$15°C$	Mean diurnal temperature
E_a	60 kJ/mol	Activation energy for aerobic respiration
R_u	8.314 J/mol.K	Universal gas constant
Varied model parameters		
K	$10^{-3}, 10^{-4}, 10^{-5} m/s$	Hydraulic conductivity
S	10^{-2}, 10^{-3}, 10^{-4}	Channel slope
T_{amp}	$0, 1, 3$ and $5°C$	Amplitude of temperature fluctuation

2009). The modified version of Kozeny-Carman Equation (Koltermann & Gorelick 1995, Porter et al. 2013) is given by $K = \frac{142*(D_c \times 1000)^{1.62}}{24 \times 3600}$ where D_c in mm and K in m/s. To explore different heat transport time scales we varied hydraulic conductivity from 10^{-3} m/s, 10^{-4} m/s and 10^{-5} m/s and channel slopes from $10^{-2}, 10^{-3}$ and 10^{-4}. Apart from the variability of hydraulic parameters, we also varied the peak amplitude of temperature (T_{amp}) and used the values 0°, 1°C, 3°C and 5°C. We provide a list of constants and varied model parameters used for performing the numerical simulations in Table 1.

4.3 Results and Discussion

4.3.1 Flow field and temperature field

The local bedform topography at the sediment-water interface (SWI) induce pressure gradient and modulate the flow of water (Figure 4.4 (B)) and heat (Figure 4.4 (C)) into the streambed. Variations in bedform topography alters the spatial distribution of heat within the hyporheic zone (HZ) (See Figure 4.4 (C)). Notice that the flow is steady and hence any variations in heat distribution solely relies on the resultant hyporheic flow due to the bedform aspect ratio and temperature variations in the water-column. Visually, the changes in the flow field is difficult to perceive, however the temperature change is inducing change in magnitude and direction of exchange flow (see Figure 4.4 (B)), primarily closer to the SWI and stagnation points. This is in line with the findings of Winter (1998). It is important to note that this distribution of flow and temperature field is dependent on transport

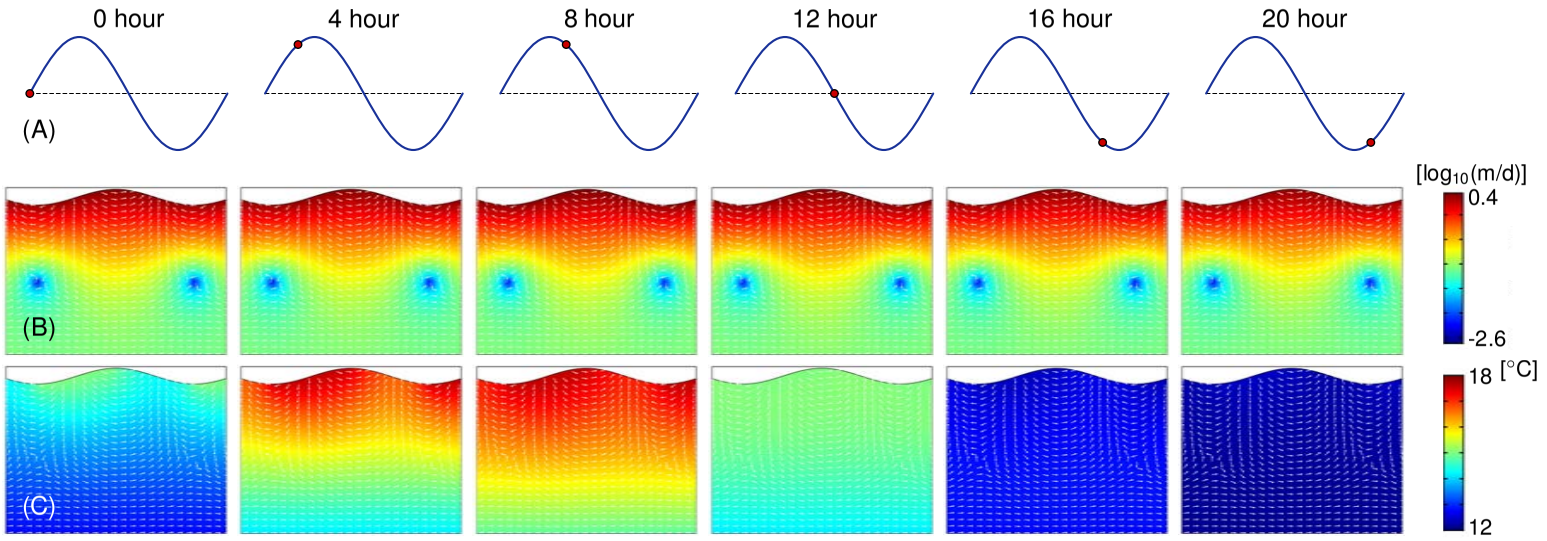

FIGURE 4.4: Snapshots of the (B) flow field (white arrows represent direction and not proportional to magnitude) within the sediment at different times. Row (A) depicts the the temporal change in temperature. Coloured surface represents the magnitude of Darcy flux vector in log scale m/d. Second row depicts (C) thermal dynamics with flow field within the sediment at different times. Coloured surface represents the temperature in °C. For all panels, temperature amplitude is 3 °C, bedform aspect ratio is 0.1, the slope is 10^{-3} and the hydraulic conductivity is 10^{-3} m/s. Vertical and horizontal axis are scaled by the bedform wavelength.

time scales determined by parameters such as hydraulic conductivity and channel slopes, discussed in detail in the next sections.

Figure 4.4 (C) depicts the temporal evolution of heat dynamics with respect to different different temperatures during the day. Complicated but predictable thermal dynamics are observed within the streambed. The transient temperature affects the spatial thermal distribution during different times of the day. For example, thermal forcing penetrates deeper into the streambed after the peak increase is attained (See Figure 4.4 columns 8 hr and 16 hr) compared to the times before the peak is attained. This finding is in line with Cardenas & Wilson (2007*a*). Owing to the heat convection caused by the advective flow strong changes in temperature are observed at the downwelling regions of the bedform. Therefore, warm and cool temperatures within the streambed were more pronounced in downwelling regions. The heat distribution was observed relatively less heterogeneous during the colder times of the day.

4.3.2 Hyporheic exchange flux and flux-weighted temperature leaving the HZ

We coupled flow with heat using a temperature-dependent relationship of viscosity and density of water *i.e.* using the equations 4.11 and 4.12. The major driving force being topography in the model set-up, any change in flow fields and the hyporheic exchange flux within the bedform is caused by the temperature change. Variations in the temperature causes hydraulic conductivity to change. This is due to the dependency of the hydraulic conductivity on temperature-dependent density and dynamic viscosity ($K = \kappa\rho g/\mu_d$).

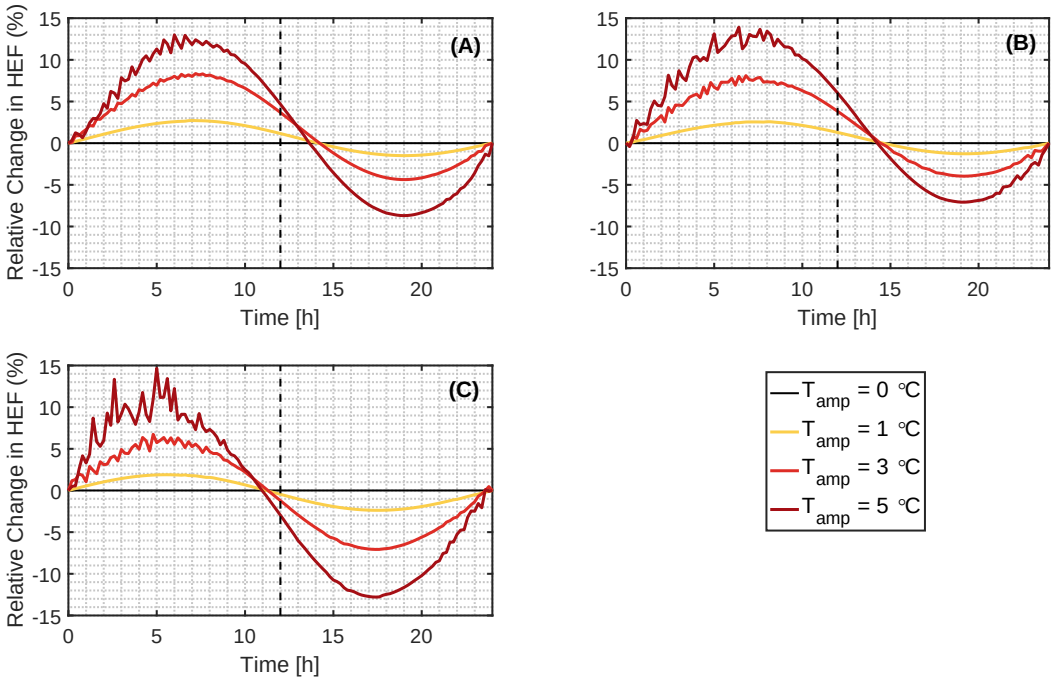

FIGURE 4.5: Relative change in hyporheic exchange flux [%] as a function of time (*hours*) for the T_{amp} of 0 °C, 1 °C, 3 °C and 5 °C for the values of hydraulic conductivity A) 10^{-3}, B) 10^{-4} and C) 10^{-5}. Slope value used is 10^{-3} and bedform aspect ratio of 0.1.

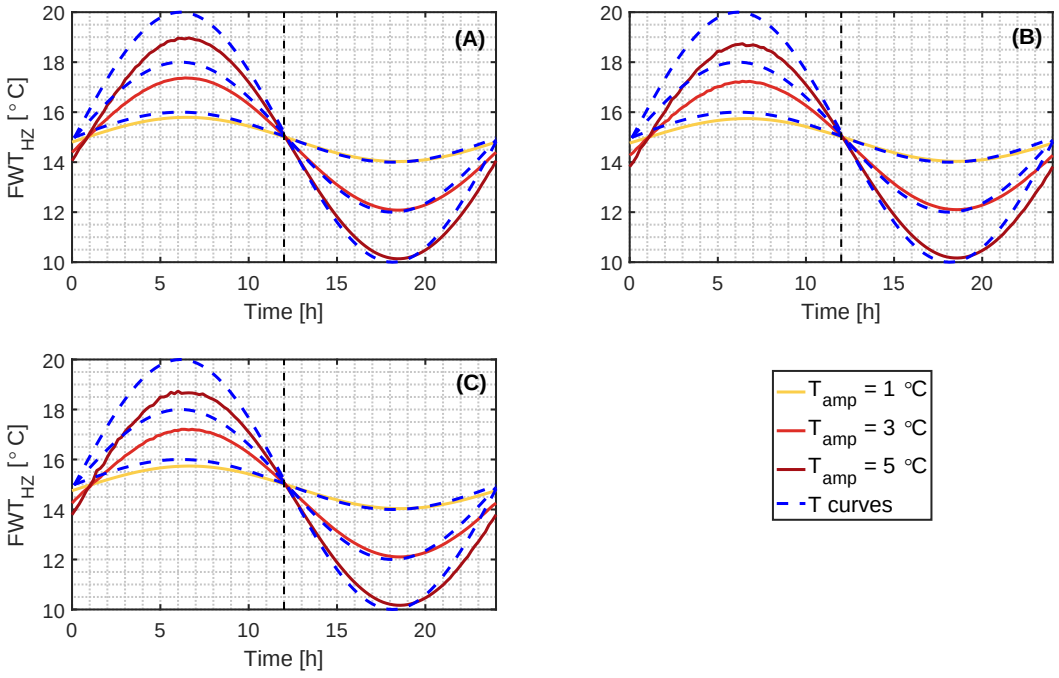

FIGURE 4.6: Flux weighted temperature [%] leaving the HZ as a function of time (*hours*) for the T_{amp} of 1 °C, 3 °C and 5 °C for the values of hydraulic conductivity A) 10^{-3}, B) 10^{-4} and C) 10^{-5}. Slope value used is 10^{-3} and bedform aspect ratio of 0.1.

We found that while hyporheic exchange flux across the SWI expectedly increased with increasing temperature, the trend observed did not coincide with the trend of imposed temperature curve (Figure 4.5). Decreasing hydraulic conductivity exhibited a negative shift in lag in the discharge of hyporheic waters. The left phase shift of the hyporheic exchange flux for higher hydraulic conductivity can be explained by the warm hyporheic waters present deeper within the streambed after the highest amplitude peak of the surface water column is attained. Conductive and convective heat flow increases with increase in temperature. The change in hyporheic flux is more pronounced when the temperatures are higher, when compared to the cooler parts of the day. Moreover, increased temperature amplitude also increased the relative change (%) change in hyporheic exchange flux. This is in agreement with the findings by Cardenas & Wilson (2007*a*) where authors showed that thermally induced fluid viscosity variations cause periodic but non symmetric changes in fluid flux through the sediments. In addition, decrease in the magnitude of hydraulic conductivity exhibits slight decrease in the percentage increase of the hyporheic exchange flux. The results indicate that even without considering variables such as evaporation and flow dynamics, temperature-induced dynamic viscosity leads to substantial increase or decrease in hyporheic exchange flux. When taken into consideration other potential external drivers such as solar radiation, tree shading, air temperature, groundwater inputs, and wind speed (Burkholder et al. 2008), the heat input to the HZs may considerably change and so the hyporheic exchange flux. Numerical artefacts were observed to increase with increased temperature amplitude T_{amp} and decreased hydraulic conductivity K.

We evaluated the flux-weighted temperature leaving the HZ to understand and explain the influences of hyporheic exchange on surface water temperature cycles

(Figure 4.6). The simulation results show that the diurnal temperature cycles in discharged hyporheic waters are cooled, buffered and lagged (definition of buffered and lagged used from Arrigoni et al. (2008)). These findings are in line with Arrigoni et al. (2008). The lagged and buffered temperatures are associated to the discharge of cooler temperatures for warmer part of the surface water temperature cycles and warmer for the cooler part. However, we also found out that this lag and buffering is highly dependent on heat transport timescales *i.e.* on the values of hydraulic conductivity. For shorter heat transport timescales (see Figure 4.6 (A)), the hyporheic waters are relatively less cooled when compared to scenarios with longer heat transport timescales. The results also indicate that the differences between the stream-water temperature and the hyporheic water temperature is larger during the warmer times of the day whereas the temperature of stream waters and hyporheic waters almost coincide during cooler times— particularly for lower temperature amplitudes. In the presence of transient thermal mosaic of heat dampening in the streambed , the crucial explanations for the differential behaviour of FWT cycles is attributed to the advection and dispersion of surface water temperature cycles. The warmer phase in temperature causes maximum variations in the fluxes, causing increased subsurface flow velocities compared to the colder phase of the day, hence exhibits similar temperatures to the surface-water temperature cycles. The result indicate that HZs can provide a cooler habitat for biota and hatchery for salmonid and invertebrate eggs. Thus HZ can provide effective refuge to temperature-sensitive species. The presence of buffered and lagged temperature variations throughout the day points the dynamic behaviour of HZ and its ability to provide cooler habitats even during warm parts of the day

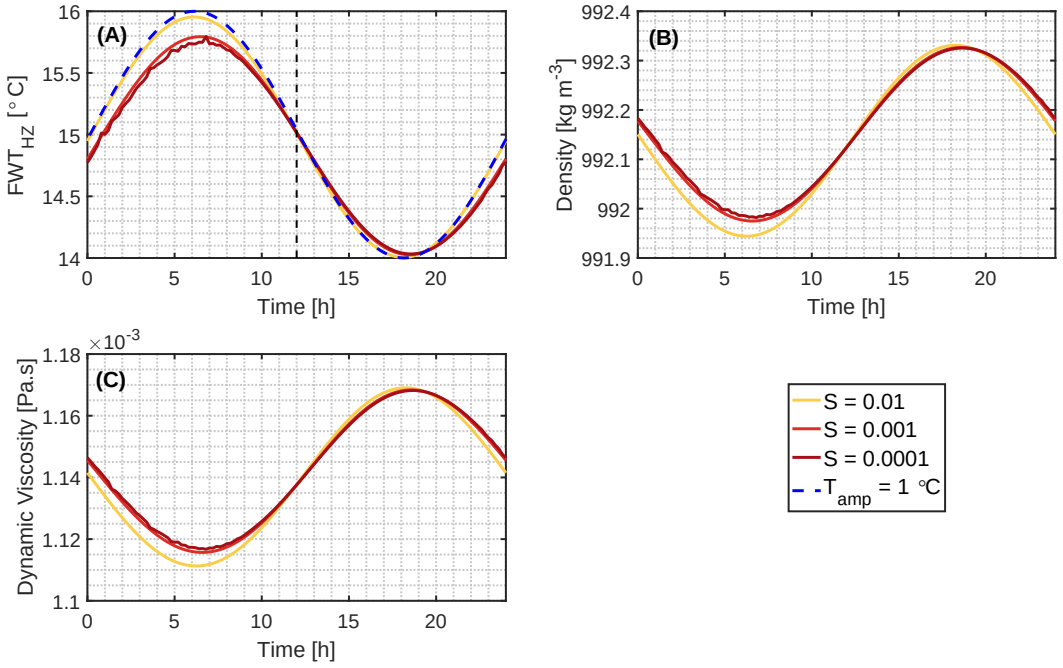

FIGURE 4.7: Depiction of impact of channel slopes on (A) flux weighted temperature [%] leaving the HZ as a function of time (*hours*) for the T_{amp} of 1 °C, variations in (B) density of water and (C) dynamic viscosity due to change in temperature cycle with an amplitude of 1°C for the slope values of 0.01, 0.001 and 0.0001. For all panels, hydraulic conductivity is 10^{-3} and bedform aspect ratio of 0.1.

4.3.3 Impact of channel slopes

To further explore the impact of another crucial moderator namely, ambient groundwater underflow on heat propagation, we performed simulations with varying channel slopes (0.01, 0.001 and 0.0001). The simulation results highlight the importance of ambient groundwater flow (proportional to channel slope) and its moderating role under both steady flow conditions and varying temperature fluctuations of the water column (Figure 4.7).

Values of channel slopes that determines the ambient groundwater flow in the streambed, strongly modulates the hyporheic thermal characteristics as well as density and dynamic viscosity of water in the streambed. Flux-weighted temperature leaving the HZ nearly coincides with the temperature oscillations in the stream water for higher channel slope value ($S = 0.01$ in Figure 4.7). However, for the decreased value of slopes the temperature leaving the stream is cooled and lagged (see $S = 0.001$ and $S = 0.0001$ in Figure 4.7). Steeper channel slopes ($S = 0.01$) promote higher underflow velocities, this results in rapid influx and outflux of heat to and fro the SWI. The importance of streambed slopes on hyporheic exchange has been highlighted for steady state discharge conditions by Cardenas & Wilson (2007*a*) and Tonina & Buffington (2009).

4.3.4 Thermal peclet number

The relative dominance of heat convection *vs* conduction is captured by dimensionless Peclet number (Pe_T) that depends on local bedfom patterns, hydrodynamic and thermal properties of streambed and the oscillations in surface water temperature.

Spatial and temporal distribution of Pe_T (in log scale) are presented in Figure 4.8. It is apparent that when the Pe_T is large, mainly evident near to the peaks of the temperature amplitude (Figure 4.8 (B)), heat convection dominates. When Pe_T is small, mainly evident close to the mean stream water temperatures, heat conduction dominates.

Under warmer temperatures, the value of $Pe_T > 0$ was primarily observed closer to the SWI. Conduction is mainly active around the stagnation zones at all times during the day. The results demonstrate that the heat-convection dominant regions enlarges after the peak-amplitude is attained (see Figure 4.8 (B) 8 hour). The transition between convection and conduction processes (*i.e.* when $Pe_T = 0$, see the white line in Figure 4.8 (B)), also moves considerably with stream temperature oscillations. This transition is more dynamic in the warmers parts of the day. Pe_T show higher sensitivity to small changes in temperature during the warmer phase of the day. This is mainly because advection dominates the heat exchange due to increased in the fluid flux in the sediments. As also shown by the Cardenas & Wilson (2007*a*), mechanical dispersion may have a measurable, however minor impact on the temperature field. It is important to note that as the heat convection highly depends on channel flow rates and conduction depends on thermal properties of streambed sediments, the spatial distribution of heat processes domination can vary to a large extent.

4.3.5 Temperature-dependent reaction rate

Hyporheic zones are subject to spatially and temporally varying temperatures. A diel temperature pattern following stream water penetrate through the SWI and

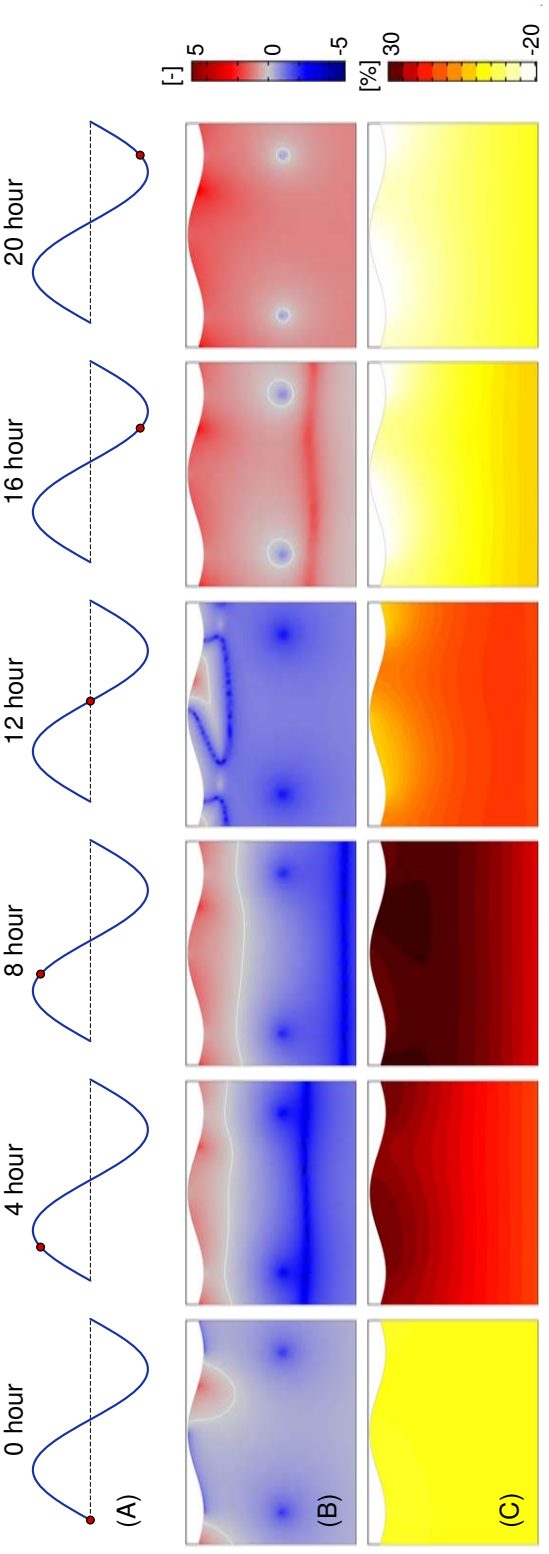

FIGURE 4.8: Snapshots of the spatial distribution of (B) thermal Peclet number (in log scale) at different times. Row (A) depicts the the temporal change in temperature. Second row depicts (C) temperature-dependent reaction-rate (%) using Arrhenius equation at different times of the day. For all panels, temperature amplitude is 3 °C, bedform aspect ratio is 0.1, channel slope is 10^{-3} and the hydraulic conductivity is 10^{-3} m/s. Vertical and horizontal axis are scaled by the bedform wavelength.

result in a dynamic temperature distribution within streambed, which could potentially affect the biogeochemical reactions in the HZ. Biogeochemical reaction rates are strongly controlled by, and coupled to hydrodynamic processes as evident by the simulation outcomes (Figure 4.8 (C)). Furthermore, most biogeochemical reactions are sensitive to temperature, especially bacterially mediated nitrogen transformation reactions. Solubility of solutes like dissolved oxygen is also considerably dependent on the factors like temperature and pH which in turn highlights the overall importance of temperature on the biogeochemical processes within the HZ.

The simulation results indicated that there was substantial variation in the reaction rates with changes in surface water temperature. As expected, the general pattern shows the increase in reaction rate with the increase in temperature and the eventual decrease when the temperatures cool down. However, the snapshots (Figure 4.8 (C)) highlights that the spatial distribution of reaction rates were highly dependent on temperature distribution in the streambed and indicates the relative importance of heat transfer processes in determining the reaction rates at different depths within the HZ.

According to the Arrhenius relationship, the reaction rate increases with increasing temperature, and the simulation results demonstrate similar patterns. The highest reaction rates are observed at the times of the day when the maximum peak was attained. When the temperature starts to decline and reach the mean temperatures, the HZ can still exhibit high reactive period. This is mainly due to the lagged transfer of heat in the HZs. Further decline in the temperatures causes low reactive regions close to the SWI where the water is downwelling. Interestingly, during the times of the day with lower temperatures, high percentage of reaction rate were observed in deeper hyporheic depths *i.e.* $t = 12$ and 16 hour.

The temporal variability induced by oscillating temperatures is highly complex to be captured in the field experiments. This is because measurements of reaction rates may not be the representative of the system. Results also indicate that it would also be very crucial to get the specific location (depth) which could provide the daily averaged reaction rate to represent the potential reactive zones. For instance, during the hours of the day with lower amplitude of temperature, when usually assumed that HZs is a low or inactive reactive zone, there is a potential of reactions occurring at certain depths and longer flow paths. Provided that the heat propagation could also be lagged and buffered depending on the hydraulic parameters, there are possible uncertainties and misinterpretation involved with the field measurements.

4.3.6 Geomorphic controls on thermal dynamics

The fully coupled heat-flow model using temperature-dependent dynamic viscosity and density caused variations in the flow velocities. Increased flow velocities due to increased temperature amplitude of diurnal oscillations in temperature (T_{amp}) cause deeper penetration of the heat into the streambed. The dominance of the thermal convection is directly related to change in hydraulic conductivity, channel gradient and temperature oscillations in stream water.

The modelling results demonstrated that bedform topography and diurnal temperature oscillations induce significant and distinct thermal patterns within the streambed. The thermal patterns observed were in agreement with those presented by Cardenas & Wilson (2007*a*). Hyporheic flow induced by the topography along the streambed is the crucial driver of hyporheic exchange flows as they are considerably

responsible for altering the head gradients at the SWI (Elliott & Brooks 1997, Norman & Cardenas 2014). However, the results indicate that hydraulic conductivity and channel slopes that determine the heat transport scales are also primary controls of heat transfer in the streambed. Knowing that heat propagation is directly related to the exchange flows, these drivers and controls determine the thermal heterogeneity within the HZs. Noticeable impact is visible for the variations in the channel slopes that controlled the ambient groundwater flow within the streambed. It is also observed that the effect of the ambient groundwater flow on hyporheic fluxes is more pronounced for lower channel slope values. Increased hyporheic exchange flux is observed with the increase in temperature amplitude (T_{amp}) of the water column.

Our simulation results provide an overview of the impact of oscillations in temperature at various depths within the streambed. The imposed high temperature at the interface creates the memory effects of the temperature within the longer subsurface flow paths or the region where conduction dominates. Similar behaviour can be observed when the lowest temperature is imposed at the SWI, however this is highly dependent on the other hydraulic parameters like hydraulic conductivity and channel slopes. This presents a great deal of significance when we simulate temperature-dependent reaction rates using the Arrhenius equation. When temperature at the boundary of the SWI is assumed to be constant, these memory effects are not taken into consideration. Hence, locations or regions of biogeochemical hotspots with high reactive environment are observed even during times of the day when not predicted. The biogeochemical activity may occur within greater depths of the streambed where the residence times of water and solutes is higher compared to the shallower regions which are closer to the SWI.

4.3.7 Biogeochemical and ecological implications

Temperature acts as a *master variable* for various physical, chemical and biological processes occurring in the river-aquifer system (Cardenas & Wilson 2007*a*, Krause et al. 2014). Implementation of the Arrhenius relationship in the simulations briefly uncovers the potential implications of thermal dynamics on the biogeochemical processes.

The inclusion of the heat transport domain in the simulations can be complex as it includes numerous processes and simultaneous influences such as solar radiation, tree-shading or shading by vegetation, buoyancy effects, groundwater inflows, evaporation, (Story et al. 2003, Malcolm et al. 2004, Webb et al. 2008). Combined effects of these complex processes can spatially and temporally impact the hydrodynamic and thermal behaviour in the river-aquifer systems. Out of these processes, hyporheic exchange has been also found to be a primary control on the mixing, transport and spatio-temporal patterns of dissolved oxygen, nutrients and contaminants, redox reactions and physio-chemical habitat characteristics such as the riverbed temperature. Hence, hyporheic exchange controls residence times of water, solutes and contaminants within regions of variable reactivity.

Hyporheic zones are hot spots for nitrogen cycling and affect the fate of nitrogen molecules and compounds in aquatic systems (Krause et al. 2009, 2013, Zheng et al. 2016). Interplay and competition between the availability of reactants, temperature variations, flow dynamics, hydro-morphology of streambed, sediment properties results in naturally complex environment for biogeochemical transformations in the HZs. Field investigations and laboratory experiments have shown that the availability of labile dissolved organic carbon and oxygen depends on the environmental

factors such as temperature. Oxygen uptake rate is also a function of temperature and pH conditions (Zarnetske et al. 2011, 2012). Other biogeochemical reaction rates are also temperature-dependent (by Arrhenius equation) which therefore makes it essential to gain a mechanistic understanding of the thermal propagation and dynamics within the HZs. The outcomes of the sensitivity analysis show that diurnal fluctuations in temperature has a substantial effect on the hyporheic exchange flux and dynamic distribution of thermal conditions which eventually impact the spatial and temporal variability in reactive environment within the HZs.

4.3.8 Limitations of the study

The proposed reduced-order numerical model of an idealized, uniform and single-type of bedform is used to gain better mechanistic understanding of heat transportation within the HZs. While performing a systematic study, a wide range of plausible scenarios in terms of hydraulic conductivity, channel slope values, variations in diurnal oscillations of temperature are considered. However, there are also other variables and impactful drivers that have not been taken into account in this study. This includes complex three-dimensional flow field as well as the lateral hyporheic exchange, bedform migration and variability in streambed structural properties. The sediment bed is considered to be homogeneous and isotropic which is not usually the case in the natural systems. Furthermore, different grain sizes would require different times to thermally equilibrate. Local thermal equilibrium of the temperature of the fluid and solid phases at the interface is assumed to be equal. A better understanding of thermal patterns induced by various bedforms subject to different flow conditions also requires separate attention. This is because there could also be an increase in the stream temperature and hence the hyporheic

temperature due to anthropogenic inputs, for *e.g.* from urban waste water, which is also the result of increased stream-stage (Kinouchi et al. 2007).

4.4 Conclusions

The proposed two-dimensional reduced-order model is used to systematically explore the effects of temperature fluctuations in surface water, ambient groundwater flow and hydraulic conductivity on bedform-induced hyporheic exchange processes. This study integrates geomorphological controls and temperature dependence on hyporheic exchange flux and potential reaction rates within the streambed when dynamic change in temperature fluctuations is taken into consideration. Spatio-temporal distribution of the heat indicates stronger temperature variations in the downwelling regions of the bedforms. Higher thermal heterogeneous behavior was observed during warmer times of the day. Temperature-dependent viscosity and density considerably varied the relative change in hyporheic exchange fluxes. The trend observed for hyporheic exchange fluxes was both lagged and cooled, however the shift was highly dependent on the values of hydraulic conductivity. Hyporheic zones attenuated the surface-water temperature signals mainly for the warmer parts of the day and showed dependency on both hydraulic conductivity and channel slopes. Cooled and lagged temperatures owing to the thermal properties of the streambed were shown to affect the spatio-temporal distribution of reaction rates.

This study highlighted the importance of inclusion of heat processes in the study of hyporheic exchange processes. Temperature variations not only alter the hydrodynamics in the streambed but also impact the temperature-sensitive biogeochemical

reactions. Hence, it is essential to gain intricate understanding of the thermal propagation and thermal dynamics in the hyporheic zones. Such understanding can contribute to the better prediction of hyporheic chemistry as well as protection of habitat of aquatic species which is crucial for overall ecosystem functioning.

Chapter 5
REDUCED-ORDER MODELS FOR SIMULATING BEDFORM-INDUCED HYPORHEIC EXCHANGE UNDER TRANSIENT FLOW CONDITIONS

Reduced-order models are becoming more common to gain mechanistic understanding and predict hyporheic exchange processes. The parameterisation of these models typically assumes significant simplifications of channel characteristics, streambed physical and chemical properties, and groundwater inflows and outflows. Whilst reduced-order models have been essential for theoretical understanding of exchange fluxes and biogeochemical cycling at aquifer-river interfaces under steady state, and more recently, under transient stream flow conditions, generalized model simulations are rarely validated by field observations. Here, we test the applicability of reduced-order models to accurately represent the hyporheic exchange flow processes in a sequence of different bedforms, including step-pool and low-gradient run, by comparing them with high-resolution simulation of the bedforms. Model simulations are validated with observations of head observations and tracer breakthrough curves at multiple depths and locations during a range of streamflow conditions (including low-flow, base-flow and high-flow conditions) in a first-order boreal stream in Northern Sweden. Our results indicate that step-pool sequences of streambed topographic features with subsurface heterogeneity are adequately simulated by our model. In addition, delayed release of conservative tracers in the upwelling regions was predicted by the model which is usually not covered in the typical sampling time-frame. However, the spatial patterns of simulated hyporheic exchange flow paths and breakthrough curves in a low-gradient run differ from field-observations. Upstream and downstream bedforms are shown to have a significant impact on the simulated exchange flow paths of low-gradient run in the validated model. Our results, therefore, suggest that mechanistic knowledge derived from the simulation of bedforms should be considered with caution. The limitations of currently-used modelling approaches to upscale process-understanding from individual bedform simulations therefore need to be acknowledged.

5.1 Introduction

5.1.1 Process-based modelling of hyporheic exchange processes

Process-based models are increasingly deployed to study hyporheic exchange processes (Elliott & Brooks 1997, Cardenas & Wilson 2007*b*, Gomez-Velez et al. 2014). They have been used effectively to couple complex fluid hydrodynamics, biogeochemical and heat propagation processes occurring in the hyporheic zones from pore-scales to catchment scales (Walsh & Saar 2010, Boano et al. 2010, Cardenas & Wilson 2007*a*, Chen et al. 2010). They are based on principles of mass, momentum and energy balance to connect the forces acting at the sediment-water interface and inducing flow and transport into the streambed. As a result, they have immensely helped us to improve our mechanistic understanding of the nature of exchange flows in the streambed and also the role of residence times of water and solutes on biogeochemical transformations in the hyporheic sediments. However, there has been a pertinent challenge of bridging the gap of translating the understanding of spatial small-scale (geomorphic units) hyporheic exchange to large-scales such as in river-reaches and catchments (Boano et al. 2014).

5.1.2 Hyporheic interactions at multiple-scales

Hyporheic exchange flows are a resultant of complex interactions of drivers and controls at multiple scales. Multi-scale distributions of hyporheic subsurface flow

paths is a function of streambed topography, channel gradient, sediment permeability, spatial distribution of hydraulic heads and other sediment properties (Tonina & Buffington 2009, Buffington & Tonina 2009, Boano et al. 2014, Krause, Hannah, Fleckenstein, Heppell, Kaeser, Pickup, Pinay, Robertson & Wood 2011, Gomez-Velez et al. 2014, Cardenas 2008). These driving forces and controls trigger the hyporheic flow paths of many scales, potentially ranging from centimetres to kilometres (Poole et al. 2008, Wörman et al. 2007, Stonedahl et al. 2010, Cardenas 2008, Revelli et al. 2008). This resultant spatial variability of the hyporheic exchange as a consequence of complex topographic features is highlighted by Caruso et al. (2016).

The hydrodynamic factors interact with biogeochemical factors across wide range of spatial and temporal scales and eventually determine complex patterns of nested flow paths. The aforementioned variability of the HZ has a direct consequence on residence times, which range from seconds in shallow subsurface flow paths to years in longer and deeper paths, affecting the types and rates of biogeochemical transformations at different depths in the streambed. Therefore, the hyporheic flow induced by various drivers and controls do not necessarily contribute equally to the biogeochemical transformations at the different scales (Marzadri et al. 2012, Haggerty et al. 2009). This makes hyporheic zone as a complex reactive zone owing to the variations of not only flow path lengths at shallow and deeper paths of the hyporheic zones but also the rates of transformations at different depths. Recent modelling studies have suggested that small-scale driven hyporheic exchange flow accounts for more net hyporheic fluxes when compared to large-scale (*e.g.* meandering rivers) hydrostatically driven hyporheic exchange (Stonedahl et al. 2010).

5.1.3 Reduced-order models

Numerous studies found in the literature use reduced-order models of idealized, uniform and single type of bedform-induced hyporheic exchange (Cardenas & Wilson 2007*b*, Singh et al. 2019, Wu et al. 2018, Gomez-Velez et al. 2017). The term *reduced-order* indicates that the framework of the model assumes and captures first-order drivers and controls of the hyporheic exchange processes, hence ignoring complexities such as sediment heterogeneity, depth-decaying hydraulic conductivity in the streambed, groundwater inflows and outflows or impacts of critical flows that may cause migration of streambed sediments and other materials. Moreover, combination of several bedform morphologies with topographic structure of the catchment determines the overall hyporheic exchange flows (Caruso et al. 2016, Schmadel et al. 2017, Ward et al. 2018). This includes nested flow paths, however in many of the reduced-order models only shorter and local flow paths are taken into account. Nevertheless, such assumptions facilitate comprehensive investigations primarily from numerous simulations owing to the reduced computational effort.

Wide use of reduced-order models also demands to see how accurate they are in prediction of hyporheic fluxes and residence times. As hyporheic flow is a resultant of multiple scale interactions, it is important to evaluate the importance of different scales on biogeochemical gradients developed in the hyporheic zones. Even though reduced-order models have vastly increased our mechanistic understanding of hyporheic exchange fluxes, retention time of water and solutes, and biogeochemical cycling in the river-aquifer systems under steady flow conditions and more recently under temporally-variable flow condition, the simulations results are seldom validated by field observations.

5.1.4 Focus of presented research

In this study, we use the observations of hydraulic heads, residence times and breakthrough curves of conservative tracers in a small first-order boreal stream to test the applicability of reduced-order models. Two bedform features are modeled: (i) step-pool ($\approx$ 3 m); and (ii) a low-gradient run ($\approx$ 8 m). The assumptions of homogeneous and isotropic sediments, constant hydraulic conductivity, neutral groundwater conditions and negligible storage is made for modelling both the bedforms. The high-resolution simulated results are then compared with field-observations.

5.2 Methodology

5.2.1 Research site

Research presented here is a part of a large-scale field and experimental study conducted in Krycklan Catchment (see Figure 5.1) in the month of August in 2017. The catchment is located $\approx$ 50 km northwest of Umeä, Sweden and has an area of 110 ha, out of which 71 % consists of forest and 25 % of mire and the elevation range from 231 to 283 masl (Mojarrad, Betterle, Singh, Olid & Wörman 2019, Laudon & Ottosson Löfvenius 2016). Catchment is characterized by a cold and humid climate, experiencing heavy snow during winter months (Leach et al. 2017). In the past, several experimental and modelling studies have been performed in this research catchment (*e.g.* Mojarrad, Betterle, Singh, Olid & Wörman (2019), Laudon et al. (2013), Laudon & Ottosson Löfvenius (2016), Mojarrad, Riml, Wörman & Laudon (2019)).

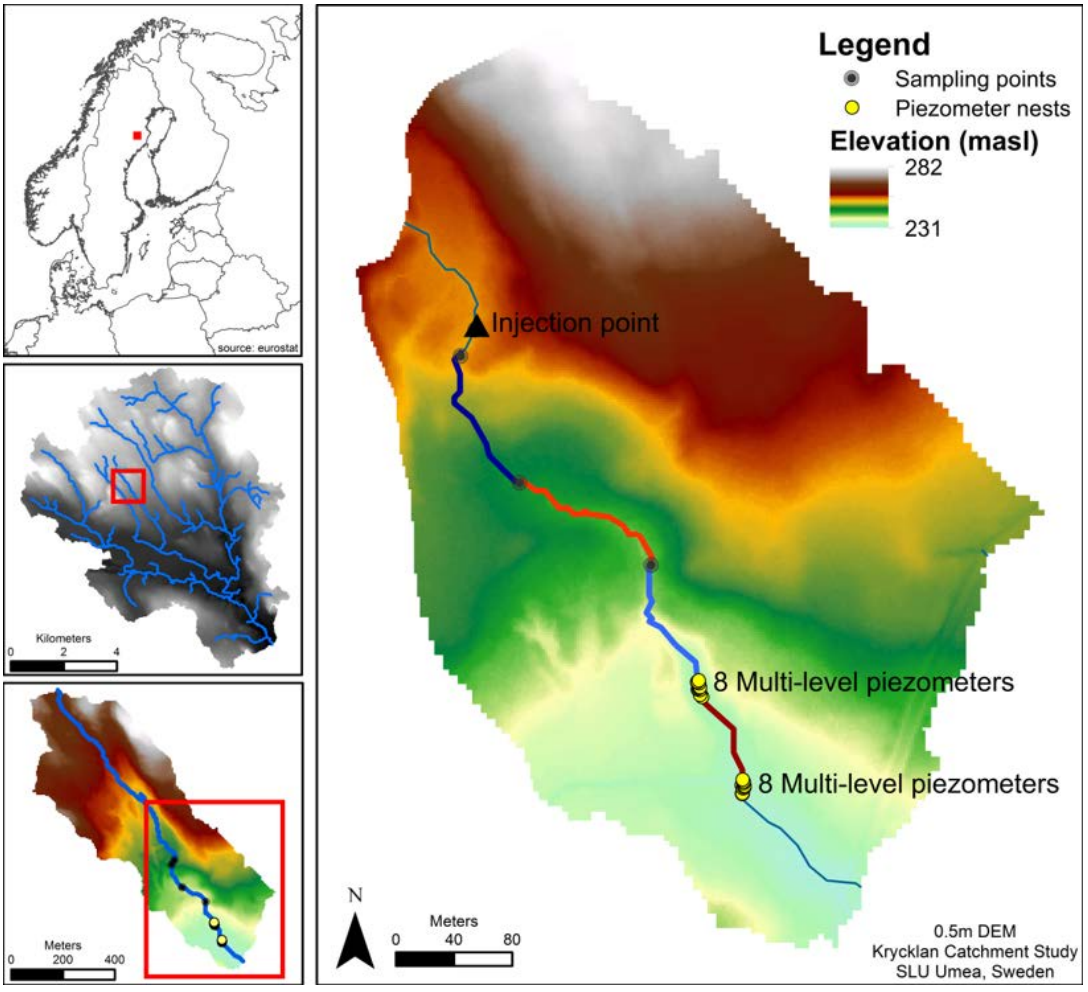

FIGURE 5.1: Maps showing the Krycklan catchment, the sub-catchment and the topography. Map on the right also depicts the location of installation of 8 multi-level piezometer. Our focus in this chapter is the upstream location that includes piezometers from 1 to 8. Also shown is the injection point (black triangle). This figure is from the work presented by Brekenfeld et al. (April 2018*a*).

The field site presented herein is within the Krycklan catchment. This catchment has been used for environmental-related research for years and has extensive existing comprehensive data sets. Moreover, the research site is well equipped for performing transient studies which in our case involved flow manipulation using generator and weir to block the flow in the stream. In the context of the modelling presented in the study, the first-order boreal stream exhibited various types of distinct bedform features which can be used to validate the presented model.

The presented research focus on a first-order boreal stream with a length of approximately 1500 m and monitored by two stations namely C5 and C6 respectively upstream and downstream of the stream respectively. The stream is primarily fed by Lake Stortjärn located 100 m upstream of station C5 and is fed by a mire system. The mean daily discharge has been noted to be $12.8\,ls^{-1}$ (2014-2017) and average slope is 3.7 % (Laudon et al. 2013). Sediment properties along the river stretch show variability and consists of dense organic matter, sand, and cobble/boulder (Leach et al. 2017). Field experiments have been performed at two sites: (1) upstream site with a longitudinal length of ≈ 14 m *i.e.* from piezometers P1 to P8 (2) downstream site with a longitudinal length of ≈ 8.8 m *i.e.* PZ9 to PZ16. Only the upstream site is considered in the present discussion. The field-observed data for hydraulic measurements and breakthrough curves was presented by Brekenfeld et al. (April 2018*a*) and Brekenfeld et al. (December 2018*b*).

5.2.2 Synthesis of field experiment

The upstream site was monitored using eight multi-level piezometers (depth of 5, 10, 15 and 20 cm in the streambed). Piezometers were placed with pre-conducted

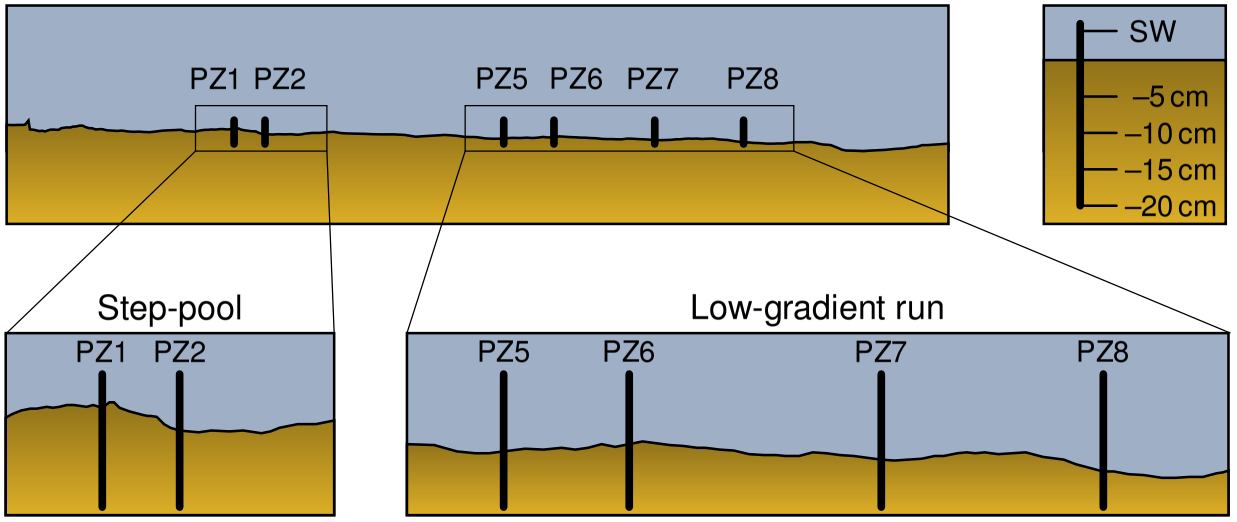

FIGURE 5.2: Depiction of the upstream site and topography. Upstream site mainly consisted of a step-pool (PZ1 and PZ2) and a low-gradient run (P5 to P8). The concentrations of conservative tracers were measure at surface water and at 4 depths in the streambed (5, 10, 15 and 20cm) shown by the sub-figure on top-right.

surveys to capture important topographic features in the site. The hydraulic conductivity measured in the site was between 5×10^{-4} m/s at shallower depth (*i.e.* $2-5$ cm) and values of 10^{-6} m/s at deeper depths (*i.e.* $10-15$ cm). For convenience, we have chosen the $K = 10^{-4}$ m/s in our simulations. The width of the channel at low flows is about 40 cm and at high is 60 cm. The water level is measured at each piezometer at specific times using salt method and the water level was continuously logged for the corresponding period (upstream of piezometer P1). This is illustarted in the Figure 5.3.

Flow manipulations were made for the reported period. This was done by manipulating the discharge of the stream downstream of lake Stortjärn as well as the lake water level. The manipulations were conducted by closing a gate of a V-notch weir roughly 50 m downstream of the lake outlet. To create normal *i.e.* base-flow conditions, V-notch weir was partly blocked. This had a negligible effect on the discharge in the stream and the water level in the lake. For low-flow conditions, the weir was completely blocked and hence no water could flow over the weir. Finally, the flood pulse *i.e.* high-flow conditions were generated with a pump directly downstream of the weir and keeping the weir completely blocked. The first flood pulse was on 19th August, 2017 with the duration of 12 hrs and the second flood pulse was on 21st of August, 2017 was rather a short flood pulse and lasted for about 3 hrs and finally the third flood was on 23rd August and had a duration of 16 hrs.

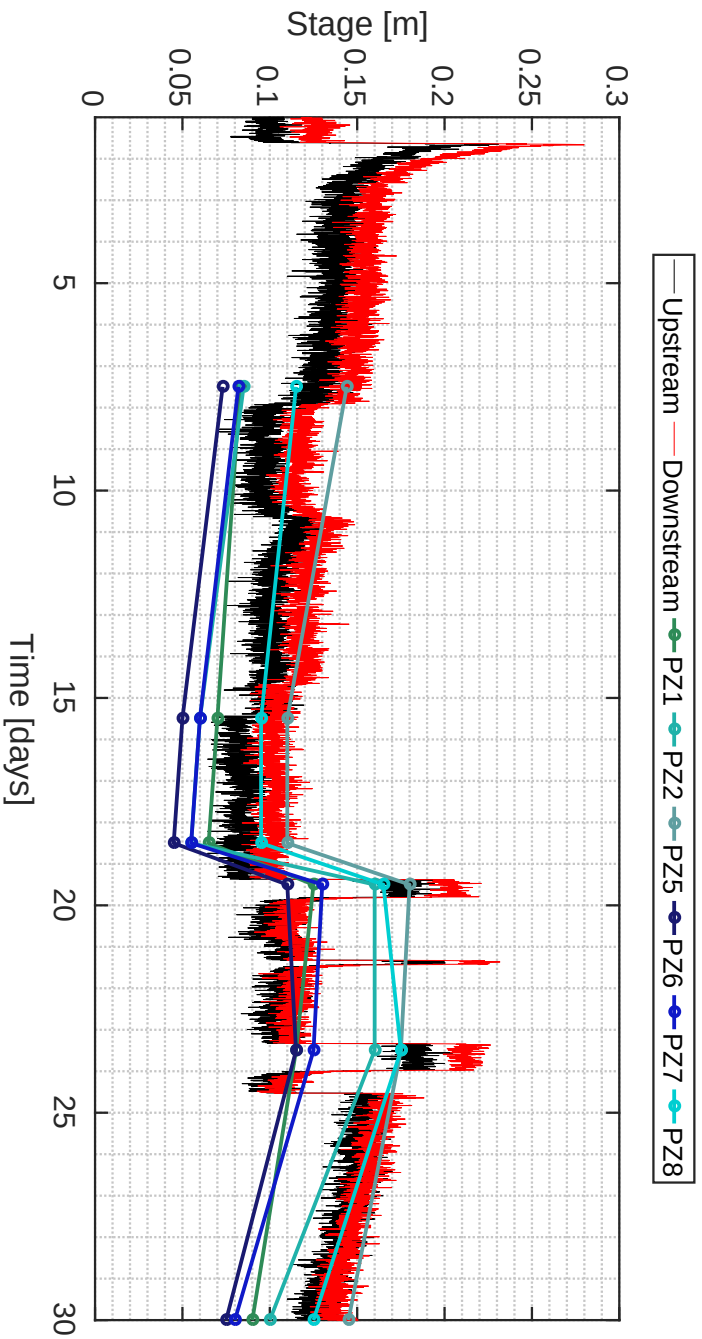

FIGURE 5.3: Depiction of stage hydrographs for the month of August in 2017. Upstream stage was measured few metres upstream of piezometer 1 (black curves) and downstream stage was measured few metres below piezometer 8 (red curves). Also shown is the water level recorded at piezometer locations for certain times during the period of the experiment.

5.2.3 Modeling domain and framework

5.2.3.1 Conceptual model

The model focused on the step-pool sequence (PZ1 to PZ2) and a low-gradient run (PZ5 to PZ8). Note that PZ1 is located towards the upstream and PZ8 is located towards the downstream end. We implement a detailed flow, transport and residence time models in the model domain. Modelling domain,Ω, represents homogeneous and isotropic stream sediments with the properties defined which was observed in the site. It is bounded at the top by the SWI, $\partial\Omega_{SWI}$, which was measured at the site. At the bottom, model domain is bounded by a horizontal boundary ($\partial\Omega_b$) and at sides by the lateral boundaries, $\partial\Omega_u$ and $\partial\Omega_d$. The dimensions are selected to avoid boundary effects in the numerical simulations. The models are constructed and computed in COMSOL Multiphysics. The size and density of the mesh elements were dependent on the streambed topography perturbations ($\partial\Omega_{SWI}$). The higher the fluctuation, the lower the size of the mesh element. Telescopic refinement close to the sediment-water interface is needed in order to capture the effect of local, fast-flowing hyporheic circulation cells and to compute accurate flux integrals along the boundaries.

5.2.3.2 Head distribution at sediment-water interface and modelling of flow

The water stage was logged at five minutes intervals close to P1 piezometer. It was also measured at various other piezometers at specific times. This is illustrated in

the Figure 5.3. The longitudinal and height measurements were made to capture the topography in the site.

With measured $H(t)$ [L] *i.e.* the time-varying river stage, we describe the pressure distribution at the sediment-water interface , $\partial\Omega_{SWI}$. For simplicity, an expression for prescribed head distribution that assumes a linear combination of head fluctuations induced by large- and small-scale bed topography (Wörman et al. 2006, Stonedahl et al. 2010):

$$h_{SWI}(x,t) = H(t) - Sx + h_d(t)\sum_{i=1}^{N} a_i sin\left(\frac{2\pi}{\lambda_i}x + \phi_i\right) \tag{5.1}$$

$H(t)$ [L] is the time-varying river stage, S is the slope. a_i and λ_i are the amplitudes and wavelengths of the i-th harmonic respectively, along the longitudinal direction. The dynamic head follows the bed topography with a phase shift of ϕ_i, and $h_d(t)$ is the intensity of the dynamic head fluctuations (Elliott & Brooks 1997) defined by

$$h_d(t) = 0.28\frac{U_s(t)^2}{2g}\begin{cases}\left(\dfrac{2\sigma_{Z_{\mathrm{SWI,s}}}}{0.34\,H(t)}\right)^{3/8} & \text{for } \dfrac{2\sigma_{Z_{\mathrm{SWI,s}}}}{H(t)} \leq 0.34 \\ \left(\dfrac{2\sigma_{Z_{SWI,s}}}{0.34\,H(t)}\right)^{3/2} & \text{for } \dfrac{2\sigma_{Z_{\mathrm{SWI,s}}}}{H(t)} > 0.34\end{cases}, \tag{5.2}$$

where the mean velocity is estimated with the Chezy equation for a rectangular channel as $U_s(t) = M^{-1}H(t)^{2/3}S^{1/2}$ with M is the Manning coefficient [$\mathrm{L}^{-1/3}\mathrm{T}$] (Dingman 2009).

Flow within the domain is driven by pressure gradients at the sediment-water interface, $\partial\Omega_{SWI}$. Neglecting the storage term, a reasonable assumption for submerged channel sediments, flow within the domain is described by the following

version of the groundwater flow equation and Darcy's law

$$\nabla \cdot \left[\rho \frac{\kappa}{\mu} \big(\nabla p + \rho g \nabla z \big) \right] = 0 \tag{5.3}$$

where $\mathbf{x} = (x, y)$ is the spatial location vector with dimension of [L], $p(\mathbf{x}, t)$ is pressure [$\mathrm{ML^{-1}T^{-2}}$], g is the acceleration due to gravity [$\mathrm{LT^{-2}}$], κ is the permeability [$\mathrm{L^2}$], ρ is fluid density [$\mathrm{ML^{-3}}$], μ_d is fluid dynamic viscosity [$\mathrm{ML^{-1}T^{-1}}$], $h = \dfrac{p}{\rho g} + z$ is hydraulic head [L], and Darcy velocity is $\mathbf{q} = -\dfrac{\kappa}{\mu}(\nabla p + \rho g \nabla z)$ [$\mathrm{LT^{-1}}$].

Assuming that bedforms repeat periodically along the channel, we implemented a periodic boundary condition for the lateral boundaries ($\partial\Omega_u$ and $\partial\Omega_d$; $p(x = -L, y, t) = p(x = 2L, y, t) + \rho g[h_{SWI}(x = -L, t) - h_{SWI}(x = 2L, t)]$). Under neutral groundwater conditions (*i.e.* without gaining and losing groundwater conditions), the only groundwater flow constraining the hyporheic zone is the ambient groundwater flow driven by the channel gradient (*i.e.* horizontal under-flow component), and therefore no-flow is assumed for lower boundary ($\partial\Omega_b$). The depth of this boundary, d_b was selected to minimize boundary effects. Finally, the solution under steady state (*i.e.* , baseflow conditions) is used as the initial condition for the transient simulations.

The sediment-water interface ($\partial\Omega_{SWI}$) can be discretized into inflow ($\partial\Omega_{IN} = \{\mathbf{x} \mid (\mathbf{n} \cdot \mathbf{q} < 0) \ \wedge (\mathbf{x} \in \partial\Omega_{SWI})$) and outflow sub-boundaries ($\partial\Omega_{OUT} = \{\mathbf{x} \mid (\mathbf{n} \cdot \mathbf{q} > 0) \ \wedge (\mathbf{x} \in \partial\Omega_{SWI})$) such that $\partial\Omega_{SWI} = \partial\Omega_{IN} \cup \partial\Omega_{OUT}$ with $\mathbf{n}$ an outward vector normal to the boundary. Notice that these boundaries are dynamic in nature, contracting and expanding with variations in the the time-varying river stage, $H(t)$.

5.2.3.3 Solute transport model and delineation of the hyporheic zone

The *advection-dispersion equation* (ADE) is used to model the transport of conservative solutes within the sediments

$$\theta \frac{\partial C}{\partial t} = \nabla \cdot (\mathbf{D} \nabla C) - \nabla \cdot (\mathbf{q} C) \tag{5.4}$$

where C is concentration [ML^{-3}], $\mathbf{q}$ is the Darcy flux [LT^{-1}], and $\mathbf{D} = \{D_{ij}\}$ is the dispersion-diffusion tensor defined as Bear (1972):

$$D_{ij} = \alpha_T |\mathbf{q}| \delta_{ij} + (\alpha_L - \alpha_T) \frac{q_i \, q_j}{|\mathbf{q}|} + \frac{\theta}{\xi_m} D_m \tag{5.5}$$

with α_T and α_L the transverse and longitudinal dispersivities [L] respectively, D_m the effective molecular self-diffusion coefficient, $\xi_m = \theta^{-1/3}$ is the fluid tortuosity (defined here with the Millington and Quirk model (Millington & Quirk 1961)), and δ_{ij} is the Kronecker delta function.

Modeling the transport of a conservative tracer allows us to explore the mixing and extend of the HZ. We assume that the concentration of the tracer in the stream water column is C_s, and therefore a prescribed boundary condition $C(\mathbf{x}, t) = C_s$ is used along the SWI's inflow areas ($\partial\Omega_{IN}$). Outflow areas ($\partial\Omega_{OUT}$) along the SWI are advective boundaries where $\mathbf{n} \cdot (\mathbf{D} \nabla C) = 0$. Lateral boundaries ($\partial\Omega_u$ and $\partial\Omega_d$) are periodic boundaries $C(x = -L, y) = C(x = 2L, y)$ and the bottom boundary ($\partial\Omega_b$) is a no-flow boundary $\mathbf{n} \cdot (\mathbf{q} C - \mathbf{D} \nabla C) = 0$. An initial condition for the concentration field is obtained from a steady-state simulation of the transport model (Eq. (5.4)) under baseflow conditions (*i.e.* , $H_s = H_0$). In this case, the hyporheic zone is defined as the zone with at least 90 % of the pore water originated from the stream

(*i.e.* , $C \geq 0.9C_s$). This definition is similar to the one proposed by Triska et al. (1989) and Gomez-Velez et al. (2014, 2017). Through the manuscript, we refer to this definition as the *biogeochemical definition* of the hyporheic zone.

5.2.3.4 Residence time model

The hyporheic zone residence time describes the time that water and solutes are exposed to the stream sediment biogeochemical conditions. Herein, we evaluate the impacts of transient flow—driven by stream stage fluctuations, on the first moment of the HZ's residence time distribution. To this end, we use the approach outlined in Gomez-Velez et al. (2012), Gomez-Velez & Wilson (2013), and Gomez-Velez et al. (2017) where the moment of the residence time are described by an ADE of the form

$$\frac{\partial(\theta a_1)}{\partial t} = \nabla \cdot (\theta \mathbf{D} \nabla a_1) - \nabla \cdot (\mathbf{v} \theta a_1) + \theta a_0 \tag{5.6a}$$

$$a_1(\mathbf{x}, t) = 0 \quad \text{on } \partial\Omega_{IN} \tag{5.6b}$$

$$\mathbf{n} \cdot (\theta \mathbf{D} \nabla a_1) = 0 \quad \text{on } \partial\Omega_{OUT} \tag{5.6c}$$

$$a_1(x = -L, y) = a_1(x = 2L, y) \text{ for } \partial\Omega_u \text{ and } \partial\Omega_d \tag{5.6d}$$

$$\mathbf{n} \cdot (\mathbf{q} a_1 - \mathbf{D} \nabla a_1) = 0 \quad \text{on } \partial\Omega_b \tag{5.6e}$$

$$a_1(\mathbf{x}, t = t_0) = a_{10} = \int_0^\infty \tau \Psi_0(\mathbf{x}, \tau) \, \mathrm{d}\tau \tag{5.6f}$$

where $a_1(\mathbf{x}, t)$ [T] is the first moment of the residence time distribution $\Psi(\mathbf{x}, t, \tau)$ [T^{-1}] which is defined as

$$a_1(\mathbf{x}, t) = \int_0^\infty \tau \Psi(\mathbf{x}, t, \tau) \, \mathrm{d}\tau, \text{ for } n = 1, 2, \ldots \tag{5.7}$$

5.3 Results and Discussion

5.3.1 Flow field and hyporheic zone extent

The temporal evolution of flow field for step-pool and low-gradient run are illustrated in Figure 5.4 A and B. Dynamic pressure distribution along the sediment-water interface changes flow field (magnitude and direction) causing expansion and contraction of the hyporheic zone. The shape of the stage and bedform topography determine the resultant impact on the magnitude and direction of flow field.

The hyporheic zone formed for the step-pool bedforms is much larger in comparison to the low-gradient run. Hydrodynamically, the low-gradient run is shown to either have no HZ or HZ formations very close to the sediment-water interface. The inflow ($\partial\Omega_{IN}$) and outflow areas ($\partial\Omega_{OUT}$) vary considerably along the sediment-water interface. This results in the development of number stagnation zones in the streambed varying in size and depths. The spatial scale of hyporheic exchange is dependent on bedform sizes and amplitudes (Buffington & Tonina 2009), where the deeper subsurface flow paths are prone to decreased velocities when compared to fast flowing hyporheic cells close to the sediment-water interface. Larger and enhanced bedform features lead to increased local pressure, enlarging the size of the hyporheic zones.

Impact of the flow conditions is mainly evident around the areas of stagnation zones. It can be seen that the size of the stagnation zones decreases due to increased vertical velocities caused due to increased stage. This was in line with the finding of (Singh et al. 2019)(see Chapter 2). Transience in flow often lead to changes in

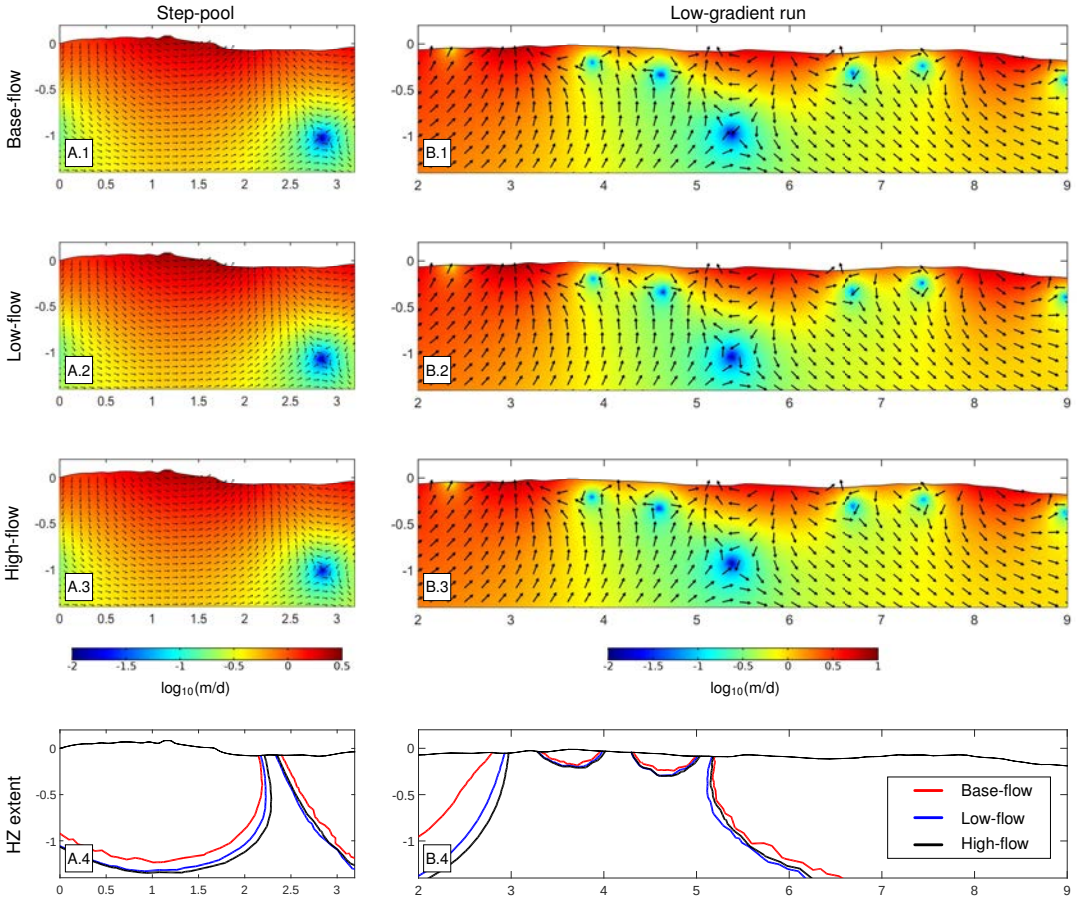

FIGURE 5.4: Snapshots of flow field within two sequences of bedforms - step-pool (first column) and low-gradient run (second column). Black arrows represent direction and is not proportional to magnitude. Coloured surface represents the magnitude of Darcy flux vector in log_{10}m/d. Rows correspond to flow conditions namely - base-, low- and high-flow conditions. Piezometers 1 and 2 were located in step-pool sequence and piezometers 5, 6, 7 and 8 in low-gradient run.

the location and size of stagnation zones, which oscillate in depth and size during the flow fluctuations, resulting in the emergence of highly reactive zones owing to the hydraulic response to the dynamic flow conditions. It is important to note that the presented model formulation doesn't apply for low or no flow conditions. The estimation of pressure distribution using the Equation 5.2, assumes that there is a a magnitude of river stage at all points, if not then the denominator becomes 0. Hence out model is not designed to capture extremely dry or no flow conditions and hence there are limitations of the model with respect to low flows.

The HZ extent according to the biogeochemical definition is shown in the Figure 5.4 - A.4 and B.4. The dynamic response of the HZ which is not very evident in the illustrations is highlighted in Figure 5.4 - A.4 and B.4. The HZs expand with time and increase with intensity of flow conditions. As the biogeochemical definition in the HZ is relatively more stable—as it is based on mass and retention process, its expansion and contraction is much slower and does not coincides with the hydraulic pressure wave.

5.3.2 Vertical hydraulic gradient

Figure 5.5 illustrates the field-observations and simulation results of vertical hydraulic gradient (VHG) observed at the piezometers 1 and 2. PZ 1 and PZ2 are associated with a step-pool sequence categorised by downwelling and upwelling regions respectively. Negative VHG is observed in the field at the locations of PZ1 that indicated that the flux is predominantly downwards in the streambed. The modelling observations also indicated a similar trend (blue dotted lines in Figure 5.5). Positive VHG is observed at the locations of PZ2 *i.e.* regions associated with

upward flux. This is again replicated by the modeled results. It is important to note that the estimated value for VHG— estimated using the modeled results include the same stage that has also been used as the input in the model. Therefore, hydraulic head at any point mimics the pressure fluctuations at the interface because of the assumption of negligible storage. Hence, the difference in the head at a point and the stage adjacent to the piezometer is not able to capture the dynamics involved with stage. However, when piezometric head is plotted solely, the dynamics involved with stage fluctuations are captured and is comparable with the field observations (Figure 5.5, 2nd sub-plot).

For the low gradient run, *i.e.* locations with PZ 5, 6, 7 and 8, the model is able to predict the direction of the flux for most of the piezometers (Figure 5.6) except for the PZ 5. In addition, a reversal of VHG was observed for PZ6 after the high-flow event which is not indicated in the modeled results. The reversal in VHG was also observed by (Dudley-Southern & Binley 2015) for increased river stage in some of the locations of the their field-site. The present model does not take into account groundwater gaining and losing conditions, it is not able to predict the reversal of VHG at PZ6. In the simulations of the low-gradient run, hyporheic zones are formed very close to the sediment-water interface with close proximity of inflow and outflow boundaries. Few deviations were observed for the modeled results for low-gradient run. This could be the due to the assumption of no lateral exchange in the streambed and/or absence of streambed heterogeneity in the model domain. However, it is also important to note that the numerical results are accounted for the field-measured locations of the piezometers which are also prone to some error.

Vertical hydraulic gradient is an important measure to estimate whether the hyporheic flux is upwards or downwards. It has been widely used to inform about

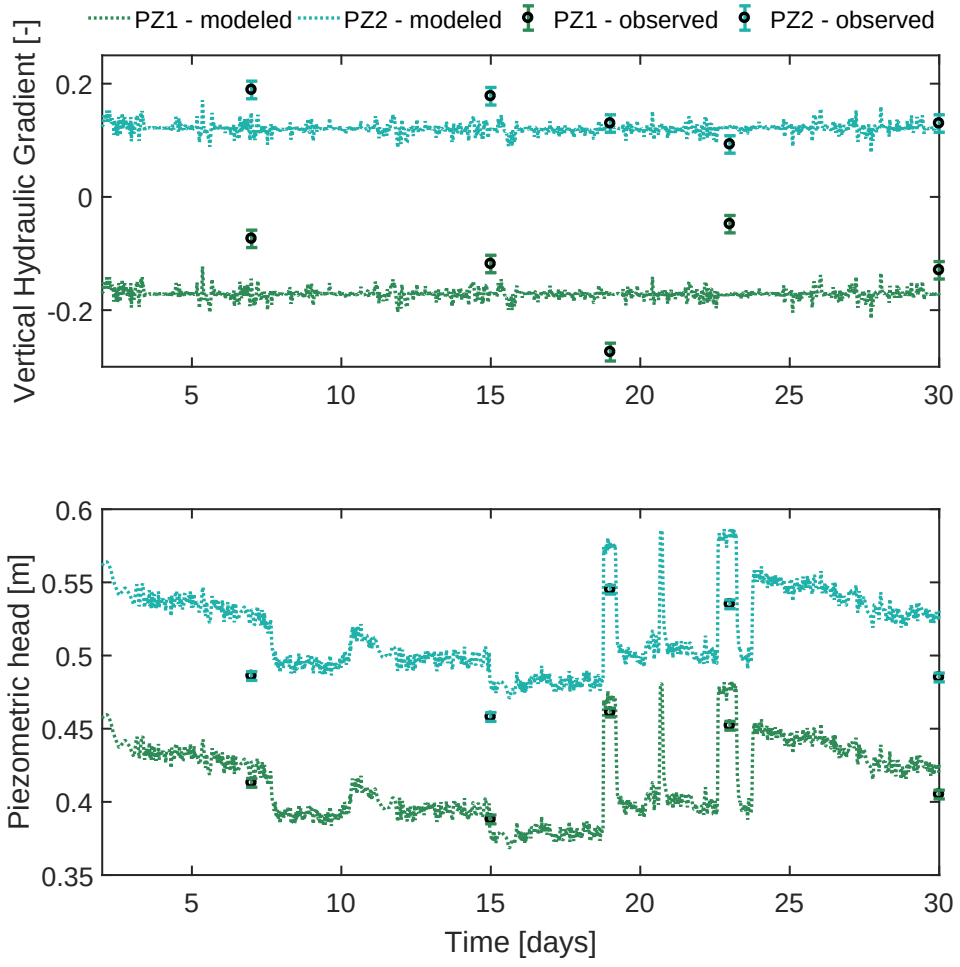

FIGURE 5.5: Comparison between modeled and field-measured vertical hydraulic gradient[-] as a function of time (days in the month of August, 2017). The second sub-plot depicts the comparison between modeled and field-measured piezometric head [m] as a function of time (days in the month of August, 2017). Values correspond to the locations of piezometers PZ1 and PZ2.

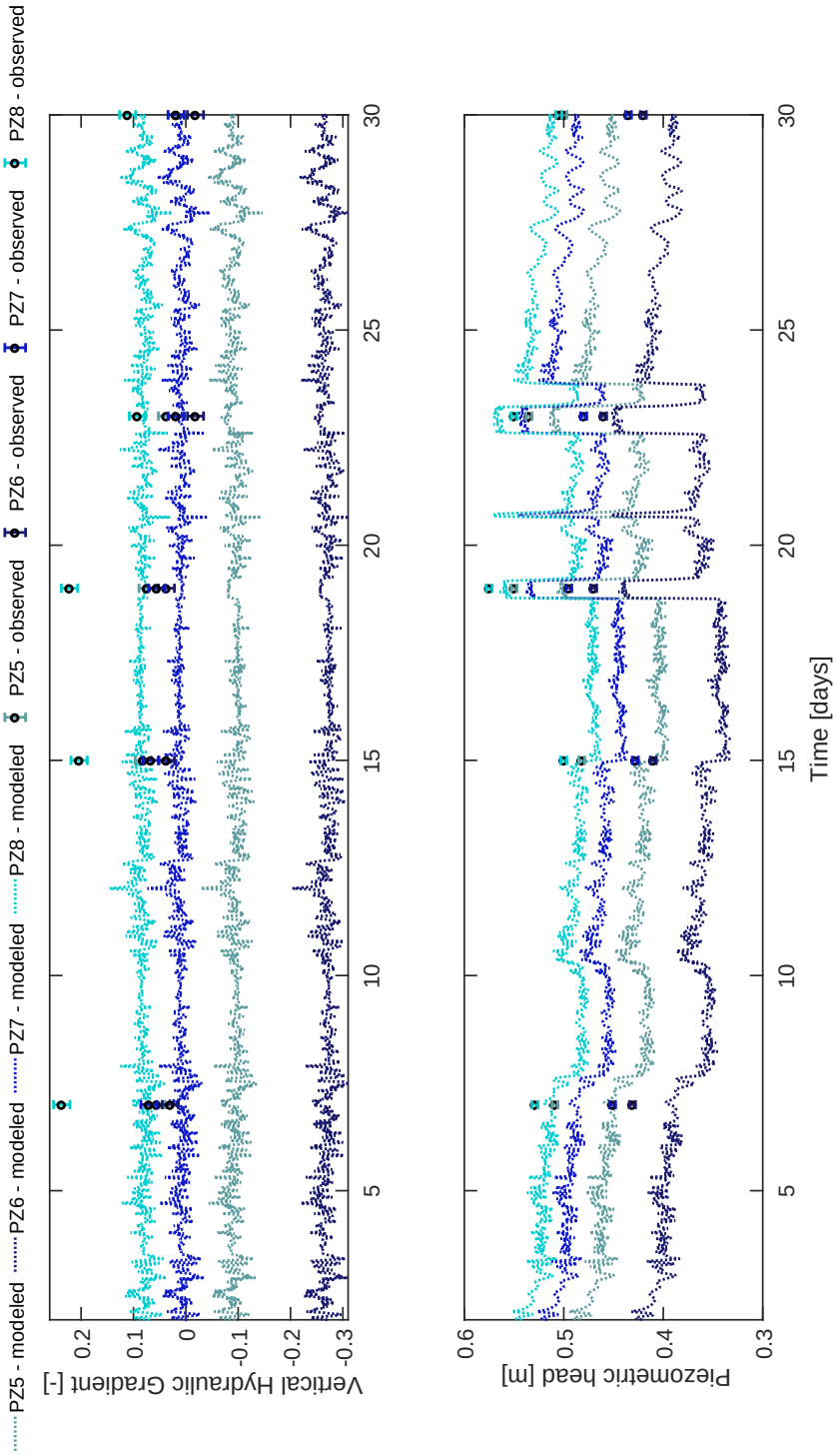

FIGURE 5.6: Comparison between modeled and field-measured vertical hydraulic gradient [-] as a function of time (days in the month of August, 2017). The second sub-plot depicts the comparison between modeled and field-measured piezometric head [m] as a function of time (days in the month of August, 2017). Values correspond to the locations of piezometers PZ5, PZ6, PZ7 and PZ8.

direction and magnitude of hyporheic fluxes (Krause et al. 2012). Groundwater gaining conditions compress the hyporheic zone and losing conditions oppose the hyporheic flow paths to emerge out of the sediment-water interface. Therefore, the formation of hyporheic zones and the extent in penetration and variations in residence time is potentially decreased by groundwater gaining or losing conditions. As the numerical and experimental studies show that to have any significant impact in hyporheic characteristics, the groundwater fluxes should exceed hyporheic fluxes. We assume this is not the case in the simulations, and hence we assume neutral groundwater conditions (Boano et al. 2014). However, in the natural settings there was no measure of dynamic change in hyporheic exchange fluxes and is thus challenging to ascertain whether the system is a gaining or losing system.

5.3.3 Residence time

Observations from vertical hydraulic gradients inform about the upwelling and downwelling regions in the step-pool sequence. The residence time of water at different depths *i.e.* 0 cm (close to SWI), 5 cm, 10 cm, 15 cm and 20 cm are modeled at the sampling locations of PZ1 and PZ2 (Figure 5.7).

Hyporheic water with different residence times is observed in the modeled results at different depths of PZ1 , with the oldest at the depth of 20 cm. As the depth increases, the residence time of the water also increases. This sampling location comprise of subsurface flow paths with downward gradient. For PZ2, which is comprised of fluxes upwards exhibits waters with higher residence times. Expectedly, the increase in residence times with increase in hyporheic depths is also observed. Isotope

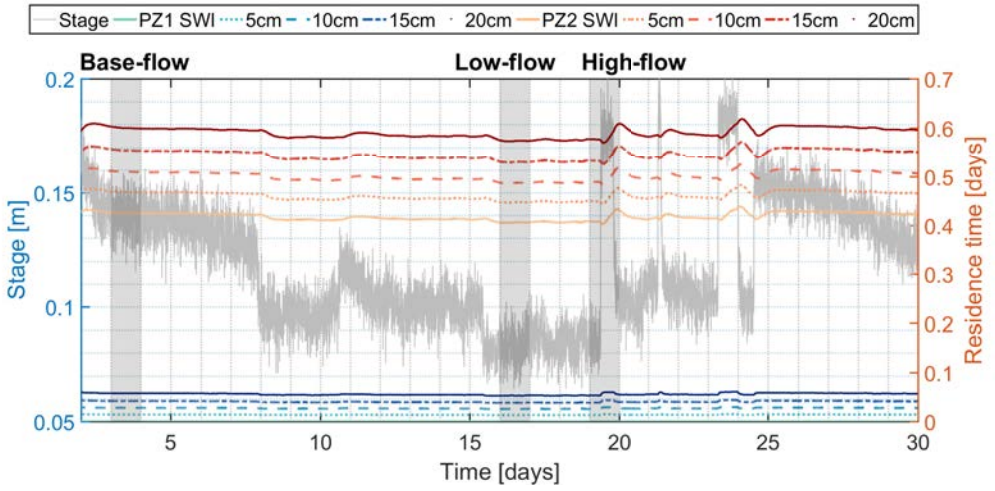

FIGURE 5.7: Residence time of hyporheic water in days at different depths (SWI, 5 cm, 10 cm, 15 cm and 20 cm). Warmer colour is for piezometer 1 and colder colour is for piezometer 2. Darker shades indicates higher residence time. Gray colour depicts the stage. The grey shaded region depicts the injection period used to compare the modeled and field-observed data for the breakthrough curves in Figures 5.8 and 5.9.

signature analysis on the samples from PZ2 indicated presence of deep groundwater (Brekenfeld et al. December 2018*b*). The simulation results demonstrated higher residence times around those locations, mainly due to the development of stagnation zones. However, deep groundwater is an indication of gaining conditions and the model assumes conditions without gaining or losing groundwater conditions. The analysis of potential additional impacts of net gains and losses of water and the resulting interference has been well documented by Wu et al. (2018).

Under high discharge conditions, modelling observations indicate an increase in residence time of water. The increase is more pronounced for the locations at PZ2 than PZ1 . Moreover, the separation in the extent of variations in residence time is higher for the depths at PZ2. This is due to the elongation of the hyporheic flow paths due to increased pressure gradient.

The recovery of the residence time from the sudden high discharge is relatively slow. This indicates release of older water after the high discharge event for a longer period of time. This behaviour of hyporheic waters is crucial from the perspective of solute retention within the reactive hotspots and the stimulation of transformations or slow release of contaminants and hence potentially providing increased time for redox reactions and biogeochemical transformations in the streambed.

An increased stream stage promotes increased downwelling of surface water that also increases the residence time of upwelling hyporheic waters. Hence, the stage does not only affect the transportation of organic matter and nutrients in the streambed but also increases the potential of nitrate removal due to increased residence time of surface-water solutes in the streambed (Zimmer & Lautz 2014).

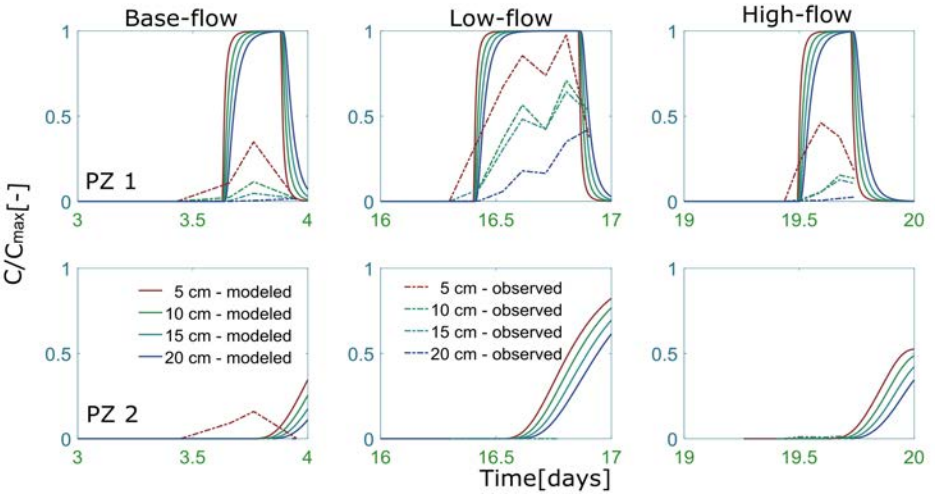

FIGURE 5.8: modeled and field-measured breakthrough curves as a function of time for the piezometers PZ1 and PZ2 locations. Time corresponds to the tracer injected on the days to capture effects of base, low and high flow conditions. Solid coloured lines correspond modeled breakthrough curves and dashed coloured lines correspond to field-measured breakthrough curves. Different colours represent different depths *i.e.* 5 cm, 10 cm, 15 cm and 20 cm within the streambed.

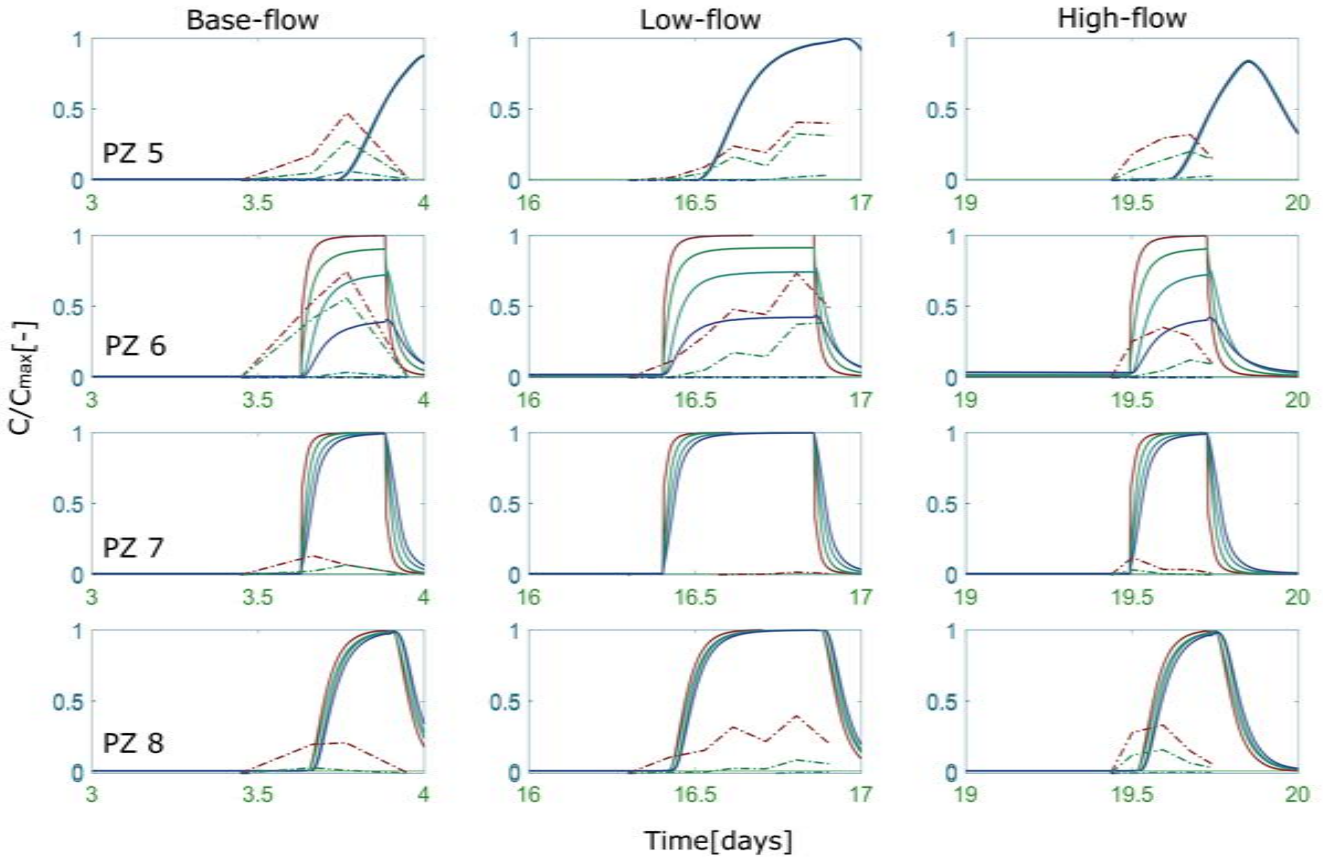

FIGURE 5.9: Modeled and field-measured breakthrough curves as a function of time for the piezometers PZ5, PZ6, PZ7 and PZ8 locations. Time corresponds to the tracer injected on the days to capture effects of base, low and high flow conditions. Solid coloured lines correspond modeled breakthrough curves and dashed coloured lines correspond to field-measured breakthrough curves. Different colours represent different depths *i.e.* 5 cm, 10 cm, 15 cm and 20 cm within the streambed.

5.3.4 Breakthrough curves of conservative tracer

The combination of Raz and Rru concentrations—which is considered as conservative is measured from the samples collected at different depths at the piezometer locations. In total there were six injections to capture the effect of different flow conditions. Here, we focus on three injections highlighted in Figures 5.7. The field-observed and model-estimated breakthrough curves for base, low and high-flow conditions at different depths of piezometer 1 and 2 are presented in Figure 5.8, and of piezometer 5, 6, 7 and 8 in Figure 5.9.

Numerical breakthrough curves for PZ1 location demonstrate the concentration of the conservative tracer is transferred at a faster rate owing to the locations associated with downwelling regions. Conversely, at PZ2 location, the concentrations are transported at a much slower rate. It is also evident that concentration at depth of 5 cm increases or decreases at a faster rate when compared to deeper depths. Delayed response in the transport of conservative tracer at the upwelling-dominated locations indicate that field observations are not sufficient to capture the tracer concentrations within the time of sample collection and thus require a longer sampling period. This is primarily because the tracers may be retained for relatively longer period which is usually not covered within the typical sampling time-frame. The results indicate that the hyporheic zone can cause a delayed release of conservative solute tracers. This release is highly dependent on discharge conditions—this is also in line with the findings of Harvey et al. (2012) where the results showed that post-flood the stored tracer was released slowly from subsurface flow paths.

In the field observations, tracers are seen to only penetrate to a depth of 5 cm or less. This could be a result of complexity involved in natural systems which include

depth decaying hydraulic conductivity, stream heterogeneity and lateral exchanges in the streambed. As the model does not take into account these complexities as it shows the idealized transport of conservative tracers to the streambed.

5.3.5 Reduced-order models for mechanistic understanding of hyporheic exchange processes

Process-based reduced-order models are increasingly used to understand hyporheic exchange processes, however they are rarely validated by field observations. In this study, the applicability of reduced-order models for the representation of hyporheic exchange processes under transient flow conditions is evaluated. In the previous chapters, the results are presented in dimensionless form. As mentioned by Gomez-Velez et al. (2017), by deploying a dimensional framework reduces computational demands and enhances transferability of the reduced-complexity model to a broad range of geomorphological settings. When the proposed model used the input from the field observations, the results depict that the model dimensionality and assumptions are more valid for small sandy bedforms where vertical hyporheic exchange are dominant whereas in a long gradient run lateral hyporheic exchange may be more dominant which is not considered in the presented model. Most of model validations are performed in a controlled environment (*e.g.* flumes) and for steady flow conditions. Here, the data from a natural setting is used and includes temporally-variable discharge conditions. Results from VHG can successfully predict the direction of the flux for most of the locations, but for the accurate prediction of the magnitude, higher spatial and temporal resolution of field-observation data is required. Results of VHG for a longer sub-reach *i.e.* long-gradient run needs to be dealt with

caution. As the resultant hyporheic subsurface flow paths is a function of complex interactions of not only local-scale streambed topography and properties but can potentially be influenced by the hyporheic flow paths at many scales. The nested flow paths created as a result of physical processes, can impact solute transport, residence times and eventually biogeochemical transformations.

Timely-variations in stream discharge occur frequently, this influences spatial and temporal distribution of hydraulic heads along the sediment-water interface. This variation also affects the hyporheic exchange in the streambed. The increased discharge affect oxygen availability, temperature distribution, availability of nutrients in the streambed. Time-dependent reduced-order models can unravel the potential of a hyporheic zone to act as a reactive zone for a longer time after a high-flow event. As shown in the results of residence times for step-pool sequences, waters with higher residence times is observed at different depths after the end of an event. Similar behaviour is observed in the modeled results of breakthrough curves. The upwelling dominant regions in step-pool sequence show delayed appearance of tracer concentrations, the time period of which was not sampled in the field. Hence, longer sampling in such identified upwelling regions can further highlight the retention ability of the streambed. Higher residence times for a longer period and increased infiltration of surface water rich in oxygen, nutrients, dissolved organic carbon will likely enhance processes such as denitrification in the streambed.

In the natural systems, its can be challenging to identify and locate the reactive hotspots in the hyporheic zones. ROMs can potentially help to locate stagnation zones and understand the complete absence or small amount of tracer concentrations at certain depths. Low-gradient run was associated with stagnation zones in close proximity to sediment-water interface. Laboratory analysis of collected water

samples from the field is used to demonstrate the presence of tracer concentrations at such locations and depths. These are measured to be either negligible or in small quantities within the sampling timescales.

The results demonstrate that ROMs are a useful tool for mechanistic understanding of the hyporheic exchange processes. Even with assumptions such as negligible storage, homogeneous and isotropic sediments, constant hydraulic conductivity and no gaining or losing groundwater conditions. ROMs are shown to predict the HZ behaviour especially for the short and local flow patterns. A fundamental flow and transport model of hyporheic exchange processes combined with high resolution field-data can be used to enhance the accuracy of prediction of the hyporheic zone behaviour under transient flow conditions. Parametrization of the reduced-order model is carried out using the stream parameters which are obtained by direct measurements in the field. However, upscaling of such processes needs to be handled carefully. This is because interplay of various hyporheic drivers and controls and also interactions between neighbouring bedform features can exhibit complex multi-scale mosaic of hyporheic subsurface flow paths. This may result in range of subsurface velocities leading to range of water and solute transport timescales in the hyporheic zone.

5.4 Conclusions

This study compares the field-measured and model estimated hydraulic head measurements and tracer breakthrough curves at multiple depths in order to test the applicability of a reduced-order model. The results indicate that a reduced-order model can predict the direction and magnitude of hyporheic exchange fluxes for a

step-pool sequence. Moreover, a delayed release of conservative tracers in the upwelling regions was predicted by the model. However, for the low-gradient run the simulated results exhibited minor deviations from the field-observations. As the magnitude of fluxes is highly dependent on the sediment properties, high resolution topographical observations and groundwater discharge and recharge, for the accurate predictions of hyporheic fluxes inclusion of complexities such as heterogeneity and complexity needs to be taken into account. The simulated results, therefore, suggest that mechanistic knowledge derived from the simulation of reduced-order models should be considered with caution and limitations of our ability to upscale processes in river-aquifer systems using reduced-order simulations needs to be acknowledged.

Chapter 6
CONCLUSIONS AND FUTURE WORK

6.1 Summary

The primary focus of this thesis was to explore the dynamic behaviour of hyporheic zones and emphasise the importance of transience in the study of hyporheic zones. This was achieved by using reduced-order process-based models and imposing dynamic boundary conditions at the sediment-water interface. Firstly, synthetically-generated peak-flow events and diurnal surface water temperature signals were used and then the reduced-order model was validated with the field-observations. In above chapters, the importance of dynamic hyporheic zones in relation to its impacts on residence times of water and solutes, temperature-dependent reaction rates and potential implications on biogeochemistry were of main focus.

Systematically, complex impacts of peak-flow events (with different characteristics in terms of duration of the event, skewness of the events and event's intensity) along with streambed topography on hyporheic exchange flow patterns and dynamics were explored. This was performed for a comprehensive range of scenarios for an idealized, uniform and single-type of bedform. A two-dimensional model consisting of sinusoidal bedforms and implemented flow, transport and residence time models was deployed. Then for further understanding, hydrograph scenarios with variations in lag between the occurrence of two events, magnitude and duration of the events were designed. Time-lag between two events covered scenarios with complete overlapping *i.e.* superimposition of two events, partial overlapping and scenarios with no overlapping *i.e.* representing repeated peak-flow events. Moreover, conservative

tracers were introduced in order to decipher contribution and potential mixing of the events. This was implemented in order to comprehend solute retention processes in the hyporheic zones. In the following chapter, the two-dimensional coupled flow and heat model was implemented to systematically explore the effects of temperature fluctuations in surface water, ambient groundwater flow and hydraulic conductivity on bedform-induced hyporheic exchange processes. This study integrated geomorphological controls and temperature dependence on hyporheic exchange flux and potential reaction rates within the streambed when diurnal surface-water temperature fluctuations is taken into consideration. To further check the applicability of reduced-order models, the model was validated with field observations of pressure heads and breakthrough curves. in this study, parametrization of the reduced-order models was done using the stream parameters which was obtained by direct measurements in the field. This included bedform topography, hydraulic conductivity and stream stage fluctuations.

6.2 Research contributions

Interplay between streambed topography, channel slope and temporally-variable discharge resulted in complex exchange of water and solute fluxes between the surface water and hyporheic zones. The presented results exhibited dynamic expansion and contraction of the HZs during the duration of the event, however in several cases this expansion was counteracted by strong ambient horizontal flow induced by large channel slope values. Noteworthy impact of peak-flow events was demonstrated on the residence time of the water in hyporheic zones. Intensification of discharge of younger and older hyporheic water out of the SWI was evident at high intensities

and longer duration of the event. Primarily, for streambed profiles with low slopes, peak-flow events caused more discharge of older water for the higher bedform aspect ratios (i.e for dunes and ripples). The direct influence of which was observed in the efficiency of the hyporheic zones in developing larger areas of potential nitrification and denitrification.

When superimposed and repeated peak-flow events were taken into account, the hydrodynamics of hyporheic zones ,and transport and retention of water within the streambed changed substantially. Instantaneous change in temporally variable hyporheic flow field was observed due to rapid pressure wave propagation within the streambed, however the expansion based on geochemical definition was relatively more stable. Flux -weighted mean residence time showed high dependence on time-lag between the two events *i.e.* longer the lag between , higher the variability in the flux-weighted mean residence times, hence demonstrating higher potential to discharge older hyporheic waters. Numerical breakthrough curves were found to be flatter for the events with increased separation and longer duration of the second event. Higher magnitude of the second event caused the breakthrough curves to become steeper, when compared to low magnitude and longer duration of the second event. Therefore, breakthrough curves for such events can unravel the biogeochemical signature of the water that is being transported in and out of the hyporheic zones. This implies that depending on the event properties, the potential of the hyporheic water with different chemical properties to retain in the hyporheic zones may determine the types and rates of redox reactions and therefore overall water quality and chemistry.

Inclusion of heat processes demonstrated importance of temperature in determining hyoporheic exchange fluxes. Spatio-temporal distribution of the heat indicated stronger temperature variations in the downwelling regions of the bedforms. Higher thermal heterogeneous behaviour was observed during warmer times of the day. Temperature-dependent viscosity and density considerably varied the relative change in hyporheic exchange fluxes. The trend observed for hyporheic exchange fluxes was both lagged and cooled, however the shift was highly dependent on the values of hydraulic conductivity. Hyporheic zones attenuated the surface-water temperature signals mainly for the warmer times of the day and showed dependency on both hydraulic conductivity and channel slopes. Cooled and lagged temperatures owing to the thermal properties of the streambed were shown to affect the spatio-temporal distribution of reaction rates.

Comparison between the field-measured and model predicted hydraulic head measurements and tracer breakthrough curves at multiple depths in order to test the applicability of a reduced-order model unravelled interesting results. The results indicated that a reduced-complexity model can predict the direction and magnitude of hyporheic exchange fluxes for a step-pool sequence. Moreover, a delayed release of conservative tracers in the upwelling regions was predicted by the model. However, for the low-gradient run the simulated results exhibited minor deviations from the field-observations. As the magnitude of fluxes is highly dependent on the sediment properties, high resolution topographical observations and groundwater discharge and recharge, for the accurate predictions of hyporheic fluxes inclusion of complexities such as heterogeneity and complexity needs to be taken into account. The simulated results, therefore, suggest that mechanistic knowledge derived from the

simulation of reduced-order models should be considered with caution and limitations of our ability to upscale processes in river-aquifer systems using reduced-order simulations needs to be acknowledged.

Intricate understanding of processes such as denitrification is important to maintain water quality and aquatic life in the riverine systems. This is because denitrification process reduces nitrates from river-aquifer continuum, through a chain of intermediate reactions. However, incomplete denitrification in the streams result in the release of N_2O, an ozone-depleting substance into the atmosphere instead of molecular nitrogen (Briggs et al. 2015). Any dynamic alterations in river-stage due to external hydrologic forcing can have substantial impact on streambed nutrient cycling and transformations. Such forcing can transport organic matter (and even contaminants) deep into the streambed, potentially increasing its contact time to favourable conditions required for transformations. As in the case of denitrification process, a peak-flow event could lead to the transport of organic matter deeper into the alluvium where anoxic environments are present for the completion of the process. Moreover, temperature variations in surface water not only alter the hydrodynamics in the streambed but also impact the temperature-sensitive biogeochemical reactions. Hence, it is essential to gain intricate understanding of the thermal propagation and thermal dynamics in the hyporheic zones. Such understanding can contribute to the better prediction of hyporheic chemistry as well as protection of habitat of aquatic species which is crucial for overall ecosystem functioning. Thorough investigation of river morphological and riparian characteristics, and combination of peak-flow event scenarios can be potentially adopted for managing and restoring river water chemistry.

6.3 Recommendations for future research

While, for the work presented here, a broad range of multi-parametric study (with regards to bedform topography, channel gradient, peak-flow event characteristics, temperature fluctuations) were considered, there remain further variables and potentially impactful drivers that have not been analysed in this thesis such as variability in streambed structural properties (Gomez-Velez et al. 2014) or the impacts of critical flows with the potential to mobilize the streambed materials (Simpson & Meixner 2012, Wu et al. 2015). Combination of several bedform morphologies with topographic structure of the catchment determines the overall hyporheic exchange fluxes (Caruso et al. 2016, Schmadel et al. 2017, Ward et al. 2018). This includes nested flow paths, however in this thesis only the shorter and local flow paths were taken into consideration . Furthermore, gaining or losing groundwater conditions were not included. The analysis of potential additional impacts of net gains and losses of water and the resulting interference with peak-flow event driven hyporheic exchange remain as the focus of future investigations.

With regards to heat transport processes, more complex models involving higher dimensionality and differentiating effects of streambed spatial heterogeneity in both hydraulic and thermal properties may help to unravel better predictability of hyporheic exchange fluxes and temperature-dependent reaction rates. The sediment bed is considered to be homogeneous and isotropic which is not usually the case in the natural systems. Different grain sizes would take different times to get thermally equilibrate. Local thermal equilibrium that is temperature of fluid and solid phases at the interface are assumed to be equal. A better understanding of thermal patterns induced by various bedforms subject to different flow conditions also requires

separate focus. This is because there could also be an increase in the stream temperature and the hyporheic temperature due to anthropogenic inputs, for eg. from urban waste water, which is also the result of increased stream-stage (Kinouchi et al. 2007). Upscaling of heat transfer processes can be achieved by better linking of the small scale features to integrative models of net heat fluxes at larger scales.

Herein, mainly conservative solute transport processes were taken into account. In addition of inclusion of aforementioned complexities, the model can be extended to couple reactive transport processes as well. As streams are usually prone to carry dissolved organic carbon, fine particles as well as contaminants both metal and non-metals, it is essential to understand its transport and possible attenuation in the hyporheic zones. Dynamic nature of hyporheic zones also effect the reactive loads in the subsurface. The conservative substances that are carried along with surface water may become non-conservative in the subsurface (Boano et al. 2014). Integrative process-based models with coupled flow, heat and reactive transport processes can help the management and restoration of the river-aquifer systems by predicting potential reactive loads and turnover in the hyporheic zones.

REFERENCES

Acornley, R. M. & Sear, D. A. (1999), 'Sediment transport and siltation of brown trout (salmo trutta l.) spawning gravels in chalk streams', *Hydrological processes* **13**(3), 447–458.

Anderson, M. P. (2005), 'Heat as a ground water tracer', *Ground Water* **43**(6), 951–968.

Arrigoni, A. S., Poole, G. C., Mertes, L. A. K., O'Daniel, S. J., Woessner, W. W. & Thomas, S. A. (2008), 'Buffered, lagged, or cooled? disentangling hyporheic influences on temperature cycles in stream channels', *Water Resources Research* **44**(9).

Azizian, M., Boano, F., Cook, P. L. M., Detwiler, R. L., Rippy, M. A. & Grant, S. B. (2017), 'Ambient groundwater flow diminishes nitrate processing in the hyporheic zone of streams', *Water Resources Research* **53**(5), 3941–3967.

Bear, J. (1972), *Dynamics of fluids in porous media*, American Elsevier Publishing, New York.

Bejan, A. (1993), *Heat transfer*, John Wiley & Sons, New York.

Bernard-Jannin, L., Brito, D., Sun, X., Jauch, E., Neves, R., Sauvage, S. & Sánchez-Pérez, J.-M. (2016), 'Spatially distributed modelling of surface water-groundwater exchanges during overbank flood events–a case study at the garonne river', *Advances in water resources* **94**, 146–159.

Blaschke, A. P., Steiner, K.-H., Schmalfuss, R., Gutknecht, D. & Sengschmitt, D. (2003), 'Clogging processes in hyporheic interstices of an impounded river, the danube at vienna, austria', *International Review of Hydrobiology: A Journal Covering all Aspects of Limnology and Marine Biology* **88**(3-4), 397–413.

Boano, F., Camporeale, C., Revelli, R. & Ridolfi, L. (2006), 'Sinuosity-driven hyporheic exchange in meandering rivers', *Geophysical Research Letters* **33**(18).

Boano, F., Demaria, A., Revelli, R. & Ridolfi, L. (2010), 'Biogeochemical zonation due to intrameander hyporheic flow', *Water resources research* **46**(2).

Boano, F., Harvey, J. W., Marion, A., Packman, A. I., Revelli, R., Ridolfi, L. & Wörman, A. (2014), 'Hyporheic flow and transport processes: Mechanisms, models, and biogeochemical implications', *Reviews of Geophysics* **52**(4), 603–679.

Boano, F., Revelli, R. & Ridolfi, L. (2007), 'Bedform-induced hyporheic exchange with unsteady flows', *Advances in Water Resources* **30**(1), 148–156.

Boano, F., Revelli, R. & Ridolfi, L. (2013), 'Modeling hyporheic exchange with unsteady stream discharge and bedform dynamics', *Water Resources Research* **49**(7), 4089–4099.

Boulton, A. J., Datry, T., Kasahara, T., Mutz, M. & Stanford, J. A. (2010), 'Ecology and management of the hyporheic zone: stream–groundwater interactions of running waters and their floodplains', *Journal of the North American Benthological Society* **29**(1), 26–40.

Boulton, A. J., Fenwick, G. D., Hancock, P. J. & Harvey, M. S. (2008), 'Biodiversity, functional roles and ecosystem services of groundwater invertebrates', *Invertebrate Systematics* **22**(2), 103–116.

Boulton, A. J., Findlay, S., Marmonier, P., Stanley, E. H. & Valett, H. M. (1998), 'The functional significance of the hyporheic zone in streams and rivers', *Annual Review of Ecology and Systematics* **29**(1), 59–81.

Brekenfeld, N., Comer-Warner, S., Singh, T., Blaen, P., Lupon, A.and Gómez-Gener, L., Blume, T., Morgner, M.and Laudon, H., Hannah, D. M., Bishop, K. H., Sponseller, R., Kettridge, N. & Krause, S. (April 2018*a*), The effect of contrasting discharges on the metabolic activity of a small boreal stream, European Geosciences Union.

Brekenfeld, N., Comer-Warner, S., Singh, T., Blaen, P., Lupon, A.and Gómez-Gener, L., Blume, T., Morgner, M.and Laudon, H., Hannah, D. M., Bishop, K. H., Sponseller, R., Kettridge, N. & Krause, S. (December 2018*b*), The hyporheic zone as a hotspot of c-cycling in a small boreal stream: Lessons learnt from experimental flow manipulations, American Geosciences Union.

Bridge, J. S. (2009), *Rivers and Floodplains: Forms, Processes, and Sedimentary Record*, Wiley.

Briggs, M. A., Day-Lewis, F. D., Zarnetske, J. P. & Harvey, J. W. (2015), 'A physical explanation for the development of redox microzones in hyporheic flow', *Geophysical Research Letters* **42**(11), 4402–4410.

Brown, L. E., Hannah, D. M. & Milner, A. M. (2006), 'Hydroclimatological influences on water column and streambed thermal dynamics in an alpine river system', *Journal of Hydrology* **325**(1-4), 1–20.

Brunke, M. & Gonser, T. (1997), 'The ecological significance of exchange processes between rivers and groundwater', *Freshwater biology* **37**(1), 1–33.

Bruno, M. C., Maiolini, B., Carolli, M. & Silveri, L. (2009), Impact of hydropeaking on hyporheic invertebrates in an alpine stream (trentino, italy), *in* 'Annales de

Limnologie-International Journal of Limnology', Vol. 45, EDP Sciences, pp. 157–170.

Bruno, M. C., Siviglia, A., Carolli, M. & Maiolini, B. (2013), 'Multiple drift responses of benthic invertebrates to interacting hydropeaking and thermopeaking waves', *Ecohydrology* **6**(4), 511–522.

Buffington, J. & Tonina, D. (2009), 'Hyporheic exchange in mountain rivers II: Effects of channel morphology on mechanics, scales, and rates of exchange', *Geography Compass* **3**(3), 1038–1062.

Burkholder, B. K., Grant, G. E., Haggerty, R., Khangaonkar, T. & Wampler, P. J. (2008), 'Influence of hyporheic flow and geomorphology on temperature of a large, gravel-bed river, clackamas river, oregon, usa', *Hydrological Processes* **22**(7), 941–953.

Caissie, D. (2006), 'The thermal regime of rivers: a review', *Freshwater biology* **51**(8), 1389–1406.

Cardenas, M. B. (2008), 'Surface water-groundwater interface geomorphology leads to scaling of residence times', *Geophysical Research Letters* **35**(8).

Cardenas, M. B. (2015), 'Hyporheic zone hydrologic science: A historical account of its emergence and a prospectus', *Water Resources Research* **51**(5), 3601–3616.

Cardenas, M. B., Lagmay, A. M. F., Andrews, B. J., Rodolfo, R. S., Cabria, H. B., Zamora, P. B. & Lapus, M. R. (2012), 'Terrestrial smokers: Thermal springs due to hydrothermal convection of groundwater connected to surface water', *Geophysical Research Letters* **39**(2).

Cardenas, M. B. & Wilson, J. L. (2006), 'The influence of ambient groundwater discharge on exchange zones induced by current–bedform interactions', *Journal of Hydrology* **331**(1), 103–109.

Cardenas, M. B. & Wilson, J. L. (2007*a*), 'Effects of current–bed form induced fluid flow on the thermal regime of sediments', *Water Resources Research* **43**(8).

Cardenas, M. B. & Wilson, J. L. (2007*b*), 'Exchange across a sediment–water interface with ambient groundwater discharge', *Journal of hydrology* **346**(3-4), 69–80.

Cardenas, M. B., Wilson, J. L. & Zlotnik, V. A. (2004), 'Impact of heterogeneity, bed forms, and stream curvature on subchannel hyporheic exchange', *Water Resources Research* **40**(8).

Caruso, A., Ridolfi, L. & Boano, F. (2016), 'Impact of watershed topography on hyporheic exchange', *Advances in water resources* **94**, 400–411.

Casas-Mulet, R., Alfredsen, K., Hamududu, B. & Timalsina, N. P. (2015), 'The effects of hydropeaking on hyporheic interactions based on field experiments', *Hydrological processes* **29**(6), 1370–1384.

Chen, C., Packman, A. I., Zhang, D. & Gaillard, J.-F. (2010), 'A multi-scale investigation of interfacial transport, pore fluid flow, and fine particle deposition in a sediment bed', *Water Resources Research* **46**(11).

Comer-Warner, S. A., Romeijn, P., Gooddy, D. C., Ullah, S., Kettridge, N., Marchant, B., Hannah, D. M. & Krause, S. (2018), 'Thermal sensitivity of co2 and ch4 emissions varies with streambed sediment properties', *Nature communications* **9**.

Conant, B. (2004), 'Delineating and quantifying ground water discharge zones using streambed temperatures', *Groundwater* **42**(2), 243–257.

Constantz, J. (2008), 'Heat as a tracer to determine streambed water exchanges', *Water Resources Research* **44**(4), 1–20.

Cooper, H. H. & Rorabaugh, M. I. (1963), Ground-water movements and bank storage due to flood stages in surface streams, Ground Water Hydraulics Water Supply Paper 1536-J, US Geological Survey.

De Marsily, G. (1986), *Quantitative hydrogeology: Groundwater hydrology for engineers*, 1 edition edn, Academic Press.

Dingman, S. L. (2009), *Fluvial Hydraulics*, Oxford University Press, USA, Oxford ; New York.

Drummond, J. D., Larsen, L. G., González-Pinzón, R., Packman, A. I. & Harvey, J. W. (2017), 'Fine particle retention within stream storage areas at base flow and in response to a storm event', *Water Resources Research* **53**(7), 5690–5705.

Dudley-Southern, M. & Binley, A. (2015), 'Temporal responses of groundwater-surface water exchange to successive storm events', *Water Resources Research* **51**(2), 1112–1126.

Elliott, A. H. & Brooks, N. H. (1997), 'Transfer of nonsorbing solutes to a streambed with bed forms: Theory', *Water Resources Research* **33**(1), 123–136.

Evans, E. C., Greenwood, M. T. & Petts, G. E. (1995), 'Thermal profiles within river beds', *Hydrological Processes* **9**(1), 19–25.

Evans, E. C. & Petts, G. E. (1997), 'Hyporheic temperature patterns within riffles', *Hydrological Sciences Journal* **42**(2), 199–213.

Fenchel, T., Blackburn, H., King, G. M. & Blackburn, T. H. (2012), *Bacterial biogeochemistry: the ecophysiology of mineral cycling*, Academic press.

Fischer, H., Kloep, F., Wilzcek, S. & Pusch, M. T. (2005), 'A river's liver–microbial processes within the hyporheic zone of a large lowland river', *Biogeochemistry* **76**(2), 349–371.

Fritz, B. G. & Arntzen, E. V. (2007), 'Effect of rapidly changing river stage on uranium flux through the hyporheic zone', *Groundwater* **45**(6), 753–760.

Gomez-Velez, J. D. & Harvey, J. W. (2014*a*), 'A hydrogeomorphic river network model predicts where and why hyporheic exchange is important in large basins', *Geophysical Research Letters* **41**(18), 6403–6412.

Gomez-Velez, J. D. & Harvey, J. W. (2014*b*), 'A hydrogeomorphic river network model predicts where and why hyporheic exchange is important in large basins', *Geophysical Research Letters* p. 2014GL061099.

Gomez-Velez, J. D., Harvey, J. W., Cardenas, M. B. & Kiel, B. (2015), 'Denitrification in the Mississippi river network controlled by flow through river bedforms', *Nature Geoscience* **8**, 941–945.

Gomez-Velez, J. D., Krause, S. & Wilson, J. L. (2014), 'Effect of low-permeability layers on spatial patterns of hyporheic exchange and groundwater upwelling', *Water Resources Research* **50**(6), 5196–5215.

Gomez-Velez, J. D. & Wilson, J. L. (2013), 'Age distributions and dynamically changing hydrologic systems: Exploring topography-driven flow', *Water Resources Research* **49**(3), 1503–1522.

Gomez-Velez, J. D., Wilson, J. L. & Cardenas, M. B. (2012), 'Residence time distributions in sinuosity-driven hyporheic zones and their biogeochemical effects', *Water Resources Research* **48**(9).

Gomez-Velez, J. D., Wilson, J. L., Cardenas, M. B. & Harvey, J. W. (2017), 'Flow and residence times of dynamic river bank storage and sinuosity-driven hyporheic exchange', *Accepted for publication in Water Resources Research* .

Gooseff, M. N. (2010), 'Defining hyporheic zones–advancing our conceptual and operational definitions of where stream water and groundwater meet', *Geography Compass* **4**(8), 945–955.

Gu, C., Hornberger, G. M., Herman, J. S. & Mills, A. L. (2008), 'Effect of freshets on the flux of groundwater nitrate through streambed sediments', *Water resources research* **44**(5).

Haggerty, R., Martí, E., Argerich, A., Von Schiller, D. & Grimm, N. B. (2009), 'Resazurin as a "smart" tracer for quantifying metabolically active transient storage in stream ecosystems', *Journal of Geophysical Research: Biogeosciences* **114**(G3).

Hannah, D. M., Malcolm, I. A. & Bradley, C. (2009), 'Seasonal hyporheic temperature dynamics over riffle bedforms', *Hydrological Processes* **23**(15), 2178–2194.

Harvey, J. & Gooseff, M. (2015), 'River corridor science: Hydrologic exchange and ecological consequences from bedforms to basins', *Water Resources Research* **51**(9), 6893–6922.

Harvey, J. W., Böhlke, J. K., Voytek, M. A., Scott, D. & Tobias, C. R. (2013), 'Hyporheic zone denitrification: Controls on effective reaction depth and contribution to whole-stream mass balance', *Water Resources Research* **49**(10), 6298–6316.

Harvey, J. W., Drummond, J. D., Martin, R. L., McPhillips, L. E., Packman, A. I., Jerolmack, D. J., Stonedahl, S. H., Aubeneau, A. F., Sawyer, A. H., Larsen, L. G. & Tobias, C. R. (2012), 'Hydrogeomorphology of the hyporheic zone: Stream solute and fine particle interactions with a dynamic streambed', *Journal of Geophysical Research: Biogeosciences* **117**(G4).

Hinton, M. J., Schiff, S. L. & English, M. C. (1997), 'The significance of storms for the concentration and export of dissolved organic carbon from two precambrian shield catchments', *Biogeochemistry* **36**(1), 67–88.

Inamdar, S. P., Christopher, S. F. & Mitchell, M. J. (2004), 'Export mechanisms for dissolved organic carbon and nitrate during summer storm events in a glaciated forested catchment in new york, usa', *Hydrological Processes* **18**(14), 2651–2661.

Jiang, X.-W., Wang, X.-S., Wan, L. & Ge, S. (2011), 'An analytical study on stagnation points in nested flow systems in basins with depth-decaying hydraulic conductivity', *Water Resources Research* **47**(1).

Jones, N. E. (2014), 'The dual nature of hydropeaking rivers: Is ecopeaking possible?', *River Research and Applications* **30**(4), 521–526.

Jung, M., Burt, T. P. & Bates, P. D. (2004), 'Toward a conceptual model of floodplain water table response', *Water Resources Research* **40**(12).

Kaplan, L. A. & Bott, T. L. (1989), 'Diel fluctuations in bacterial activity on streambed substrata during vernal algal blooms: effects of temperature, water chemistry, and habitat', *Limnology and Oceanography* **34**(4), 718–733.

Kaufman, M. H., Cardenas, M. B., Buttles, J., Kessler, A. J. & Cook, P. L. M. (2017), 'Hyporheic hot moments: Dissolved oxygen dynamics in the hyporheic zone in response to surface flow perturbations', *Water Resources Research* **53**(8), 6642–6662.

Kennedy, C. D., Genereux, D. P., Corbett, D. R. & Mitasova, H. (2009), 'Spatial and temporal dynamics of coupled groundwater and nitrogen fluxes through a streambed in an agricultural watershed', *Water Resources Research* **45**(9).

Kinouchi, T., Yagi, H. & Miyamoto, M. (2007), 'Increase in stream temperature related to anthropogenic heat input from urban wastewater', *Journal of Hydrology* **335**(1-2), 78–88.

Kleineidam, S., Rügner, H. & Grathwohl, P. (2004), 'Desorption kinetics of phenanthrene in aquifer material lacks hysteresis', *Environmental science & technology* **38**(15), 4169–4175.

Koltermann, C. E. & Gorelick, S. M. (1995), 'Fractional packing model for hydraulic conductivity derived from sediment mixtures', *Water Resources Research* **31**(12), 3283–3297.

Krause, S., Blume, T. & Cassidy, N. J. (2012), 'Investigating patterns and controls of groundwater up-welling in a lowland river by combining fibre-optic distributed temperature sensing with observations of vertical hydraulic gradients', *Hydrology and Earth System Sciences* **16**(6), 1775–1792.

Krause, S., Boano, F., Cuthbert, M. O., Fleckenstein, J. H. & Lewandowski, J. (2014), 'Understanding process dynamics at aquifer-surface water interfaces: An introduction to the special section on new modeling approaches and novel experimental technologies', *Water Resources Research* **50**(2), 1847–1855.

Krause, S., Hannah, D. M. & Blume, T. (2011), 'Interstitial pore-water temperature dynamics across a pool-riffle-pool sequence', *Ecohydrology* **4**(4), 549–563.

Krause, S., Hannah, D. M., Fleckenstein, J. H., Heppell, C. M., Kaeser, D., Pickup, R., Pinay, G., Robertson, A. L. & Wood, P. J. (2011), 'Inter-disciplinary perspectives on processes in the hyporheic zone', *Ecohydrology* **4**(4), 481–499.

Krause, S., Heathwaite, L., Binley, A. & Keenan, P. (2009), 'Nitrate concentration changes at the groundwater-surface water interface of a small Cumbrian river', *Hydrological Processes* **23**(15), 2195–2211.

Krause, S., Tecklenburg, C., Munz, M. & Naden, E. (2013), 'Streambed nitrogen cycling beyond the hyporheic zone: Flow controls on horizontal patterns and depth distribution of nitrate and dissolved oxygen in the upwelling groundwater of a lowland river', *Journal of Geophysical Research: Biogeosciences* **118**(1), 54–67.

Langmuir, I. (1915), 'Chemical reactions at low temperatures', *Journal of the American Chemical Society* **37**(5), 1139–1167.

Laudon, H. & Ottosson Löfvenius, M. (2016), 'Adding snow to the picture–providing complementary winter precipitation data to the krycklan catchment study database', *Hydrological Processes* **30**(13), 2413–2416.

Laudon, H., Taberman, I., Ågren, A., Futter, M., Ottosson-Löfvenius, M. & Bishop, K. (2013), 'The krycklan catchment study—a flagship infrastructure for hydrology, biogeochemistry, and climate research in the boreal landscape', *Water Resources Research* **49**(10), 7154–7158.

Leach, J. A., Lidberg, W., Kuglerová, L., Peralta-Tapia, A., Ågren, A. & Laudon, H. (2017), 'Evaluating topography-based predictions of shallow lateral groundwater discharge zones for a boreal lake-stream system', *Water Resources Research* **53**(7), 5420–5437.

Lenk, M. & Saenger, N. (2000), 'Exchange processes in the river bed and their influence on temperature variations', *Internationale Vereinigung für theoretische und angewandte Limnologie: Verhandlungen* **27**(1), 427–430.

Liang, X., Zhan, H. & Schilling, K. (2018), 'Spatiotemporal responses of groundwater flow and aquifer-river exchanges to flood events', *Water Resources Research* **54**(3), 1513–1532.

Malard, F., Mangin, A., Uehlinger, U. & Ward, J. V. (2001), 'Thermal heterogeneity in the hyporheic zone of a glacial floodplain', *Canadian Journal of Fisheries and Aquatic Sciences* **58**(7), 1319–1335.

Malcolm, I. A., Soulsby, C. & Youngson, A. F. (2002), 'Thermal regime in the hyporheic zone of two contrasting salmonid spawning streams: ecological and hydrological implications', *Fisheries Management and Ecology* **9**(1), 1–10.

Malcolm, I. A., Soulsby, C., Youngson, A. F., Hannah, D. M., McLaren, I. S. & Thorne, A. (2004), 'Hydrological influences on hyporheic water quality: implications for salmon egg survival', *Hydrological Processes* **18**(9), 1543–1560.

Malzone, J. M., Anseeuw, S. K., Lowry, C. S. & Allen-King, R. (2016), 'Temporal Hyporheic Zone Response to Water Table Fluctuations', *Groundwater* **54**(2), 274–285.

Malzone, J. M., Lowry, C. S. & Ward, A. S. (2016), 'Response of the hyporheic zone to transient groundwater fluctuations on the annual and storm event time scales', *Water Resources Research* .

Marzadri, A., Tonina, D. & Bellin, A. (2012), 'Morphodynamic controls on redox conditions and on nitrogen dynamics within the hyporheic zone: Application to gravel bed rivers with alternate-bar morphology', *Journal of Geophysical Research: Biogeosciences* **117**(G3).

Marzadri, A., Tonina, D., Bellin, A. & Valli, A. (2016), 'Mixing interfaces, fluxes, residence times and redox conditions of the hyporheic zones induced by dune-like bedforms and ambient groundwater flow', *Advances in Water Resources* **88**, 139–151.

McCallum, J. L. & Shanafield, M. (2016), 'Residence times of stream-groundwater exchanges due to transient stream stage fluctuations', *Water Resources Research* .

Millington, R. J. & Quirk, J. P. (1961), 'Permeability of porous solids', *Transactions of the Faraday Society* **57**, 1200–1207.

Mojarrad, B. B., Betterle, A., Singh, T., Olid, C. & Wörman, A. (2019), 'The effect of stream discharge on hyporheic exchange', *Water* **11**(7), 1436.

Mojarrad, B. B., Riml, J., Wörman, A. & Laudon, H. (2019), 'Fragmentation of the hyporheic zone due to regional groundwater circulation', *Water resources research* **55**(2), 1242–1262.

Mouw, J. E. B., Stanford, J. A. & Alaback, P. B. (2009), 'Influences of flooding and hyporheic exchange on floodplain plant richness and productivity', *River research and applications* **25**(8), 929–945.

Nield, D. A. & Bejan, A. (2013), *Convection in porous media*, Springer New York, New York, NY.

Nimick, D. A., Gammons, C. H., Cleasby, T. E., Madison, J. P., Skaar, D. & Brick, C. M. (2003), 'Diel cycles in dissolved metal concentrations in streams: occurrence and possible causes', *Water Resources Research* **39**(9).

Norman, F. A. & Cardenas, M. B. (2014), 'Heat transport in hyporheic zones due to bedforms: An experimental study', *Water Resources Research* **50**(4), 3568–3582.

Ocampo, C. J., Oldham, C. E. & Sivapalan, M. (2006), 'Nitrate attenuation in agricultural catchments: Shifting balances between transport and reaction', *Water Resources Research* **42**(1).

O'Connor, B. L. & Harvey, J. W. (2008), 'Scaling hyporheic exchange and its influence on biogeochemical reactions in aquatic ecosystems', *Water Resources Research* **44**(12).

Packman, A. I., Salehin, M. & Zaramella, M. (2004), 'Hyporheic exchange with gravel beds: basic hydrodynamic interactions and bedform-induced advective flows', *Journal of Hydraulic Engineering* **130**, 647.

Pinay, G., Peiffer, S., De Dreuzy, J.-R., Krause, S., Hannah, D. M., Fleckenstein, J. H., Sebilo, M., Bishop, K. & Hubert-Moy, L. (2015), 'Upscaling nitrogen removal capacity from local hotspots to low stream orders' drainage basins', *Ecosystems* **18**(6), 1101–1120.

Poole, G. C., O'daniel, S. J., Jones, K. L., Woessner, W. W., Bernhardt, E. S., Helton, A. M., Stanford, J. A., Boer, B. R. & Beechie, T. J. (2008), 'Hydrologic spiralling: the role of multiple interactive flow paths in stream ecosystems', *River Research and Applications* **24**(7), 1018–1031.

Porter, L. B., Ritzi, R. W., Mastera, L. J., Dominic, D. F. & Ghanbarian-Alavijeh, B. (2013), 'The kozeny-carman equation with a percolation threshold', *Groundwater* **51**(1), 92–99.

Rau, G. C., Andersen, M. S., McCallum, A. M., Roshan, H. & Acworth, R. I. (2014), 'Heat as a tracer to quantify water flow in near-surface sediments', *Earth-Science Reviews* **129**, 40–58.

Revelli, R., Boano, F., Camporeale, C. & Ridolfi, L. (2008), 'Intra-meander hyporheic flow in alluvial rivers', *Water Resources Research* **44**(12).

Ryan, R. J. & Boufadel, M. C. (2006), 'Influence of streambed hydraulic conductivity on solute exchange with the hyporheic zone', *Environmental Geology* **51**(2), 203–210.

Salazar, O., Vargas, J., Nájera, F., Seguel, O. & Casanova, M. (2014), 'Monitoring of nitrate leaching during flush flooding events in a coarse-textured floodplain soil', *Agricultural Water Management* **146**, 218–227.

Sanz-Prat, A., Lu, C., Amos, R. T., Finkel, M., Blowes, D. W. & Cirpka, O. A. (2016), 'Exposure-time based modeling of nonlinear reactive transport in porous media subject to physical and geochemical heterogeneity', *Journal of contaminant hydrology* **192**, 35–49.

Sanz-Prat, A., Lu, C., Finkel, M. & Cirpka, O. A. (2015), 'On the validity of travel-time based nonlinear bioreactive transport models in steady-state flow', *Journal of contaminant hydrology* **175**, 26–43.

Sawyer, A. H., Cardenas, M. B., Bomar, A. & Mackey, M. (2009), 'Impact of dam operations on hyporheic exchange in the riparian zone of a regulated river', *Hydrological Processes: An International Journal* **23**(15), 2129–2137.

Schmadel, N. M., Ward, A. S., Lowry, C. S. & Malzone, J. M. (2016), 'Hyporheic exchange controlled by dynamic hydrologic boundary conditions', *Geophysical Research Letters* p. 2016GL068286.

Schmadel, N. M., Ward, A. S. & Wondzell, S. M. (2017), 'Hydrologic controls on hyporheic exchange in a headwater mountain stream', *Water Resources Research* **53**(7), 6260–6278.

Simpson, S. C. & Meixner, T. (2012), 'Modeling effects of floods on streambed hydraulic conductivity and groundwater-surface water interactions', *Water resources research* **48**(2).

Singh, T., Wu, L., Gomez-Velez, J. D., Lewandowski, J., Hannah, D. M. & Krause, S. (2019), 'Dynamic hyporheic zones: Exploring the role of peak flow events on bedform-induced hyporheic exchange', *Water Resources Research* **55**(1), 218–235.

Stonedahl, S. H., Harvey, J. W., Wörman, A., Salehin, M. & Packman, A. I. (2010), 'A multiscale model for integrating hyporheic exchange from ripples to meanders', *Water Resources Research* **46**(12).

Story, A., Moore, R. D. & Macdonald, J. S. (2003), 'Stream temperatures in two shaded reaches below cutblocks and logging roads: downstream cooling linked to subsurface hydrology', *Canadian Journal of Forest Research* **33**(8), 1383–1396.

Tonina, D. & Buffington, J. M. (2009), 'Hyporheic exchange in mountain rivers I: mechanics and environmental effects', *Geography Compass* **3**(3), 1063–1086.

Tonina, D. & Buffington, J. M. (2011), 'Effects of stream discharge, alluvial depth and bar amplitude on hyporheic flow in pool-riffle channels', *Water Resources Research* **47**(8).

Trauth, N. & Fleckenstein, J. H. (2017), 'Single discharge events increase reactive efficiency of the hyporheic zone', *Water Resources Research* **53**(1), 779–798.

Triska, F. J., Kennedy, V. C., Avanzino, R. J., Zellweger, G. W. & Bencala, K. E. (1989), 'Retention and transport of nutrients in a third-order stream in northwestern california: hyporheic processes', *Ecology* pp. 1893–1905.

Vivoni, E. R., Bowman, R. S., Wyckoff, R. L., Jakubowski, R. T. & Richards, K. E. (2006), 'Analysis of a monsoon flood event in an ephemeral tributary and its downstream hydrologic effects', *Water Resources Research* **42**(3).

Walsh, S. D. C. & Saar, M. O. (2010), 'Macroscale lattice-boltzmann methods for low peclet number solute and heat transport in heterogeneous porous media', *Water Resources Research* **46**(7).

Ward, A. S., Gooseff, M. N., Voltz, T. J., Fitzgerald, M., Singha, K. & Zarnetske, J. P. (2013), 'How does rapidly changing discharge during storm events affect transient storage and channel water balance in a headwater mountain stream?', *Water Resources Research* **49**(9), 5473–5486.

Ward, A. S., Schmadel, N. M. & Wondzell, S. M. (2018), 'Time-variable transit time distributions in the hyporheic zone of a headwater mountain stream', *Water Resources Research* **54**(3), 2017–2036.

Ward, A. S., Schmadel, N. M., Wondzell, S. M., Gooseff, M. N. & Singha, K. (2017), 'Dynamic hyporheic and riparian flow path geometry through base flow recession in two headwater mountain stream corridors', *Water Resources Research* **53**(5), 3988–4003.

Webb, B. W., Hannah, D. M., Moore, R. D., Brown, L. E. & Nobilis, F. (2008), 'Recent advances in stream and river temperature research', *Hydrological processes* **22**(7), 902–918.

Westrich, J. T. & Berner, R. A. (1988), 'The effect of temperature on rates of sulfate reduction in marine sediments', *Geomicrobiology Journal* **6**(2), 99–117.

Winter, T. C. (1998), *Ground water and surface water: a single resource*, Vol. 1139, DIANE Publishing Inc.

Wondzell, S. M. & Swanson, F. J. (1999), 'Floods, channel change, and the hyporheic zone', *Water Resources Research* **35**(2), 555–567.

Woodside, W. & Messmer, J. H. (1961), 'Thermal conductivity of porous media. I. Unconsolidated sands', *Journal of Applied Physics* **32**(9), 1688–1699.

Wörman, A., Packman, A. I., Marklund, L., Harvey, J. W. & Stone, S. H. (2006), 'Exact three-dimensional spectral solution to surface-groundwater interactions with arbitrary surface topography', *Geophysical Research Letters* **33**(7).

Wörman, A., Packman, A. I., Marklund, L., Harvey, J. W. & Stone, S. H. (2007), 'Fractal topography and subsurface water flows from fluvial bedforms to the continental shield', *Geophysical Research Letters* **34**(7).

Wu, G., Shu, L., Lu, C., Chen, X., Zhang, X., Appiah-Adjei, E. K. & Zhu, J. (2015), 'Variations of streambed vertical hydraulic conductivity before and after a flood season', *Hydrogeology Journal* **23**(7), 1603–1615.

Wu, L., Singh, T., Gomez-Velez, J. D., Nützmann, G., Wörman, A., Krause, S. & Lewandowski, J. (2018), 'Impact of dynamically changing discharge on hyporheic exchange processes under gaining and losing groundwater conditions', *Water Resources Research* **54**(12), 10–076.

Zarnetske, J. P., Haggerty, R., Wondzell, S. M. & Baker, M. A. (2011), 'Dynamics of nitrate production and removal as a function of residence time in the hyporheic zone', *Journal of Geophysical Research: Biogeosciences* **116**(G1).

Zarnetske, J. P., Haggerty, R., Wondzell, S. M., Bokil, V. A. & González-Pinzón, R. (2012), 'Coupled transport and reaction kinetics control the nitrate source-sink function of hyporheic zones', *Water Resources Research* **48**(11).

Zheng, L. & Cardenas, M. B. (2018), 'Diel stream temperature effects on nitrogen cycling in hyporheic zones', *Journal of Geophysical Research: Biogeosciences* .

Zheng, L., Cardenas, M. B. & Wang, L. (2016), 'Temperature effects on nitrogen cycling and nitrate removal-production efficiency in bed form-induced hyporheic zones', *Journal of Geophysical Research: Biogeosciences* **121**(4), 1086–1103.

Zhou, T., Bao, J., Huang, M., Hou, Z., Arntzen, E., Song, X., Harding, S. F., Titzler, P. S., Ren, H., Murray, C. J., Perkins, W. A., Chen, X., Stegen, J. C., Hammond, G. E., Thorne, P. D. & Zachara, J. M. (2018), 'Riverbed hydrologic exchange dynamics in a large regulated river reach', *Water Resources Research* **54**(4), 2715–2730.

Zimmer, M. A. & Lautz, L. K. (2014), 'Temporal and spatial response of hyporheic zone geochemistry to a storm event', *Hydrological Processes* **28**(4), 2324–2337.